Continuum Damage Mechanics (CDM) Modelling of Dislocation Creep in 9-12% Cr Creep Resistant Steels

Muhammad Ghalib Stracey

This dissertation is submitted for the degree of Master of Science in Engineering

In the Department of Mechanical Engineering

University of Cape Town

Plagiarism Declaration

1. I know the meaning of plagiarism and declare that all the work in the document, save for that which is properly acknowledged, is my own. This thesis/dissertation has been submitted to the Turnitin module (or equivalent similarity and originality checking software) and I confirm that my supervisor has seen my report and any concerns revealed by such have been resolved with my supervisor
2. I have not allowed, and will not allow anyone to copy my work with the intention of passing it off as his or her own work.

Signed by candidate

Muhammad Ghalib Stracey

Signature removed

Student Number: STRMUH001

Date:

Abstract

The generation of electricity to meet an ever-growing demand has become a defining characteristic of the modern world for both developed and developing nations alike. This, coupled with the intensifying concern with pollution and its effects on the environment has put immense pressure on how quickly and efficiently power is produced. Being the most prevalent source of electricity generation, coal fired power plants have been subject to increasing scrutiny and study in an effort to improve the efficiency at which they operate. Hence, coal fired power plants are being run at increased temperatures and pressures such as those observed in Super-critical and Ultra-super-critical plants. This has by extension put excessive demand on materials used in these plants specifically within the boiler and superheater pipe sections where the most extreme thermodynamic conditions are experienced. The most commonly used materials for these applications are in the family of ferritic/martensitic 9-12% Cr steels chosen for their superior material properties especially during long-term exposure as coal fired power plants typically operate for over 20 years before being decommissioned.

One of the lesser understood aspects of 9-12%Cr steels is with regard to their long-term material properties specifically that of creep degradation and deformation. This has been partially due to the reliance of creep life predictions in the past being based on accelerated creep testing and empirically based modelling. With the relatively recent revelations of empirically based modelling shown to be inaccurate when extrapolated to the long-term, a need has been identified amongst researchers to develop more accurate models based on physical relationships and material microstructure. Moreover, the insight obtained from modern experimental techniques and technologies as well as ever-expanding computing capabilities provide an opportunity to produce microstructurally based models with a high degree of complexity. Thus motivated, the focus of this dissertation was to develop a physically based dislocation creep model using the Continuum Damage Mechanics (CDM) approach.

A dislocation CDM model was developed and implemented in the current work for uniaxial creep loading using the numerical modelling software *Matlab*^{TM}. The CDM approach was built upon fundamental dislocation theory as well as other microstructural considerations pertaining to dislocation creep including subgrain coarsening, $M_{23}C_6$ precipitate coarsening and stress redistribution. The CDM model was found to require calibration in order to be applied to specific 9-12% Cr steels which was implemented using a parameter optimisation routine. The results obtained were compared with experimentally obtained, long-term creep-time and microstructural data for the 11% Cr steel CB8 and the 9% Cr steel P92. The CDM creep-time predictions were found to vary in accuracy depending upon the experimental data against which the model was calibrated. Upon further investigation, it was hypothesised that the discrepancy observed was due to the formation of the Modified Z-phase in some of the long term creep data but not in others which was based primarily on the differing creep exposure times of the various samples. The CDM creep-time predictions for P92 were found to be accurate when compared with experimental results regardless of creep exposure times. The apparent difference in the approximation of the creep deformation for the two steels was concluded as being due to the formation of the Modified Z-phase in CB8 but not in P92 as Modified Z-phase formation is intrinsically linked with the Cr content of the steel.

Acknowledgements

In the name of Allah, The Most gracious, the Most Merciful. Lord of the heavens and the earth. To Him belongs knowledge of all things, of which he has given man but a little.

The author would like to acknowledge the following for their help and support throughout his studies and who have made the journey through this MSc a pleasant and enlightening experience:

- To the author's parents, Ghalib and Muzne Stracey and family for their love and support throughout the undertaking of this project.
- To my supervisor, Professor Robert Knutsen for his assistance, guidance and kindness throughout the progress of this project.
- To Professor Bernhard Sonderegger for his assistance, guidance and kindness throughout the progress of this project.
- To the Technology and Human Resources for Industry Programme (THRIP) for funding this project.
- To the students and staff of the Center for Materials Engineering (CME) for their help and pleasant company.
- To the Graz Institute of Technology for their generous contribution of experimental data for use in this project.
- Finally, the author would like to thank the Department of Mechanical Engineering at the University of Cape Town for affording him the opportunity to undertake the current research.

Contents

List of Figures

List of Tables

Nomenclature

ε_{ss}	Steady state creep strain
$\dot{\varepsilon}_{min}$	Minimum creep strain rate
d	Particle diameter at time t
d_i	Initial particle diameter
$\dot{\varepsilon}$	Strain/creep rate
ρ_m	Mobile dislocation density
v	Mobile dislocation average velocity
b	Burgers vector
σ_{ex}	External applied stress
σ_i	Internal stress
σ_{eff}	Effective stress
M	Taylor factor
τ_{prec}	Precipitate contribution to total back stress
τ_{sgb}	Subgrain boundary contribution to total back stress
τ_{disl}	Dislocation contribution to total back stress
σ_{Or}	Orowan/threshold stress for orowan looping
G	Shear modulus
λ	Average inter-particle spacing
v_g	Average dislocation glide velocity
ΔG	Gibbs free energy of activation
σ_{bar}	Activation stress barrier
T	Temperature
k	Boltzman Constant ($\approx 1.38 \times 10^{-23} JK^{-1}$)
D_0	Vacancy diffusion coefficient
α	Dislocation geometric constant of the order of unity
Q_c	Activation energy for dislocation climb

H Stress redistribution variable

D_d Dislocation density damage variable

D_p Particle coarsening damage variable

D_s Subgrain evolution damage variable

D_c Solid solution damage variable

K_1 Primary creep rate constant

K_2 Primary creep limiting constant

K_{S1} Temperature independent subgrain growth constant

K_{S2} Temperature dependent subgrain growth constant

σ_0 Primary creep/ normalising stress parameter

S Subgrain size

S_i Initial subgrain size

L_{eff} Effective inter-particle spacing

Ω Atomic volume ($\Omega \approx b^3$),

R Ideal gas constant ($\approx 8.314 JK^{-1}mol^{-1}$)

R_j Frequency of atomic jumps

R_0 Atomic attempt frequency

P Probability of an available vacancy site

z Atomic jump distance

V_P Precipitate volume fraction

Err_{min} Percentage error in time at which the minimum creep rate is reached

Err_{tr} Percentage error in time at which the onset of tertiary creep occurs

$Err_{5\%}$ Percentage error in time at which 5% strain is reached

1 Introduction

The modern world has seen the rise of electricity usage from a luxury enjoyed by a few developed nations to a worldwide basic necessity. The availability of electricity has come to be a benchmark against which the success of a people is measured. This is understandable as electricity now plays a major role in almost every sector from business and agriculture to mining and everyday domestic use. However, with this proliferation in the need for electricity, ever growing pressure is put on generating enough of it to meet demand. Added to that is the growing concern for the dire state of the natural environment and the urgent need to reduce pollution and carbon emissions. This two-fold problem cannot be solved by only producing more power, but rather by doing so in a more efficient way so as to have a lower impact on the environment.

While cleaner power generating technologies have seen a profound rise in popularity in recent years, coal-fired power plants remain the most widely used form of electricity generation and is expected to continue to be so for many years to come [1]. This is mostly due to coal being abundant and relatively cheap, and coal-fired power stations being relatively easy to construct and maintain. Therefore, attention needs to be put on improving the efficiency and operating life of these power plants. The efficiency of coal-fired power plants is generally improved by raising the temperature and pressure of the steam operating conditions. Consequently the last 100 years has seen a drastic rise in these parameters (see Figure 1-1) with the result that today ultra-supercritical generators operate at over 600°C and 300 bar (30 MPa).

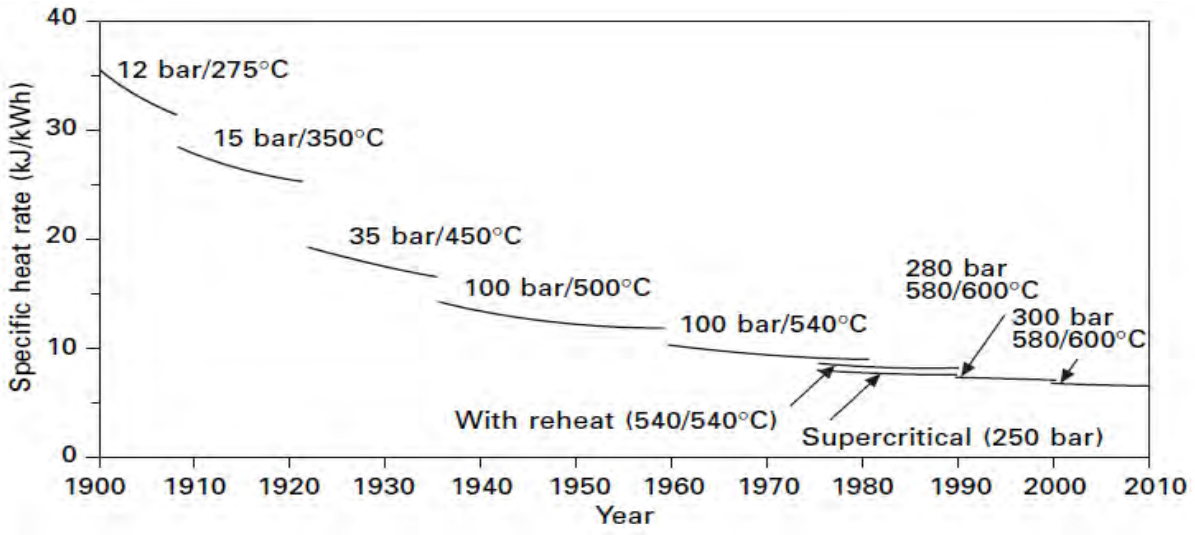

Figure 1-1 Heat rate of steam power plants in Germany as a function of steam parameters since the year 1900 [2]

The intensification of power plant operating conditions has seen a corresponding evolution in the way steels are fabricated and selected for various critical regions within the plant. These steels are required to have a high resistance to stress corrosion cracking, low thermal expansion and high creep resistance in order to withstand their extreme applications. Over the past several decades, this has led to the development of heat-resistant 9-12% Cr steels which possess all of the aforementioned characteristics. However, one of the lesser understood material properties in these steels is that of

creep strength and loss of creep strength specifically in the long term. Added to this is the tendency of short-term or accelerated creep test results to produce erroneous predictions when extrapolated to the long-term. While long-term creep tests can be more reliable, they are costly to conduct and do not produce immediate results. As coal-fired power plants often exceed 25 years of operational service [3], the lack of insight into creep degradation of 9-12% Cr steels in the long term is becoming a point of growing concern amongst researchers.

An alternative to extensive creep testing is the use of computer modelling and simulations. With the ever-growing capabilities of computer processing power, complex models and simulations can be produced far more quickly than physical testing. Added to this is the relative flexibility of computer models compared to experimental setups.

In the work presented in this dissertation a Continuum Damage Mechanics (CDM) modelling approach will be used to predict long-term dislocation creep behaviour of two types of 9-12% Cr steels. This model will be microstructurally based with emphasis on microstructural evolution and loss of creep strength. The model will be calibrated using long-term creep data for the 11% Cr steel, CB8 obtained from the Graz University of Technology. A comprehensive analysis of the various model parameters as well as the reliability of the results will be made. Finally, microstructural observations made from the model's results will be discussed.

1.1 Objectives

The objectives of the research are:

- To perform a comprehensive study of dislocation creep phenomena in 9-12% Cr steels
- To investigate current approaches in modelling dislocation creep with emphasis on the Continuum Damage Mechanics (CDM) method
- To develop and explain from physical principles a CDM model for uniaxial dislocation creep in 9-12% Cr with capabilities of producing creep-time as well as microstructural predictions
- To source and compare experimental long-term creep data to model predictions and estimations based on creep-time and microstructural observations

Ultimately, this research will aid in the development of a holistic creep model to be used in the life assessment of 9-12%Cr in coal fired power plants.

1.2 Details of Thesis Format

The thesis begins with a brief background to the development and use of 9-12% Cr steels in coal fired power plants as well as an overview of dislocation creep phenomena. Chapter 2 proceeds with a detailed analysis of the microstructure of 9-12% Cr steels with emphasis on the aspects pertinent to creep deformation. Chapter 3 introduces various fundamentals of dislocation creep modelling and goes on to examine existing CDM creep modelling approaches. In Chapter 4, data obtained from experimental creep tests for the steels CB8 and P92 is explained.

Chapter 5 details the model used for the current study and includes relevant derivations, techniques and procedures. Chapter 6 documents and discusses strain-time and microstructural results for the steel CB8. Chapter 7 follows with an assessment and discussion for the model results obtained for the steel P92. Finally, Chapter 8 highlights the major conclusions reached based on the results and Chapter 9 makes recommendations based on the conclusions drawn.

1.3 Power Plant Steels

The need for increased thermal efficiency in steam power plants has led to the development of steels with higher creep strength and an acceptable level of creep ductility. One of the greatest breakthroughs in this regard has been the development of heat-resistant ferritic-martensitic 9-12% Cr steels which was spurred by the start of public electrification in the 1950s [2]. These steels, used mostly for header and steam pipes in the steam generator regions of power plants, have seen a continuous improvement in material properties and continue to do so to this day. Some of the major factors influencing the development of heat resistant steels include [2]:

- Long-term operational experience
- Insight gained from long term creep tests
- Investigations into the influence of heat treatment on creep behaviour
- Examination of microstructure during creep loading
- Computer-aided alloy design methods
- Development of metallographic methods and equipment for the identification of precipitates
- Computer-aided creep modelling

During the early 1900s, non-alloyed carbon steels were generally used in critical regions of steam power plants. This was due to a lack of understanding of the influence of key alloying elements such as *N*, *Al* and *Mo* on creep rupture strength. As operating conditions were relatively mild at the time (12 bar, 245°C), the use of non-alloyed steels was not too problematic. The 1920s saw the beginning of the use of low alloy steels for power plant applications due to heightened operational requirements (450°C, 35 bar) [2]. These steels were selected primarily based on hot tensile and short term creep test observations. Due to limited coordination among various research programmes at the time, a wide variety of alloys were produced for the manufacture of steam boilers and turbines. Some of the alloys produced included those with chemical composition (wt%): *0.15%C-0.3-0.5%Mo*, *0.13%C-1%Cr-0.5%Mo* and *0.10%C-2.25%Cr-1%Mo* [2]. In the 1950s the use of long-term creep testing gave rise to the development of *MoV* steels with higher creep capabilities and saw the start of 9-12% Cr steels which would go on to form the basis of modern power plant steels.

One of the more important findings of the 1950s was the identification of Molybdenum as an important alloying element in increasing high temperature creep strength. The increase in creep strength due to the addition of *Mo* is the result of solution hardening as well as the precipitation of Mo_2C. While the addition of *Mo* does significantly improve the strength of the steel there is a marked decline in creep ductility with *Mo* content of above 0.35% for temperatures of above 400°C. This problem was solved by the addition of *Cr* which began the development of *CrMo* steels for use at temperatures beyond 550°C [2]. A typical *CrMo* heat resistant steel chemical composition is *0.13%C-1%Cr-0.5%Mo.*

Another crucial alloying element for increased high temperature creep strength has been identified as Vanadium. Steels with chemical compositions of *0.14%C-0.6%Mo-0.3%V* have been used preferentially for steam pipes and superheater steam pipes in the past due to their superior creep strength. The improvement in creep properties with the addition of *V* is due to the precipitation of V_4C_3 and Mo_2C.

The most prevalent ferritic steels used for thick walled components in modern day super-critical and ultra super-critical power plants are the designated P91 and P92 steels as well as other variants [4] [5]. These steels which were developed in the 1970s have complex chemical compositions with numerous alloying elements added to improve material properties [4]. Compared to earlier 9-12% Cr steels such as the *X22CrMoV12* these steels typically have a lower *C* content, reduced *Cr* content and additional alloying elements resulting in improved creep strength [4]. Table 1-1 shows the major alloying elements present in P91 and P92 steels and Table 1-2 highlights the property enhancing function of the respective elements.

Table 1-1: Chemical composition of type P91 and P92 steels in wt% [6]

	Element													
	C	**Mn**	**Si**	**S**	**P**	**Cr**	**Ni**	**Mo**	**W**	**V**	**Nb**	**N**	**B**	**Al**
P91	0.08-0.12	0.30-0.60	0.20-0.50	0.01	0.02	8.00-9.50	0.40	0.85-1.05	-	0.18-0.25	0.06-0.10	0.03-0.07	-	0.04
P92	0.07-0.13	0.30-0.60	0.50	0.01	0.02	8.50-9.50	0.40	0.30-0.60	1.50-2.00	0.15-0.25	0.04-0.09	0.03-0.07	10-60 ppm	0.04

Table 1-2: Summary of functions of alloying elements in 9-12%Cr steels [5]

Alloying Element	Function
C	Essential for the precipitation of $M_{23}C_6$ and NbC
Mn	Stabilises austenite and provides creep strength
Si	Stabilises ferrite and influences the kinetics of carbide precipitation. Also provides some corrosion resistance
Cr	Provides essential corrosion resistance as well as precipitation of $M_{23}C_6$
Mo	Provides solution hardening as well as the precipitation of Mo_2C
W	Provides microstructural stability as well as solid solution strengthening
V	Provides creep strength through the precipitation of MX
Nb	Provides creep strength through the precipitation of MX
N	Provides creep strength through the precipitation of MX
B	Reduces coarsening rate of $M_{23}C_6$ precipitates
Al	Produces AlN precipitates which stabilise austenitic grain size

1.4 Dislocation Creep Curves

Dislocation creep, as the term implies, is the time-dependent plastic deformation (creep) of a material due to the motion of dislocations. Creep in steels is usually considered at elevated temperatures (<0.4 T_m) and at stresses below the material's yield stress which differentiates it from conventional plastic deformation.

Creep tests have been used extensively over the past decades in order to characterise creep deformation. These tests are most frequently conducted at constant tensile load and at a constant temperature. The test results are typically plotted as creep curves which represent the time dependence of strain over a gauge length. Creep curves for 9-12% Cr steels are generally assumed to consist of three distinct stages. Although strictly speaking this assumption is inaccurate as each stage smoothly transitions into the next, it allows for simpler modelling of creep deformation. The three creep stages are aptly referred to as the Primary, Secondary and Tertiary stages with the Primary and Tertiary stages being transient and the Secondary stage being regarded as steady-state. The secondary creep stage generally encompasses the vast majority of the material's service life and has therefore received the most attention from researchers. However, the extent and influence of each stage on the overall creep curve can vary patently, depending on conditions of stress and temperature (see Figure 1-2).

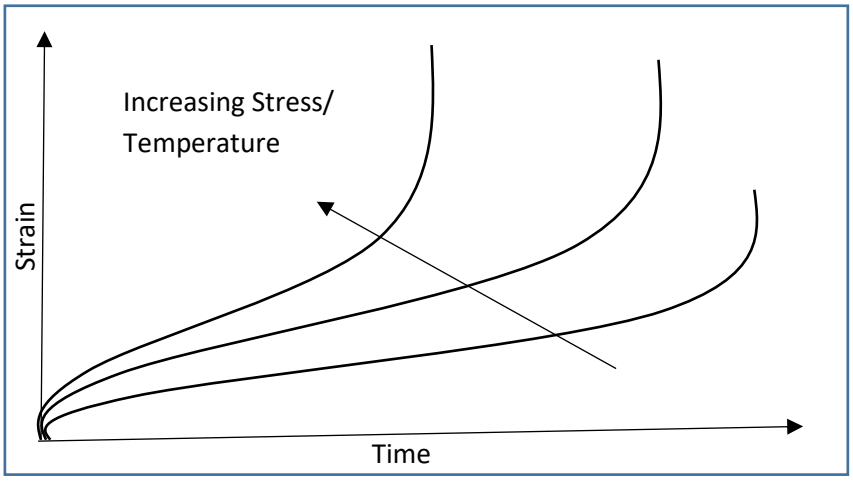

Figure 1-2: Schematic of creep curves varying with Stress/Temperature

1.4.1 *Primary Creep*

The Primary stage of creep is usually typified by a decrease in strain rate ultimately merging into the 'constant' strain region of Secondary creep. This transient behaviour is generally attributed to strain hardening – that is, the hardening effect caused by an increase in dislocation density as a result of a stress increase within a crystalline microstructure (see Figure 1-3). As basic material science dictates, an increase in dislocation density translates to a reduction in free dislocation mobility as dislocations act as obstacles to other dislocations. Since dislocation motion fundamentally leads to material deformation (strain), a lack of dislocation motion therefore has a hardening effect on the material.

An alternative explanation for the primary creep behaviour particularly in Ferritic/Martensitic steels, is that the initial dislocation structure is not in equilibrium with the applied stress and the observance of the decreasing strain rate is due to a type of stress redistribution between the applied stress, dislocation sub-structure and precipitates (see Figure 1-4). Motivation for this explanation stems from observed creep data indicating very slight variation in primary creep strain for large variations in stress and temperature testing conditions [7]. Furthermore, while austenitic steels show a marked increase in dislocation density during primary creep, the increase is comparatively slight for Ferritic/Martensitic steels which have high initial dislocation densities following phase transformation [8]. It is more than likely however that both strain-hardening as well load-transfer phenomena occur concurrently in 9-12% Cr steels, the extent of each differing depending on pre-service treatment.

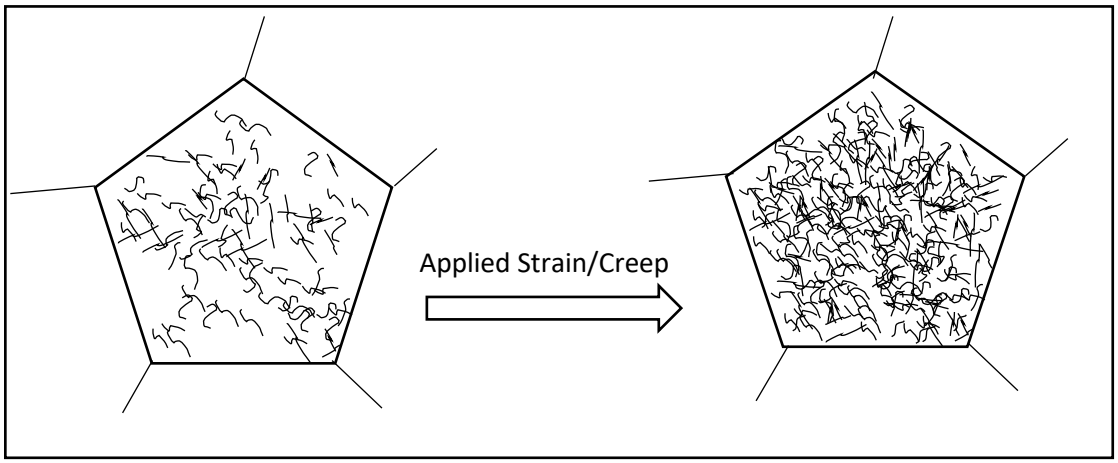

Figure 1-3: Schematic of an idealised Austenitic grain showing dislocation evolution during primary creep

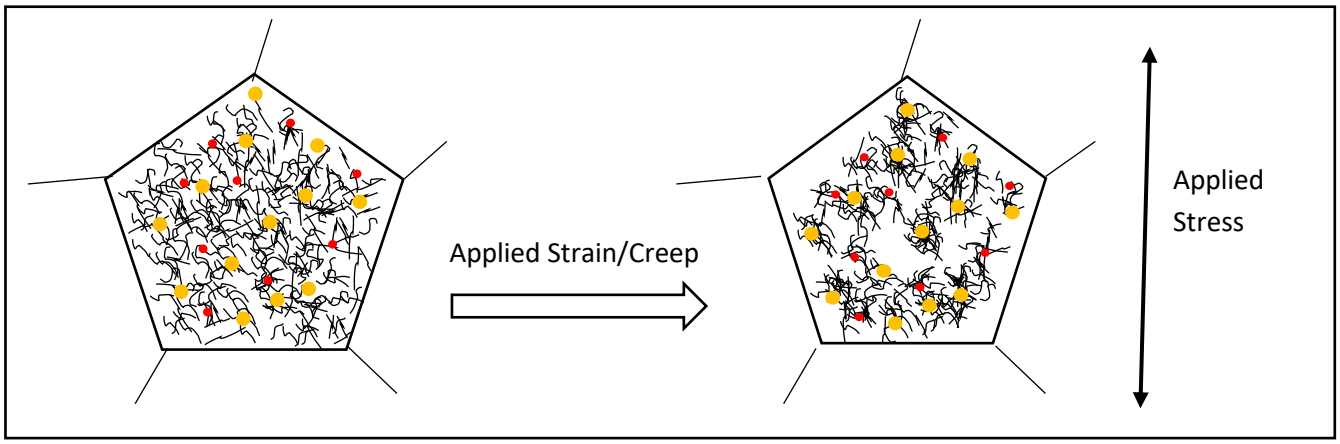

Figure 1-4: Schematic of an idealised Ferritic/Martensitic grain showing dislocation evolution due to applied stress

1.4.2 *Secondary Creep*

The secondary stage of dislocation creep generally dominates the service life of 9-12% Cr in engineering applications. It is traditionally represented as a steady-state creep region $\dot{\varepsilon}_{SS}$, in the creep curve (see Figure 1-5 (a)). However, this is a simplification as in practice the creep rate decreases during primary creep, reaches an instantaneous minimum $\dot{\varepsilon}_{min}$(see Figure 1-5(b)) before increasing, leading into the tertiary creep region [9]. This 'steady-state' behaviour is commonly attributed to the dynamic balance of mobile dislocation generation and annihilation contributing to hardening and softening of the microstructure respectively [8]. As this process is accompanied by a multitude of microstructural changes, a minimum creep rate is observed rather than one of strictly steady-state. These microstructural changes include subgrain evolution, precipitate evolution, void growth and formation of new phases each having an effect on mobile dislocation as well as the overall creep rate to varying degrees.

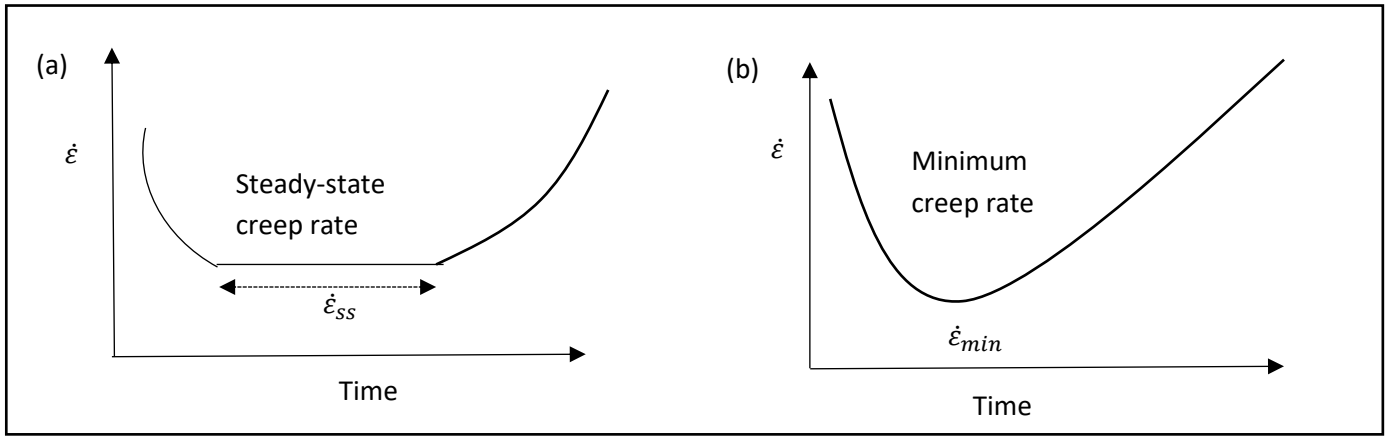

Figure 1-5: Plots of creep strain rate vs time illustrating (a) steady state creep $\dot{\varepsilon}_{ss}$ and (b) minimum creep rate $\dot{\varepsilon}_{min}$

1.4.3 *Tertiary Creep*

The tertiary creep stage is the third and final creep stage which begins at the end of the secondary creep stage and culminates in rupture. It is generally identified as an accelerated strain rate with an exponential increases in material strain over time. This behaviour has been attributed to a range of microstructural as well as mechanical factors. Among the microstructural factors are, subgrain growth and coarsening, precipitation of new phases, precipitate coarsening and void growth and coalescence.

2 Dislocation Creep Microstructure Evolution in 9-12% Cr Steels

The high temperature, high stress operating conditions under which 9-12% Cr steels are placed in coal fired power plant applications, have a significant effect on these materials' microstructure. These effects on microstructure in turn give rise to the long term loss of creep strength. The microstructure of 9-12% Cr steels is tempered martensite which is formed after normalising and tempering heat treatments [10].

In the case of Dislocation Creep, the microstructural changes of interest are those which give rise to greater mobile dislocation motion and therefore greater creep rate. Several microstructural changes have been identified over the years as being detrimental to the Dislocation Creep strength of 9-12% Cr steels [11]. These include:

I. The strain dependent coarsening of subgrains;
II. The coarsening/Ostwald Ripening of creep-strengthening precipitates;
III. The reduction in network dislocation density;
IV. The depletion of solid solution elements such as Mo/W and subsequent formation of Laves phase;
V. The degradation of fine creep strengthening MX precipitates and subsequent formation of the Z-phase.

2.1 Subgrain Evolution

The microstructural sources of creep include the migration of dislocations and subgrain boundaries. After tempering heat treatments the subgrain width is in the range of 0.3-0.7 μm [4]. Subgrain boundaries consist of network dislocations within prior austenite grains. Subgrain boundaries are often confused with martensitic lath boundaries; however, according to *Sonderegger* [12] there is a marked difference in misorientation between the two. Subgrain boundaries display random misorientation while martensitic lath boundaries show preferential axes-angle combinations [12]. The strengthening effect of subgrain boundaries is due to the fact that they are obstacles to mobile dislocations.

Subgrain boundaries are often thought of as 'hard' regions when compared with the 'soft' subgrain interior [10]. Thus, a small subgrain size equates to a high ratio of 'hard' to soft regions. However, the initial subgrain structure alone does not necessarily determine the creep properties of a Cr steel. A prime example is the 12CrMoV steel which has a finer subgrain size than does the P92 steel and yet has poorer long term creep strength[13]. This seemingly inconsistent result stems from the fact that subgrains coarsen and dislocation densities decrease in different Cr steels during service at different rates [13]. The creep strength of a steel therefore lies in its ability to maintain its initial microstructure and minimise the migration of dislocations and subgrains. This is influenced by a variety of factors the most important being precipitate and solid solution strengthening.

After creep exposure, subgrains in 9-12% Cr steels tend to have a polygonal shape [14]. While some subgrain growth has been observed during thermal ageing, it is far more significant under creep loading indicating that subgrain growth is both strain and temperature dependent [14]–[16].

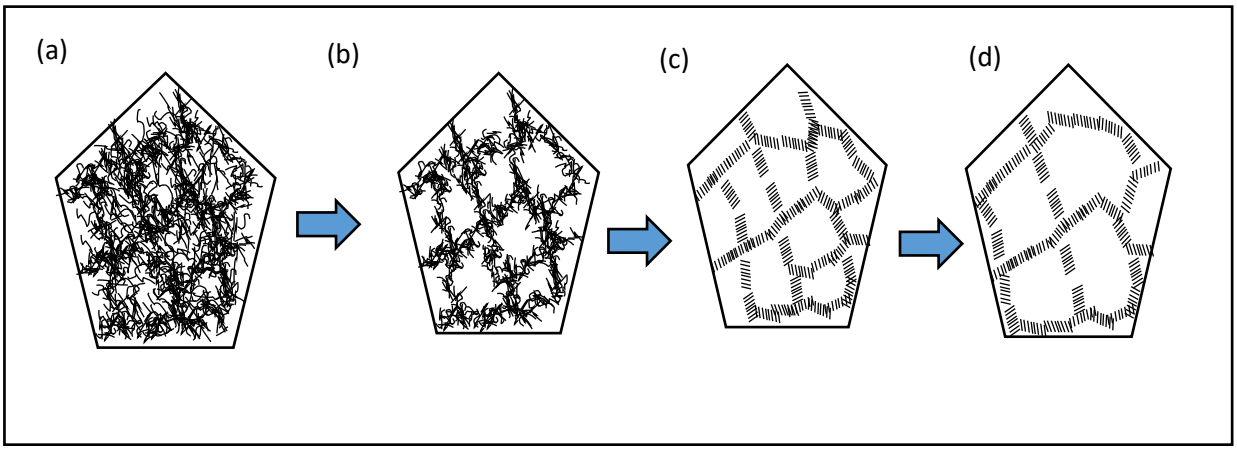

Figure 2-1 : Schematic of subgrain coarsening behaviour during dislocation creep

Figure 2-1 illustrates schematically the subgrain coarsening processes in Cr steels during creep. The initial dislocation tangles formed during tempering heat treatment (Figure (a)) begin to form into dislocation networks under applied stress (Figure (b)). Dislocations within subgrains annihilate due to high temperatures and stresses. After prolonged exposure to creep conditions network dislocations form into a more regular arrangement (Figure(c)) and begin to coarsen (Figure (d)).

2.2 Precipitate Evolution

During the steel tempering process, carbide and nitride particles precipitate on prior austenite grain boundaries (PAGB), ferrite subgrain boundaries and on dislocations within subgrains [10].Three main types of precipitate are known to have an effect on the creep strength of 9-12% Cr creep resistant steels [17]. These include metal carbide ($M_{23}C_6$) precipitates, metal carbonitride (MX) precipitates and the intermetallic Laves phase $(Fe,Cr)_2(Mo.W)$.

2.2.1 *$M_{23}C_6$ Precipitates*

$M_{23}C_6$ is a conventional notation used to denote a family of metal carbides, the most common of which is $Cr_{23}C_6$ although Ni, Mo, and Fe, are often found to substitute for Cr [17]. $M_{23}C_6$ is the most prevalent precipitate present in creep resistant steels and as such has a significant impact on the creep properties of the material. $M_{23}C_6$ carbides have been found to have a mean diameter of between 100-300nm [18]–[20] . They contribute to the overall creep strength by stabilising the initial microstructure through the pinning of grain and subgrain boundaries as well as by acting as obstacles to dislocation movement within the grain [5] [21]. $M_{23}C_6$ precipitates have been observed to coarsen during creep exposure especially near prior austenite grain boundaries. This leads to larger precipitate particles and hence greater inter-particle spacing resulting in a loss of creep strength. However, this process in $M_{23}C_6$ precipitates is significantly suppressed by the addition of a small amount of Boron [17]. The coarsening process is thermodynamically-driven as larger particles are more energetically favourable than smaller ones due to their smaller interface/volume ratio. This process is traditionally described using the Ostwald ripening law:

$$d^3 - d_i^3 = K_p t \quad (2.1)$$

Where d is the particle diameter at time t, d_i is the initial particle diameter and K_p thermodynamically based constant (see section 5.3). According to *Xu et al* [22] $M_{23}C_6$ carbides precipitate mostly on high angle boundaries with misorientation angle of 40°-60° due to high grain boundary energy. *Xu et al* [22] also noted that the average size of $M_{23}C_6$ increases significantly within the first 12000h of thermal ageing and slows down between 12000h and 25000h of exposure. This was attributed to a large increase in V concentration substituting for Fe, W and Mo in $M_{23}C_6$ between 12000h and 25000h of ageing resulting in a decrease in coarsening rate [22]

2.2.2 *MX Precipitate Evolution*

The notation MX represents a family of carbonitride precipitates present in 9-12% Cr ferritic steels which comprise mainly of strong carbide/nitride formers (Ti, Nb, V, Zr, Ta) the most common of which are the VN and NbC precipitates [17] [23]. The NbC precipitates are often referred to as primary MX precipitates as they remain undissolved throughout the heat treatment while the VN precipitates are often referred to as secondary MX as they nucleate only during tempering [23]. Both types of MX precipitates have the same NaCl type cubic crystal structure but behave differently [23].

Primary MX (NbC) precipitates at high temperatures on austenite grain boundaries and prevents grain growth during normalising heat treatments [23]. Secondary MX (VN) precipitates usually nucleate on imperfections such as dislocations within the matrix as well as on ferrite subgrain boundaries and prior austenite grain boundaries (PAGB)[10] [23]. They contribute to the overall creep strength of the steel by pinning free dislocations [17]. MX precipitates have been found to be more stable against coarsening than other precipitates present in creep resistant steels during long-term creep exposure [10].

2.2.3 *M_2X*

The M_2X family made up mainly of Cr_2N precipitates are thermodynamically stable and are often found in 9-12% Cr steels [23]. They have a hexagonal crystal structure and normally precipitate on grain boundaries and on dislocations [23]. Unlike the MX precipitates, M_2X has been found to coarsen and become large resulting in a loss of creep strength [23].

2.2.4 *Z-phase and Modified Z-phase*

The Z-phase is the name assigned to a thermodynamically stable nitride often found in the 9-12% Cr microstructure. Its role with regard to Cr steel creep strength has been the subject of debate amongst researchers for decades ranging from beneficial to extremely deleterious [23]. The original Z-phase with chemical formula CrNbN, was first observed in the 1950's by Binder et al. [24]. It has since been associated with having minor but nonetheless beneficial effects on the creep strength as it precipitates quickly and consists of small, fine rod-like particles [23].

Conversely, the modified Z-phase with chemical formula Cr(V,Nb)N which was first observed in 1985 by *Andren et al* [25] , has largely been accepted as being detrimental to the long term creep strength of 9-12% Cr steels. Unlike the original Z-phase, the modified Z-phase only precipitates after extended periods of creep exposure, often over 10 000h. It precipitates as coarse particles which has been observed to occur in parallel with the dissolution of fine MX particles. This has led researchers [26] [27] to conclude that the modified Z-phase forms by dissolving the MX particles as the two comprise of the same elements [23], [28], [29]. Thus, the detrimental effects of the modified Z-phase are twofold. First, in its depletion of the highly beneficial MX precipitates and second, in its ineffectiveness in hindering dislocation and subgrain motion due to its coarse, irregular structure.

Some researchers have suggested that the formation of the modified Z-phase is the major contributing factor to the loss of creep strength in 9-12% Cr steels and gives the creep/time graph its characteristic sigmoidal shape [30]. In a recent study by *Danielsen et al.* [31], the modified Z-phase precipitation rate was studied for both 9% Cr and 12% Cr steels with almost identical chemical composition apart from the Cr content. They found that the modified Z-phase precipitated about 20 times faster in the 12% Cr steel compared to the 9% Cr steel [31]. This finding reinforced the already widely accepted hypothesis that the modified Z-phase is significantly more detrimental in 10.5-12% Cr steels than in 9% Cr steels and can even be neglected in steels with a Cr content below 9% [32]. The Cr content has therefore clearly been highlighted as the major driving force for the formation of the modified Z-phase.

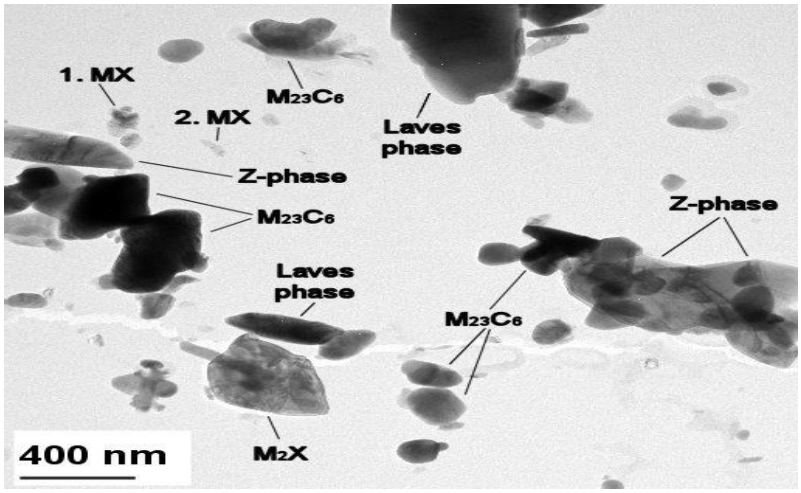

Figure 2-2: Image of the most common precipitates present in 9-12% Martensitic/Ferritic steels [23]

2.3 Dislocation Motion and Creep

Dislocation mobility and its dependence on temperature and stress are of key importance in understanding the elementary mechanics of material plasticity [33]. There are two major components which influence the flow stress of a metal. The first is the long-range interaction of mobile dislocations with the crystal microstructure and the second is the stress required to "push" the mobile dislocations over local energy barriers which hinder their movement [33]. The latter is of greater significance when considering precipitate hardened steels under creep deformation.

Short-range dislocation interaction with energy barriers takes place over such a small volume that it is strongly influenced by thermal vibrations within the lattice. Thermal activation helps dislocations to overcome these energy barriers and continue motion past the obstacle. In many cases, the energy barriers that obstruct dislocation motion are of the order of one electron-volt and involve some hundreds of atoms only [33]. Therefore added thermal energy favours overcoming these energy barriers. The Orowan equation [34] is commonly used to describe the relationship between deformation rate and dislocation mobility:

$$\dot{\varepsilon} = \rho_m v b \tag{2.2}$$

Where, $\dot{\varepsilon}$ is the deformation rate, ρ_m is the mobile dislocation density, v is the average dislocation velocity and b is the Burger's vector. The average velocity v is determined almost entirely based on the rate-controlling step. That is the step that takes the greatest amount of time to overcome.

2.3.1 *Back stress*

During the dislocation creep deformation process the externally applied stress on the material is counteracted by a resistive stress which is often referred to as the back stress or inner stress. Consequently, not all of the external stress goes into deforming the material as some of it is required to overcome this inner stress. The existence of the back stress is usually attributed to microstructural features of the material which hinder dislocation motion and hence creep deformation. In creep resistant martensitic steels these features mostly consist of immobile dislocations, subgrain boundaries and precipitates.

The back stress is traditionally accounted for by subtracting it from the applied external stress to give an effective stress value.

$$\sigma_{eff} = \sigma_{ex} - \sigma_i \tag{2.3}$$

Where, σ_{ex} is the externally applied stress and σ_i is the inner stress. The effective stress is then further used to calculate strain/creep rates using power-law relations. The internal stress can be expressed as a superposition of individual contributions from dislocations and precipitates as shown below [4].

$$\sigma_i = M\tau_i = M(\tau_{disl} + \tau_{prec} + \tau_{sgb}) \tag{2.4}$$

Where, M is the Taylor factor (usually between 2 and 3) and τ is the shear stress. While a Taylor factor of 3 is often used for modelling purposes, it should be noted that this is only strictly accurate for a specimen with uniform crystallographic texture under uniaxial loading. Furthermore, the "true" Taylor factor can be calculated based on crystallographic texture. The subscripts in the parenthesis denote

contributions from dislocations, precipitates and subgrain boundaries, respectively. The general Norton creep law is then expressed as [4]:

$$\dot{\varepsilon} = A(\sigma_{ex} - \sigma_i)^n = A\sigma_{eff}^n \tag{2.5}$$

Where A and n are constants. The largest contribution to the back stress is attributed to the shear stress due to precipitation hardening (τ_{prec}) and is quantified by the critical Orowan stress (σ_{Or}).

2.3.2 *Precipitation Strengthening*

The effect of precipitate hardening in steels can be explained in two general ways [35].

1. Increase of creep strength by direct interaction of particles with mobile dislocations acting themselves as obstacle for dislocation motion.
2. Increase of creep strength indirectly by pinning of grain and subgrain boundaries.

In the first case where precipitates interact directly with mobile dislocations, several mechanisms have been suggested to occur. These include shearing of the precipitate particles; local or general climb; precipitate dragging and the Orowan mechanism. Due to the nature of the second phase particles present in 9-12% Cr steels, the shearing of particles by dislocations is generally ignored. Also, precipitate dragging does not play a significant role in creep deformation at elevated temperatures [36]. Therefore, the only major direct precipitate-dislocation interactions are local and general climb as well as the Orowan mechanism. Since the Orowan mechanism is only slightly influenced by temperature, climb usually dominates creep at higher temperatures within the diffusional creep regime [4]. Hence the main dislocation-precipitate interaction at higher stresses and lower temperatures (dislocation creep regime) is attributed to the Orowan mechanism. The threshold stress required for plastic flow via the Orowan mechanism is given by:

$$\sigma_{Or} = C\frac{Gb}{\lambda} \tag{2.6}$$

Where, C is a constant, G is the shear modulus, b is the Burgers vector and λ is the average spacing of particles in the glide plane. The Orowan mechanism is believed to occur in three stages [4]. First, the dislocation encounters the precipitate particles and begins to bow out due to the shear stress acting in the glide plane. If the shear stress is sufficient, the dislocation bows out completely around the precipitate particles and annihilates itself, forming loops around the particles (see Figure 2-3 b). The dislocation is then able to continue to glide past until it encounters another obstacle.

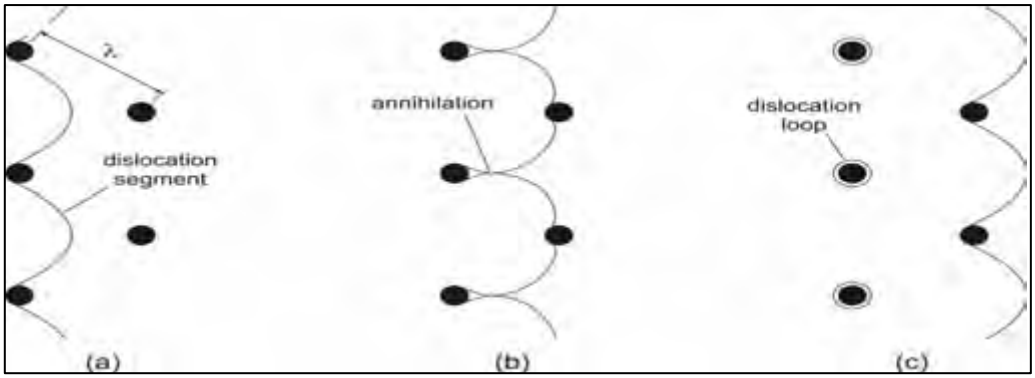

Figure 2-3 Bypassing of non-shearable particles by the Orowan mechanism [37]

2.3.3 *Particle Spacing and Distribution*

The presence of precipitate particles plays a vital role in increasing the creep strength of a large variety of steels particularly by introducing the back stress or threshold stress. Within the dislocation controlled creep regime the Orowan mechanism is the main dislocation-particle interaction mechanism. The Orowan stress τ_{Or} is mainly influenced by the mean particle spacing λ. In a recent treatment by Sonderegger *et a l*[38], a model was suggested to calculate the particle spacing λ based on random distribution of particles with arbitrary size distributions. This was done by considering the surface to surface distance between a particle and its nearest neighbour λ_{ss}. The number of particles per unit area was then calculated by considering different size classes based on particle radii as well as their number densities within a given volume. This was then used to setup a probability function to depict the probability that a nearest neighbour distance is smaller than λ_{ss}. Finally the Kocks criterion was used by setting the probability $W = 2/3$. The resulting formulation for particle spacing was given as:

$$\lambda_{ss} = \sqrt{\left(\frac{\ln(3)}{2\pi \sum_i n_{V,i} r_i} + (2r_A)^2\right)} - 2r_A \tag{2.7}$$

Where r_A is the mean projected radius, $n_{V,i}$ is the particle number density per volume. The subscript i denotes the specific particle size class. It was found that the particle spacing model showed good agreement with numerical simulations [39].

It was further suggested by [39] that the particle spacing model could be implemented into shear stress formulas to quantify the strengthening effects of numerous particle strengthening mechanisms including the Orowan mechanism. The resulting strength contribution would then be of the form:

$$\tau = C \frac{Gb}{\lambda} \ln\left(\frac{r_a}{r_i}\right) f(\theta_{crit}) \tag{2.8}$$

Where, τ is the strength contribution, *C* is a constant, *G* is the shear modulus, *b* is the burgers vector, r_i and r_a are the inner and outer cut-off radii of the dislocations respectively and θ_{crit} is the critical bow-out angle of the dislocations.

3 Creep Modelling

3.1 Glide controlled flow rule (exponential law creep)

A common approach to obtaining a creep flow rule is based on the assumption that creep is controlled by the glide of dislocations or more accurately the obstacles to dislocation glide. This approach was first suggested by *Kocks et al.* [40] in 1975. According to *Kocks et al.* obstacles to dislocation motion can be viewed as energy barriers. The velocity of a dislocation can therefore be calculated based on the time taken for a dislocation to overcome an energy barrier as well as the time it takes the dislocation to move between obstacles:

$$v_g = \frac{\Delta L}{t_0 + t_g} \tag{3.1}$$

Where, v_g is the average dislocation velocity, ΔL is the distance between two obstacles, t_0 is the time taken to overcome the obstacle and t_g is the time taken for the dislocation to glide between obstacles (see Figure 3-1). Generally the dislocation glide time t_g is negligible as it is far less than the time required to overcome the obstacle t_0 leading to:

$$t_g \approx 0 \;\&\quad v_g = \frac{\Delta L}{t_0} \tag{3.2}$$

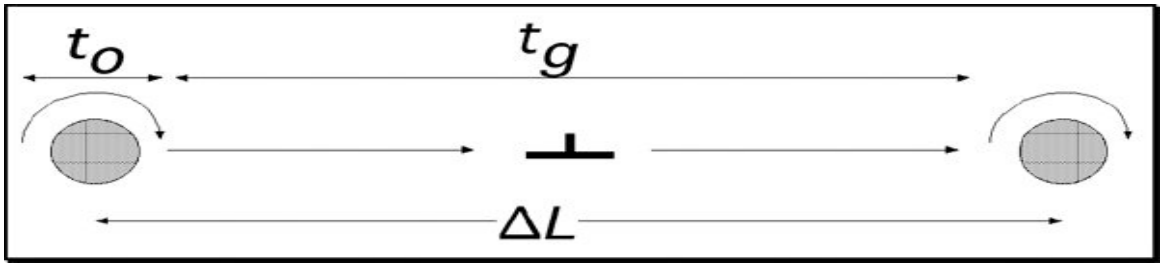

Figure 3-1: Dislocation glide and climb over obstacles [41]

Since energy barriers can be overcome by both stress and temperature, the activation energy must have some temperature dependence. Since thermal activity favours dislocation mobility, the increase in temperature should lower the height of the energy barrier.

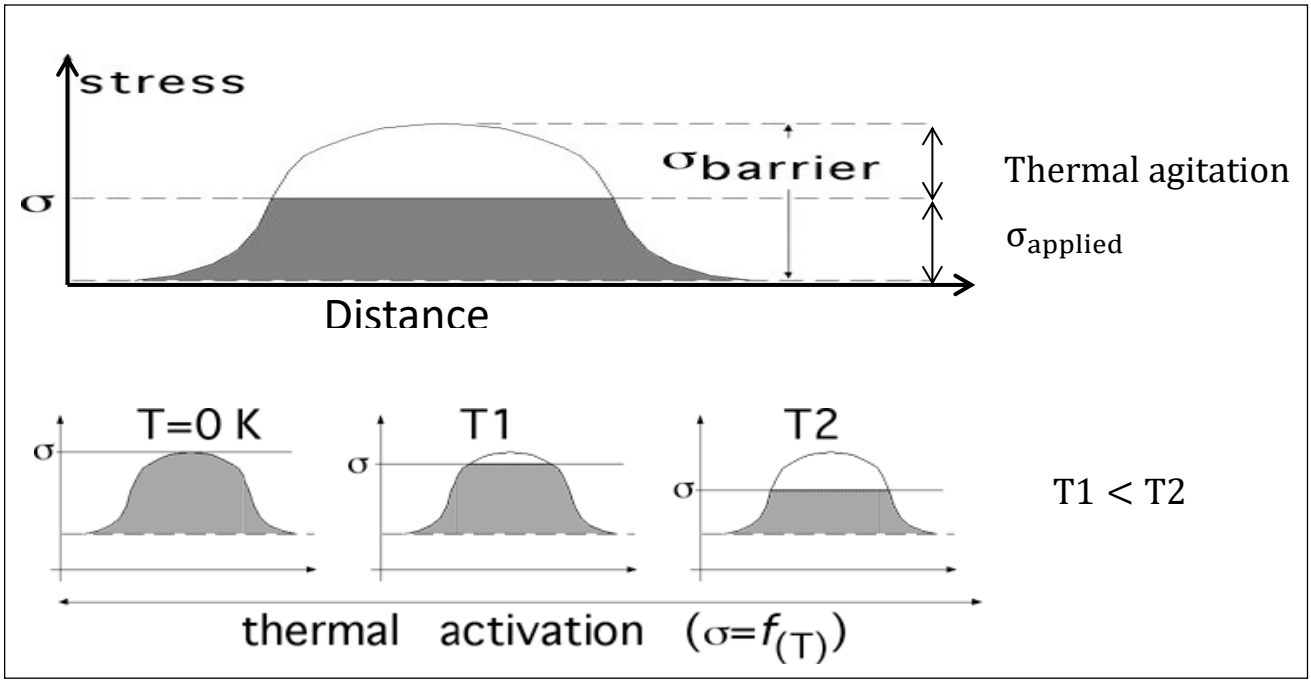

Figure 3-2: Effect of temperature on the height of an energy barrier [41]

Figure 3-2 illustrates the effect of temperature on the height of an energy barrier representing an obstacle to dislocation glide. It shows that as the temperature increases, the amount of thermal agitation also increases resulting in lower applied stress required to overcome the energy barrier. *Kocks et al.*[40] put forward an Arrhenius type equation to describe the dislocation glide velocity v_g in terms of a stress dependent Gibbs free energy of activation:

$$v_g = \beta \exp\left(-\frac{\Delta G}{kT}\right) \tag{3.3}$$

Where, β is a pre-exponent constant and $\Delta G(\sigma)$ is the Gibbs free energy of activation which can be expressed as:

$$\Delta G = \Delta F\left(1 - \frac{\sigma}{\sigma_{bar}}\right) \tag{3.4}$$

Where, ΔF is the energy required to overcome the barrier without applied stress and σ_{bar} is the stress required to overcome the energy barrier without any thermal agitation. It can be seen from equation 3.12 that if the applied stress σ is set equal to the barrier stress σ_{bar} then the Gibbs free energy of activation $\Delta G(\sigma)$ falls to zero and the obstacle can be overcome by the dislocation. However, if $\sigma < \sigma_{bar}$ then the energy barrier/obstacle cannot be overcome by stress alone ($\Delta G(\sigma) \neq 0$) and some extra thermal agitation is needed. By combining equation 3.11 and equation 3.12 an expression for dislocation glide velocity v_g can be obtained:

$$v_g = \beta \exp\left(-\frac{\Delta F}{kT}\left(1 - \frac{\sigma}{\sigma_{bar}}\right)\right) \tag{3.5}$$

A flow rule can now be obtained for glide controlled creep using the Orowan equation (equation 3.2) as well as the expression for mobile dislocation density (equation 4.4) giving:

$$\dot{\varepsilon}_{ss} = \frac{\alpha\beta\sigma^2}{b}\exp\left(-\frac{\Delta F}{kT}\left(1-\frac{\sigma}{\sigma_{bar}}\right)\right) \tag{3.6}$$

At absolute zero, no thermal agitation contributes to overcoming the energy barrier hence the applied stress σ, must be equal to the barrier stress σ_{bar} leading to the following simplifications:

$$\dot{\varepsilon}_0 = \frac{\alpha\beta\sigma^2}{b}\exp(-0) = \frac{\alpha\beta\sigma^2}{b} \tag{3.7}$$

$$\dot{\varepsilon}_{ss} = \dot{\varepsilon}_0\exp\left(-\frac{\Delta F}{kT}\left(1-\frac{\sigma}{\sigma_{bar}}\right)\right) \tag{3.8}$$

3.2 Climb controlled flow rule (power-law creep)

The most commonly used flow rules for dislocation creep today are mostly based on the climb controlled flow rule developed by *Weertman* [42] in 1957. The flow rule is centred on the assumption that dislocation climb over obstacles is the rate controlling process during steady state dislocation creep and that thermally activated vacancies dictate the rate at which dislocations climb. Vacancies can diffuse into an edge dislocation thereby replacing an atom and causing the dislocation to climb to a different glide plane and continue to glide until its motion is hindered once again. This is known as positive climb (see Figure 3-3 (a)). Alternatively the vacancy at the end of an edge dislocation can be replaced by a lattice atom causing the dislocation to once again climb to a different glide plane but in the opposite direction. This is known as negative climb (see Figure 3-3 (b)).

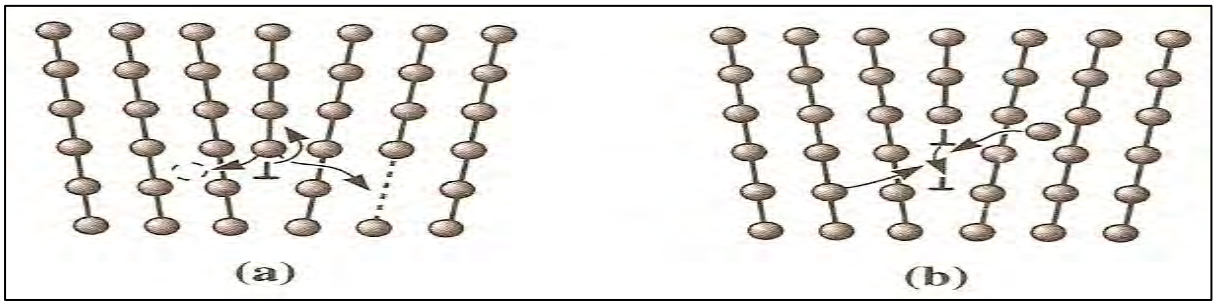

Figure 3-3: (a) Vacancy controlled (a) positive and (b) negative climb of an edge dislocation [69]

The rate at which edge dislocations climb can therefore be approximated by the rate at which vacancies diffuse within a crystal structure. This approach assumes that dislocation glide causes almost all the strain but the average velocity is determined by dislocation climb. A creep rate relationship can then be formulated based on vacancy diffusion laws, dislocation climb theory, and dislocation density approximations using Orowan's equation (equation 3.2). In this way *Weertman,* arrived at the following expression for the climb controlled dislocation creep rate [42]:

$$\frac{\partial \varepsilon}{\partial t} = \frac{\alpha \sigma^3 b D_0}{kTG^2} \exp\left(-\frac{Q_c}{RT}\right) \tag{3.9}$$

Where G is the shear modulus, α is a dimensionless constant which reflects the strength of dislocation-dislocation interaction, D_0 is the vacancy diffusion coefficient, Q_c is the activation energy associated with dislocation climb. A complete derivation of equation 4.5 can be found in section 5.1. Equation 4.5 can be simplified by combining all the constants, resulting in the general Three-power-law expression:

$$\dot{\varepsilon} = \frac{\partial \varepsilon}{\partial t} = \varepsilon_0' \, \sigma^3 \exp\left(-\frac{Q_c}{RT}\right) \tag{3.10}$$

The three-power-law expression has been found by numerous researchers to only be accurate for specific steels under specific conditions of creep. In general, the value of the stress exponent has been found to vary between 3 and 7. This has led researchers to be cautious of the power law creep formulation and to investigate alternate approaches to modelling dislocation creep [43]. Furthermore, power-law creep does not explicitly consider the effects of long term changes in microstructure such as those discussed in chapter 2, which undoubtedly influence the dislocation creep rate.

3.3 Continuum Damage Mechanics (CDM)

3.3.1 *Dyson-McClean CDM model*

In recent years there has been a trend amongst investigators towards describing dislocation creep using continuum damage mechanics. This has been especially the case for materials with complex microstructures such as 9-12% Cr creep resistant steels. The desire to model creep phenomena based on microstructure stems from the tendency of short term data and empirical models to over-estimate the long term performance of many materials [44]. Most of the current CDM creep models are based on the works of *Dyson et al*.[45]. This approach uses a set of coupled differential equations which represent the accumulated creep strain as well as various forms of microstructural evolution. It is impossible to take into account every aspect of the microstructure therefore only those aspects which contribute most to creep are assessed. The approach of *Dyson et al*. is particularly useful for particle strengthened alloys where stress is distributed between the matrix and the precipitates. The set of coupled equations can best be represented in functional form as [46]:

$$\dot{\varepsilon} = \dot{\varepsilon}(\sigma, T, H, D_i) \tag{3.11-1}$$

$$\dot{H} = \dot{H}(\sigma, T, H, D_i) \tag{3.11-2}$$

$$\dot{D}_i = \dot{D}_i(\sigma, T, H, D_i) \tag{3.11-3}$$

Equation 3.11-1 describes the strain accumulation as a function of stress (σ), temperature (T), stress redistribution between the particles and matrix (H), and the damage due to microstructural changes in the material (D_i). Two microstructural damage variables were identified by *Dyson et al*. as having a significant impact on creep in particle strengthened steels. These are the damage due to particle coarsening (D_p) and the damage due to the decrease in mobile dislocation density (D_d) resulting in strain softening. The set of coupled differential equations used by *Dyson et al*. are:

$$Creep\ rate\ equation: \quad \dot{\varepsilon} = \dot{\varepsilon}_0(1 + D_d)\exp\left(-\frac{Q_c}{RT}\right)\mathrm{Sinh}\left[\frac{\sigma(1-H)}{\sigma_0(1-D_p)}\right] \tag{3.12-1}$$

$$Backstress\ evolution: \quad \dot{H} = \frac{h'}{\sigma}\left(1 - \frac{H}{H^*}\right)\dot{\varepsilon} \tag{3.12-2}$$

$$Mobile\ Dislocation\ density: \quad \dot{D}_d = C\dot{\varepsilon} \tag{3.12-3}$$

$$Precipitate\ Coarsening \quad \dot{D}_p = \frac{K_P{}'}{3}\left(1 - D_p\right)^4 \tag{3.12-4}$$

$$Stress\ rate: \quad \dot{\sigma} = \sigma\dot{\varepsilon} \tag{3.12-5}$$

Where $\dot{\varepsilon}_0$ is a characteristic strain rate which is dependent on precipitate volume fraction and mobile dislocation density, Q_v is the activation energy associated with vacancies and formation of jogs, σ is the applied stress, σ_0 is a normalising stress associated with dislocation-particle interactions, h' is the effective modulus, H^* is the limiting value of H. The coarsening damage factor D_p is defined in terms of the initial inter-particle spacing λ_i and the particle spacing at any given time λ as:

$$D_p = \left(1 - \frac{\lambda_i}{\lambda}\right) \tag{3.13}$$

The dislocation damage factor D_d is defined in terms of the initial dislocation density ρ_i and the dislocation density at any given time ρ as:

$$D_d = \left(1 - \frac{\rho_i}{\rho}\right) \tag{3.14}$$

The model also requires 10 material constants namely; $\dot{\varepsilon}_0,\ Q_c,\ \sigma_0,\ \Delta H_s,\ T_s, h', H^*, Q_p, K_P'$ and C. While these parameters can be obtained (estimated) from theoretical derivations, they are often more accurately derived empirically from experimental data.

In a publication*, Hore et al*. [46] describe a method for obtaining initial values of $\sigma_0,\ \dot{\varepsilon}_0, Q_d,\ T_s, H^*, h'$ from experimental creep data of 2.25CrMo steel as a large amount of creep data was available. These values were used as initial guesses in producing creep data for 9CrMoVNb steel where only a limited amount of creep data was available. *Hore et al.* thereafter used an optimisation scheme to obtain an optimum data set for the material constants [46]. In so doing*, Hore et al.* showed that the chief issue of creep modelling being a scarcity of long-term creep data could be overcome by the use of an optimisation routine. The optimised material properties used by *Hore et al.* are shown in Table 3-1.

Table 3-1: Material parameters for 2.25Cr1Mo and 9CrMoVNb steels

Alloy name	**Parameter**									
	$\dot{\varepsilon}_0\ (s^{-1})$	$Q_d(kJmol^{-1})$	$\sigma_{0m}(MPa)$	$\Delta H_s\ (kJmol^{-1})$	$T_s(K)$	$h'(MPa)$	H^*	$Q_p(KJmol^{-1})$	$k_{p0}(s^{-1})$	C
2.25Cr1Mo	2.71E08	298	28	137	936	1.06E03	0.3	200	2.5E05	10
9CrMoVNb	3.0E08	300	30	140	950	1.03E04	0.3	210	2.2E05	27

Hore et al. reported that the model predictions for the 2.25Cr1Mo and 9CrMoVNb steels correlated well with experimental results at various temperatures and stresses and produced a better relationship than power law models [46].

3.3.2 *Oruganti CDM Model*

In a recent publication by *Oruganti et al* [47] a CDM model for 9-10% Cr Ferritic Steels was put forward based on the original formulations of *Dyson et al*. The model produced *by Oruganti et al*. deviates from the original works of *Dyson et al.* in its' selection of 'key microstructural features' which contribute significantly to creep. These features include MX precipitate spacing, MX coarsening and subgrain evolution.

The equation set for the *Oruganti* CDM models was formulated as:

$$Creep\ rate\ equation: \quad \dot{\varepsilon} = \dot{\varepsilon}_0' \exp\left(-\frac{Q_c}{RT}\right) \sinh\left[\frac{\sigma\left(1 - H^*(1 - D_s)\right)}{\sigma_0(1 - D_P)}\right] \tag{3.26-1}$$

$$Primary\ creep: \quad \dot{\sigma}_0 = K_1\left(1 - \frac{\sigma_0}{K_2}\right)\dot{\varepsilon} \tag{3.26-2}$$

$$Subgrain\ evolution: \quad \dot{D}_s = \frac{\dot{\varepsilon}}{S_i}\left(K_{S1} + K_{S2}\exp\left(-\frac{Q_s}{RT}\right)\right)(1 - D_S)^2 \tag{3.26-3}$$

$$MX\ evolution: \quad \dot{D}_P = \frac{K_P}{d_i^3}\exp\left(-\frac{Q_P}{RT}\right)(1 - D_P)^4 \tag{3.26-4}$$

Where $\dot{\varepsilon}_0$ is a characteristic strain rate, Q_c is the activation energy associated with vacancies and formation of jogs, σ is the applied stress, σ_0 is a normalising stress associated with dislocation-particle interactions, H^* is a limiting parameter for stress redistribution between 'soft' and 'hard' regions within the grain, K_1 and K_2 are primary creep parameters, K_{S1} and K_{S2} are coefficients corresponding to the temperature independent and temperature dependent parts of subgrain growth respectively, K_P is a coarsening rate constant, P_i is the initial particle size and Q_p is a particle coarsening activation energy.

The precipitate coarsening damage parameter is defined as:

$$D_p = \left(1 - \left(\frac{d_i}{d(t)}\right)\right) \tag{3.19}$$

Where d_i and $d(t)$ are the initial precipitate diameter and diameter at any time t repectively.

The subgrain coarsening damage parameter is defined as:

$$D_s(t) = 1 - \left(\frac{S_i}{S(t)}\right) \tag{3.19}$$

Where S_i and $S(t)$ are the initial subgrain width and width at any time t repectively.

Oruganti et al. used a formulation originally devised by *Kelly* [48] to ascertain whether or not the precipitate spacing λ, is rate controlling:

$$\lambda = \frac{1}{\sqrt{n_A}[1 + L\sqrt{n_A}]} - \frac{\pi t}{2} \tag{3.17}$$

Where n_A is the area density of particles and L is the length of the line that the particle makes upon interception with the slip plane.

The *Oruganti* model also accounts for back stress generated by subgrain boundaries bowing out between $M_{23}C_6$ particles based on the mechanics suggested by Argon and Takeuchi [49] giving the following expression:

$$\sigma_B^S = 0.26(1-v)\frac{\delta^{\frac{4}{3}}\ \theta^{\frac{1}{3}}}{b^{\frac{1}{3}}\ S}\sigma \tag{3.20}$$

Where δ is the $M_{23}C_6$ inter-particle spacing on the subgrain boundaries, θ is the average misorientation between adjacent subgrains, b is the Burger's vector, S is the average subgrain width and v is the Poisson's ratio. *Oruganti et al*. also take into account the back stress generated by block boundaries as being inversely proportional to the square of the block width B:

$$\sigma_B^B \propto \frac{\sigma}{\sqrt{B}} \tag{3.21}$$

Hence the total back stress can be written as:

$$\sigma_B = \left(\frac{K'}{S} + \frac{K''}{\sqrt{B}}\right) \tag{3.22}$$

$$\sigma_B = H^*\sigma \tag{3.23}$$

Where

$$H^* = \left(\frac{K'}{S} + \frac{K''}{\sqrt{B}}\right) \tag{3.24}$$

Due to a lack of data, values for K'' are estimated based on values of K'.

The back stress due to subgrain and block boundaries is assumed to be instantaneous and is subtracted from the applied stress where H^* determines the maximum possible back stress. The damage factor $(1-D_s)$ is associated with the back stress and takes into account the migration and annihilation of subgrains during creep. The reference stress σ_0 arises from the primary creep stage which is dependent on the evolution of the initial dislocation structure. This model has 12 parameters, 9 of which are physically bounded, 2 of which describe the primary stage (K_1 and K_2) and hence do not affect the long-term creep predictions. The final input parameter is a scaling parameter $\dot{\varepsilon}_0'$. The 9 physically based parameters are, $Q_P, K_{S1}, K_{S2}, Q_S, P_i, S_i, H^*$ and Q_C. The same parameter set was used in the *Oruganti* model over a wide stress and temperature range.

In their publication *Oruganti et al.* applied the CDM model to two different ferritic steels after standard austenisation and tempering heat treatments. The model showed good agreement with experimental results and provided more accurate predictions when compared to extrapolated predictions from experiments running for less than 10000 hours. This was attributed to weakening due to coarsening of MX carbonitrides which the CDM model took into account but which the extrapolated experimental predictions did not.

3.3.3 *Christopher CDM creep model*

A CDM creep model based on the works of *Dyson et al*. was recently investigated by *Christopher et al.*[50]. In the investigation, damage caused by coarsening of dislocation networks and subgrains as well as coarsening of precipitates was considered. The model was formulated by using a set of coupled equations to describe the creep deformation process. The master equation was set up as:

$$Creep\ rate\ equation: \qquad \dot{\varepsilon} = \dot{\varepsilon}_0(1 + D_d)\,\mathrm{Sinh}\left[\frac{\sigma(1-H)}{\sigma_{0,i}(1-D_p)}\right] \tag{4.23-1}$$

$$Back-stress\ evolution: \qquad \dot{H} = \left(\frac{h}{\sigma}\right)\left(1 - \frac{H}{H^*}\right)\dot{\varepsilon} \tag{4.23-2}$$

$$Back-stress\ limiter: \qquad \dot{H}^* = \frac{H^*(1-H^*)}{2}(1 + D_d)^{-1}\dot{D}_d \tag{4.23-3}$$

$Mobile\ dislocation\ density\ damage\ evolution$:

$$\dot{D}_d = k_2\left(\frac{\rho_{SS}}{\rho_{N,i}}\right)^{0.5}(1 + D_d)^{0.5}\,(1 - (1 + D_d)^{-1}\left(\left(\frac{\rho_{N,i}}{\rho_{SS}}\right)^{0.5}\right)\dot{\varepsilon} \tag{4.23-4}$$

$$M_{23}C_6\ coarsening\ damage\ evolution: \qquad \dot{D}_P = \frac{K_P{}'}{3}(1 - D_P)^4 \tag{4.23-5}$$

$$Stress\ evolution: \qquad \dot{\sigma} = \sigma\dot{\varepsilon} \tag{4.23-6}$$

The dislocation damage parameter D_d due to network dislocation coarsening is expressed as:

$$D_d = \left(\frac{\rho_N}{\rho_{N,i}}\right) - 1\ for\ 0 \geq D_d \geq -1, \tag{4.25}$$

Where ρ_N and $\rho_{N,i}$ are the dislocation density at any given time and initial dislocation density respectively. The damage parameter due to particle coarsening D_P, is expressed as:

$$D_P = 1 - \left(\frac{P_i}{P(t)}\right)\ for\ 0 \leq D_P \leq 1, \tag{4.26}$$

Where P_i and $P(t)$ are the initial particle diameter and particle diameter at any time t respectively. H is the normalised back stress defined as:

$$H = \sigma_K/\sigma \tag{4.27}$$

Where σ_K is a measure of strain-induced stress distribution between hard regions (subgrain boundaries) and soft regions (matrix). $\sigma_{0,i}$ is a normalising stress due to dislocation-particle interaction. The constant h is the effective modulus and H^* is the maximum value of H.

The constant k_2 is a dislocation annihilation parameter derived using the Kocks-Mecking approach [51] and $K_P{}'$ is related to the rate constant for particle coarsening from the Ostwald ripening law. The initial parameters are derived from either experimental findings or physical relationships. The normalising stress $\sigma_{0,i}$ is obtained using the Orowan stress as follows:

$$\sigma_{0,i} = \frac{kT\sigma_{or}}{\alpha G b^3} \tag{4.29}$$

$$\sigma_{or} = \frac{\alpha M G b}{L} \tag{4.30}$$

$$\sigma_{0,i} = MkT/(Lb^2) \tag{4.31}$$

Where M is a Taylor factor and L is the mean inter-particle spacing. L is calculated for $M_{23}C_6$ particles as well as MX particles using the following expression:

$$\frac{1}{L_{eff}} = \frac{1}{L_{M_{23}C_6}} + \frac{1}{LX} \tag{4.32}$$

The damage parameter for network dislocation coarsening is obtained from the Kocks-Mecking [51] approach with respect to strain:

$$\frac{d\rho}{d\varepsilon} = k_1 \rho_N^{0.5} - k_2 \rho_N \tag{4.33}$$

Where k_1 and k_2 are dislocation storage and annihilation parameters. As the network dislocation density approaches steady state, $\frac{d\rho}{d\varepsilon} = 0$ a saturation dislocation expression can be derived as $\rho_{ss} = \left(\frac{k_1}{k_2}\right)$. Therefore equation 4.33 can be rewritten as:

$$\frac{d\rho}{d\varepsilon} = k_1 \rho_N^{0.5} \left(1 - \left(\frac{\rho_N}{\rho_{SS}}\right)\right)^{0.5} \tag{4.34}$$

By integrating equation 4.34 with respect to strain, the following expression can be obtained:

$$\rho_N = \left(\rho^{0.5} - \left(\rho_{ss}^{0.5} - \rho_{N,i}^{0.5}\right) \exp\left(-\left(\frac{k_2}{2}\right)\varepsilon\right)\right)^2 \tag{4.35}$$

Due to its complex nature, the value of $\dot{\varepsilon}_0$ is obtained from experimental results using the relation:

$$\dot{\varepsilon}_0 = \frac{\dot{\varepsilon}_{at\ t=0.1h}}{\sinh\left(\frac{\sigma}{\sigma_{0,i}}\right)} \tag{4.36}$$

Once initial values for the input parameters were selected, the values for $\sigma_{0,i}, K'_p, k_2, \dot{\varepsilon}_0$ and H^* were optimised based on experimental creep test results using a least square error function. This model therefore has 8 input parameters, 5 of which require optimisation. This model was found by *Christopher et al.* to produce good creep predictions for a variety of stresses for 9Cr1Mo steel.

3.3.4 *Yin et al CDM Model*

The CDM creep modelling approach of *Yin et al.* also builds on the original work of *Dyson et al.* with particular emphasis on precipitation kinetics [52]. Using a Monte Carlo simulation, *Yin et al.* modelled intra-granular as well as inter-granular precipitate evolution of MX and $M_{23}C_6$ precipitates and incorporated it into a CDM creep model [53]. The precipitation kinetics model was set up by

considering a simulation cell which included both matrix and grain boundaries. The number of grain boundaries was then calculated using a non-equilibrium segregation model. The pre-service and service heat treatments were then divided up into time increments Δt, and precipitate nucleation, growth and dissolution was modelled [53].

$$Creep\ rate\ equation: \dot{\varepsilon} = \frac{\dot{\varepsilon}_0}{(1-D_d)(1-D_C)} \mathrm{Sinh}\left[\frac{\sigma(1-H)}{\sigma_0(1-D_p)(1-D_N)}\right] \quad (4.46\text{-}1)$$

$$Mobile\ dislocation\ damage\ evolution: \quad \dot{D}_d = C(1-D_d)^2\dot{\varepsilon} \quad (4.46\text{-}2)$$

$$Cavity\ growth\ damage: \quad \dot{D}_N = A'\varepsilon^{B'}\dot{\varepsilon} \quad (4.46\text{-}3)$$

$$Back-stress\ evolution: \quad \dot{H} = \left(\frac{h}{\sigma}\right)\left(1-\frac{H}{H^*}\right)\dot{\varepsilon} \quad (4.46\text{-}4)$$

$$Solid\ solution\ damage\ evolution: \quad \dot{D}_c = K_c D_c^{\frac{1}{3}}(1-D_c) \quad (4.46\text{-}5)$$

Where C is a material constant, A' and B' are cavity growth constants and K_c is a Wert-Zener solid solution constant. The damage due to precipitate coarsening D_P was calculated by *Yin et al.* using precipitation kinetics which included, particle nucleation, growth and coarsening.

3.3.4.1 Nucleation

The nucleation of particles was modelled using classical nucleation theory:

$$I = Z\beta^*\left(\frac{N}{x_0}\right)\exp\left(\frac{\Delta G^*}{kT}\right)\exp\left(-\frac{\tau}{t}\right) \quad (4.37)$$

Where I is the nucleation rate, N is the number of a particular type of atomic site, x_0 the molar fraction of solute atoms in the nucleus phase, ΔG^* the energy required to form the critical nucleus, t is the time and τ is the incubation time for nucleation. The coefficients Z and B^* are define as:

$$Z = \frac{V_{\theta x}(\Delta G_V)^2}{8\pi\sqrt{kTK_j\gamma_{\alpha\theta}^3}} \quad (4.38)$$

$$B^* = \frac{16\pi\gamma_{\alpha\theta}^2 D x_\alpha L_j}{a^4(\Delta G_V)^2} \quad (4.39)$$

Where $V_{\theta x}$ is the volume occupied by one atom in the nucleus, ΔG_V is the free energy change per unit volume of the nucleus, $\gamma_{\alpha\theta}$ is the interfacial free energy, D is the diffusivity, x_α is the solute concentration in the matrix, *a* the lattice parameter, L_j and K_j are shape factors defined as:

$$V = \frac{4}{3}\pi r^3 K_j \quad (4.40)$$

$$S = 4\pi r^2 L_j \quad (4.41)$$

The value for τ is usually very small such that the term $\exp\left(\frac{-\tau}{t}\right)$ is taken as unity. The number of nuclei generated per unit time is described using:

$$\Delta N(t) = Z\beta^* \left(\frac{N}{x_0}\right) \exp\left(\frac{\Delta G^*}{kT}\right) \Delta t \tag{4.42}$$

Where $\Delta N(t)$ is the number of nuclei generated in the time interval Δt. The nucleation rate changes with time as the solute concentration decreases due to precipitate formation which is reflected in the value of ΔG_v.

3.3.4.2 Growth and Coarsening

Once the number of generated nuclei reaches its limiting value determined by equation 4.42 the growth and coarsening equations control the precipitate evolution. Given the initial solute concentration and volume fraction of precipitates, the solute concentration at time *t* can be calculated using:

$$\bar{C}_t = 1 - \frac{V_f \rho_\theta N_r}{\rho_\alpha C_g} \tag{4.43}$$

Where C_g is the initial concentration of solute, V_f is the volume fraction of precipitates at any time, ρ_α and ρ_θ are the molar density of the matrix and precipitate phase respectively and N_r is the number of rate controlling atoms in the precipitate molecule. The concentration gradient in the vicinity of the surface of a particle of radius of curvature r at any time t can be approximated using:

$$g = \frac{\bar{C}_t - \bar{C}_r}{d} \tag{4.44}$$

Where d is the average interparticle spacing and C_r is the solute concentration at the surface of the particle. If g>0 then the particle grows and if g<0 the particle dissolves. Both these rates are determined using Fick's first law of diffusion. The increase in volume of a particle ΔV can therefore be calculated using:

$$\Delta V = \frac{DSg\rho_\theta}{C_\theta \rho_\theta - C_r \rho_\alpha} \Delta t \tag{4.45}$$

At each time step, each particle is allowed to grow or dissolve depending on the concentration gradient and therefore the change in volume ΔV. Also, at each time step, the average concentration in the matrix is recalculated. This entire routine was used by *Yin et al.* instead of the traditionally used Ostwald ripening law.

4 Experimental Data

For the current study, experimental creep data was required in order to calibrate as well as validate the proposed CDM model. Creep data for 9-12% Cr steels, particularly long term creep data is limited in open literature. For this reason, only two steels were used. The first was for the experimental 10% Cr steel from the COST (European Cooperation in Science and Technology) programme designated CB8 (see Table 4-1). This data was generously shared by the Graz University of Technology. The data included long term (>10000h) continuous creep strain-time results at 650°C at three different stresses: 75MPa, 85MPa and 100 MPa. The reader is directed to Appendix A-1 Section 0 for the full creep-time data. Corresponding microstructural results of subgrain and precipitate size evolution were obtained from *Sonderegger* [12] (see Appendix A-1 section 0). As these results were the most comprehensive available, they were used for the calibration of the model in this study.

In order to determine the chemical composition of the CB8 samples, electron energy loss spectroscopy and energy-dispersive X-ray spectroscopy (EDX) was used. The microstructural data included subgrain size measurements obtained from interrupted creep tests at 75 MPa and 650°C at intervals for up to 16000h of creep loading. These measurements were made using EBSD (Electron Back Scatter Diffraction) in an SEM (Scanning Electron Microscope) with a special resolution of 200nm and orientation resolution of 1- 1.5° [15].

The second set of creep data was obtained from the works of *Ennis et al* [54] available in open literature for the 9% Cr steel, P92. This data consisted of continuous creep rupture test results at 104 MPa as well as at 92 MPa both at 650°C. The publication by *Ennis et al.* also included measurements of initial subgrain and precipitate size for the samples. Transmission Electron Microscopy (TEM) of thin foil and extraction double replicas was used to obtain information on precipitate morphology and analysis. Precipitate size distribution and subgrain sizes were quantified using a line-intercept technique on enlarged TEM images.

Table 4-1: Chemical composition in wt% of COST steel CB8 [12]

Element	**C**	**Mn**	**Cr**	**Ni**	**Mo**	**V**	**Nb**	**Co**	**B**	**N**	**Si**	**P**	**S**	**Al**	**Ti**
Wt%	0.17	0.2	10.86	0.15	1.42	0.21	0.061	2.94	0.01	0.024	0.27	0.009	0.006	0.026	0.001

Table 4-2: Chemical composition in wt% of steel P92 [54]

Element	**C**	**Mn**	**Cr**	**Ni**	**Mo**	**V**	**Nb**	**N**	**Si**	**P**	**S**	**Al**
Wt%	0.10	0.4	9.0	0.40	0.5	0.23	0.052	0.05	0.50	0.02	0.50	0.04

5 Current Model

The basic structure for the CDM model used in this thesis was selected based mainly on available experimental creep data as well as the availability of literature for material constants and properties for the steels being analysed, namely CB8 and P92.

5.1 CDM Strain Rate Equation

The creep strain flow rule used for the dislocation creep CDM method is derived from the well-known Orowan equation discussed in section 2.3 and repeated here for convenience:

$$\dot{\varepsilon} = \rho_m v b \tag{2.9}$$

Where, $\dot{\varepsilon}$ is the uniaxial strain rate, ρ_m is the mobile dislocation density, v is the average dislocation velocity and b is the Burger's vector. The average velocity v is determined almost entirely based on the rate-controlling step. That is the step that takes the greatest amount of time to overcome. With regards to dislocation creep this is the time required to overcome obstacles via dislocation climb as described by *Weertman* [42].

$$v_c = \frac{\Omega}{bkT} D_v \sigma \tag{5.1}$$

Where Ω is the atomic volume ($\Omega \approx b^3$), b is the Burger's vector, *T* is temperature, D_v is the vacancy diffusion coefficient and σ is the applied stress. Strictly speaking σ is the component of the applied stress normal to the glide plane. However, it is a reasonable assumption that this normal component is directly proportional to the applied stress making the expression qualitatively sound in this regard.

D_v is a measure of the rate at which atomic jumps are made into vacancy sites and is what fundamentally dictates dislocation glide along slip planes on an atomic scale. However, in order for an atomic jump to be made, an atom needs to overcome an energy barrier associated with breaking atomic bonds with its neighbouring atoms. The frequency of atomic jumps is described using an Arrhenius type formula:

$$R_j = R_0 \exp\left(-\frac{E_m}{RT}\right) \tag{5.2}$$

Where R_0 is the 'attempt frequency' which is typically of the order of the Debye frequency and E_m is the activation energy required for an atomic jump to occur (roughly equal to 1mV). In addition to the determination of the frequency of atomic jumps, the probability of an existing vacancy site needs to be considered. This probability is expressed as:

$$P = z^2 \exp\left(-\frac{Q_d}{RT}\right) \tag{5.3}$$

Where z is the atomic jump distance. The diffusion coefficient can hence be expressed as the product of the frequency of atomic jumps and the probability of an available vacancy site:

$$D_v = PR_j = z^2 R_0 \exp\left(-\frac{Q_d}{RT}\right) \exp\left(-\frac{E_m}{RT}\right)$$

$$D_v = D_0 \exp\left(-\frac{Q_c}{RT}\right) \tag{5.4}$$

Where

$$D_0 = z^2 R_0 \; and \; Q_c = Q_d + E_m$$

According to *Weertman* [42], the mobile dislocation density ρ_m within a crystal can be described as a function of stress using the following empirical relation:

$$\rho_m = \alpha \left(\frac{\sigma}{bG}\right)^2 \tag{5.5}$$

Where G is the shear modulus and α is a dimensionless constant which reflects the strength of dislocation-dislocation interaction.

By combining the expressions for ρ_m (equation 5.5), v_c (equation 5.1) using equation 2.2, an expression for steady-state dislocation creep can be obtained giving the well-known three power creep law as discussed in section 3.2:

$$\frac{\partial \varepsilon}{\partial t} = \frac{\alpha \sigma^3 b D_0}{kTG^2} \exp\left(-\frac{Q_c}{RT}\right) \tag{4.5}$$

The inconsistency in stress exponent (see section 3.2) has been suggested to be due to microstructural features which affect creep and are not explicitly considered in the power-law creep formulation [55]. In order to account for microstructural changes occurring during creep, the CDM approach assumes a $\sinh(\sigma)$ relationship between the uniaxial creep strain rate $\dot{\varepsilon}$ and the applied stress giving:

$$\frac{\partial \varepsilon}{\partial t} = \varepsilon_0' \exp\left(-\frac{Q_c}{RT}\right) \sinh\left(\frac{\sigma}{\sigma_0}\right) \tag{5.6}$$

While the value of ε_0' does have a physical basis, it is commonly approximated empirically and considered as a scaling parameter.

σ_0 is a reference stress parameter which represents stress redistribution between initial dislocation structure and precipitates during primary creep as well as the evolution of the dislocation structure as it moves into equilibrium with the applied stress:

$$\frac{\partial \sigma_0}{\partial t} = K_1 \left(1 - \frac{\sigma_0}{K_2}\right) \frac{\partial \varepsilon}{\partial t} \tag{5.7}$$

K_1 is an empirically determined parameter which describes the rate at which equilibrium between the applied stress and initial dislocation structure is reached. K_1 has been reported to be in the range of the shear modulus [47]. K_2 represents the maximum value of σ_0 once the initial dislocation structure has moved into equilibrium with applied stress and is determined by the dislocation-precipitate stress interaction:

$$K_2 = \frac{5kTV_p^{0.5}\sigma_{or}}{\alpha G b^3} \tag{5.8}$$

Where V_p is the volume fraction of precipitates and σ_{or} is the Orowan stress expressed as:

$$\sigma_{or} = \frac{\alpha MGb}{\lambda_{eff}} \tag{5.9}$$

Where α is a geometric term for dislocations and is obtained theoretically by idealising an edge dislocation with an arbitrary line tension interacting with an obstacle (see [56] for detailed explanation). It's value can be approximated as unity[50]. λ_{eff} is the effective inter-particle spacing for $M_{23}C_6$ and MX precipitates determined using:

$$\frac{1}{\lambda_{eff}} = \frac{1}{\lambda_{M_{23}C_6}} + \frac{1}{\lambda_{MX}} \tag{5.10}$$

Table 5-1: Theoretical approximations for CDM strain rate parameters for 9-12% Cr Steels

Parameter	**Theoretical Approximation**
$R_0\ (s^{-1})$	$1 \times 10^{13}\ (Debye\ frequency)$ Ref. [57]
$z\ (nm)$	$0.25\ (burgers\ verctor)$ Ref. [50]
$D_0\ (m^2 s^{-1})$	6.2×10^{-7}
$\dot{\varepsilon}_0'\ (s^{-1})$	3.78×10^5
$Q_c\ (kJmol^{-1})$	330 Ref. [7], [45], [50]
$k\ (JK^{-1})$	1.38×10^{-23}
$R\ (Jmol^{-1}K^{-1})$	8.31
$T\ (K)$	923
M	3 Ref. [7], [50]
$\lambda_{eff}\ (nm)$	60
$\lambda_{M_{23}C_6}\ (nm)$	260
$\lambda_{MX}\ (nm)$	80
$b\ (nm)$	0.25 Ref.[7], [50]
V_p	0.02 Ref. [55]
$K_1\ (MPa)$	7.14×10^3 Ref. [7]
$K_2\ (MPa)$	9.55
α	1

The strain rate equation was modified using the CDM method to include damage parameters due to subgrain coarsening D_S, $M_{23}C_6$ coarsening D_P and, back stress evolution H^*. The rate equation was modified as per the guidelines described by *Dyson et al.* [45] and summarised in Table 5-2.

$$Creep\ rate\ equation: \qquad \dot{\varepsilon} = \dot{\varepsilon}_0' \exp\left(-\frac{Q_c}{RT}\right) \sinh\left[\frac{\sigma\left(1 - H^*(1 - D_s)\right)}{\sigma_0(1 - D_P)}\right] \tag{5.11-1}$$

Table 5-2: Summary and description of various CDM damage parameters

Damage Parameter	Description	Arithmetic Relation to Creep Rate
Precipitate Coarsening Damage Parameter D_P	Effects of precipitate coarsening resulting in larger interparticle spacing. Mostly $M_{23}C_6$ and MX type precipitates are considered	$\sinh\left(\frac{1}{1 - D_p}\right)$
Subgrain Coarsening Damage Parameter D_S	Effects of increase in average subgrain size due to subgrain coarsening and growth	$\sinh(1 - D_S)$
Back stress Evolution Damage Parameter H^*	Effects of initial dislocation structure accounting for back stress	$\sinh(1 - H^*)$

For the current model the damage parameters considered were: subgrain coarsening damage D_S, precipitate coarsening damage D_p and back stress evolution damage H^*. The damage parameter D_S was chosen on the basis of available subgrain data for the steels being investigated (CB8, P92). For the steel CB8, the average subgrain size during creep as well as thermal ageing was obtained from Sonderegger [12]. As the damage parameter D_S is structured based on subgrain size rather than network dislocation density this made it the obvious choice for the current study. The damage parameter D_p was selected to describe the coarsening of $M_{23}C_6$ precipitates as the presence of this type of coarsening has been reported for CB8 [12] as well as P92 [54] and various other 9-12% Cr steels [20], [45], [50], [58], [59]. The coarsening of MX type precipitates was ignored for the current study as they have been reported to be stable and not coarsen during creep exposure by numerous studies [4], [14], [15]. The back stress concept and its influence on creep has become the focus of significant study over the past few years and has been applied to numerous creep resistant steels including CB8 [12], [60], [61]. Therefore, it was included in the current CDM model using the damage parameter H^* as defined by Christopher *et al.* [47].

5.2 Subgrain Coarsening Damage Derivations

Subgrain growth and coarsening is a strain and temperature dependent process. The average subgrain size is assumed to be proportional to the applied strain, giving:

$$S(t) = S_i + \varepsilon K_s \tag{5.12}$$

Where K_s is a subgrain growth constant and $S(t)$ is the average subgrain width at time t and S_i is the initial subgrain width. As subgrain coarsening/growth is both temperature and strain dependent, K_s can be expanded into a temperature dependent and temperature independent constant. The temperature dependence is described using an Arrhenius type formulation giving:

$$S(t) = S_i + \varepsilon \left(K_{s1} + K_{S2} \exp\left(-\frac{Qs}{RT}\right)\right) \tag{5.12}$$

The damage parameter for subgrain coarsening is defined as:

$$D_s(t) = 1 - \left(\frac{S_i}{S(t)}\right) \tag{3.19}$$

With this formulation, the initial damage parameter value $D_s = 0$ as the subgrain size at time $t = 0$ is equal to the initial subgrain size i.e. $S(t) = S_i$. As subgrain growth/coarsening occurs, the subgrain size at time t exceeds that of the initial subgrain size giving $S(t) > S_i$ and hence $D_s(t) > 0$.

Rearranging gives:

$$S(t)/S_i = (1 - D_s)^{-1} \tag{5.13}$$

$$(1 - D_s)^{-1} = 1 + \varepsilon \left(K_{s1} + K_{S2} \exp\left(-\frac{Qs}{RT}\right)\right) \tag{5.14}$$

Differentiating with respect to time gives:

$$\frac{\partial D_s}{\partial t} = \frac{\partial \varepsilon}{\partial t}\left(K_{s1} + K_{S2} \exp\left(-\frac{Qs}{RT}\right)\right)(1 - D_s)^2 S_i^{-1} \tag{5.15}$$

Or

$$\dot{D}_s = \frac{\dot{\varepsilon}}{S_i}\left(K_{s1} + K_{S2} \exp\left(-\frac{Qs}{RT}\right)\right)(1 - D_s)^2 \tag{5.16}$$

Table 5-3: Theoretical approximations for subgrain growth and coarsening parameters in 9-12% Cr steels

Parameter	Theoretical Approximation
$K_{s1}\ (ms^{-1})$	3.9×10^{-6} Ref. [7]
$K_{S2}\ (ms^{-1})$	7.7×10^{12} Ref. [7]
$Qs\ (kJmol^{-1})$	303 Ref. [7]
$S_i\ (\mu m)$	0.7 [15] (for CB8 steel)

5.3 $M_{23}C_6$ Coarsening Damage Derivations:

The Oswald Ripening law, equation 3.1 is assumed to apply to precipitate coarsening. It relates the precipitate diameter d at time t to the initial precipitate diameter d_i:

$$d^3 - d_i^3 = K_p t \tag{2.10}$$

Where K_p is a thermodynamically based constant defined according to *Barker et al.*[62] as:

$$K_p = \frac{8}{9}\gamma V_m \sum_{i=1}^{C} \frac{\left(\frac{x_i^{\frac{\alpha}{\beta}} D_V}{RT}\right)}{\left(x_i^{\beta} - x_i^{\frac{\alpha}{\beta}}\right)^2} \tag{5.17}$$

Where γ is the precipitate interfacial energy, V_m is the molar volume of the precipitate phase, D_V is the diffusion coefficient of element i in the matrix, x_i^{β} is the mole fraction of element i in the precipitate and $x_i^{\frac{\alpha}{\beta}}$ is the mole fraction of element i at the precipitate/matrix interface. The value for K_p is often determined empirically or using thermodynamic modelling tools and has been reported to be in the range of 10^{-29} to $10^{-28}\ m^3 s^{-1}$ for $M_{23}C_6$ precipitates at 650°C in 9-12% Cr steels by various studies [20], [63] [64].

If a damage parameter is defined as:

$$D_P = 1 - \frac{d}{d_i} \tag{5.18}$$

Then,

$$\frac{d_i}{d} = 1 - D_P \tag{5.19}$$

$$\frac{d^3(t)}{d_i^3} = \frac{K_p t + d_i}{d_i^3} \tag{5.20}$$

Inverting gives:

$$\frac{d_i^3}{d^3(t)} = \frac{d_i^3}{K_p t + d_i^3} \tag{5.21}$$

Hence,

$$(1 - D_P)^{-3} = 1 + \frac{K_p t}{d_i^3} \tag{5.22}$$

Differentiating with respect to time gives:

$$3(1 - D_P)^{-(3+1)} \frac{\partial D_P}{\partial t} = \frac{K_P}{d_i^3} \tag{5.23}$$

$$\frac{\partial D_P}{\partial t} = \frac{K_P}{3d_i^3}(1 - D_P)^4 \tag{5.24}$$

Table 5-4: Theoretical approximations for M23C6 coarsening parameters in 9-12% Cr steels

Parameter	Theoretical Value
$K_p\ (m^3 s^{-1})$	4.72×10^{-28}
$x_i^{\frac{\alpha}{\beta}}$	0.0841 Ref. [63]
x_i^{β}	0.6062 Ref. [63]
$D_V\ (m^2 s^{-1})$	9.57×10^{-20} Ref. [63]
$V_m\ (m^3 mol^{-1})$	1.82×10^{-4} Ref. [52]
$\gamma\ (Jm^{-2})$	0.668 Ref. [59]

5.4 Stress-redistribution Parameter

The redistribution of stress between the hard subgrain regions and soft matrix regions can be defined in terms of a damage parameter H^* as:

$$H^* = \frac{2\phi_{sg}}{1 + 2\phi_{sg}} \tag{5.25}$$

Where ϕ_{sg} is the volume fraction of subgrain boundaries. As subgrain coarsening occurs, this leads to a change in the redistribution of stress and hence a change in the damage parameter H^* According to [50] a rate equation for the redistribution of stress between the subgrain boundaries and matrix during creep can be defined as:

$$\frac{\partial H^*}{\partial t} = \frac{H^*(1 - H^*)}{2}(1 + D_s)^{-1}\frac{\partial D_s}{\partial t} \tag{5.26}$$

Table 5-5: Theoretical approximations for stress redistribution parameters in 9-12% Cr steels

Parameter	Theoretical Value
ϕ_{sg}	0.33 Ref.[50]
H_0^*	0.40

The fundamental differential equations are summarised below:

$$Creep\ rate\ equation: \quad \dot{\varepsilon} = \dot{\varepsilon}_0' \exp\left(-\frac{Q_c}{RT}\right)\sinh\left[\frac{\sigma\left(1 - H^*(1 - D_s)\right)}{\sigma_0(1 - D_P)}\right] \tag{5.11-1}$$

$$Primary\ creep\ rate: \quad \dot{\sigma}_0 = K_1\left(1 - \frac{\sigma_0}{K_2}\right)\dot{\varepsilon} \tag{5.11-2}$$

$$Subgrain\ Damage\ Evolution: \quad \dot{D}_s = \frac{\dot{\varepsilon}}{S_i}\left(K_{S1} + K_{S2}\exp\left(-\frac{Q_s}{RT}\right)\right)(1 - D_S)^2 \tag{5.11-3}$$

$$Backstress\ Damage\ Evolution: \quad \dot{H}^* = \frac{H^*(1 - H^*)}{2}(1 + D_s)^{-1}\dot{D}_s \tag{5.11-4}$$

$$M_{23}C_6\ Damage\ Evolution: \quad \dot{D}_p = \frac{K_P}{3d_i^3}(1 - D_P)^4 \tag{5.11-5}$$

5.5 Empirically based Parameter Determinations

The CDM modelling method while being physically based is often used in conjunction with experimental and microstructural measurements to calculate 'actual' values for the various required parameters. This is done in order to produce more accurate and reliable results for the specific steels being assessed. This section details the various calculations carried out to determine the CDM parameters for the steel CB8.

5.5.1 *Creep Rate Parameters*

Some of the parameters used as an initial guess were calculated based on information extrapolated from creep-time plots. The first parameter $\dot{\varepsilon}_0'$, as derived and explained in section 5.1 ,is often considered as a scaling parameter and was calculated by plotting a graph of $\log(\dot{\varepsilon}_{min})$ against $\log\left(sinh\left(\frac{\sigma H^*}{\sigma_0}\right)\right)$ for a set of creep curves for CB8 for applied stress of 75, 85 and 100 MPa as shown in Figure 5-1. This was done by firstly assuming that the damage parameters $D_P = D_S = 0$ which is motivated by the assumption that the minimum strain rate is reached relatively early within the creep deformation timeline and therefore degradation due to particle and subgrain evolution is negligible. Also, at $\dot{\varepsilon}_{min}$ (the time at which the minimum creep rate is reached) the stress distribution between the 'soft' matrix and 'hard' particles, H^* is taken as being at its maximum value. Thus, the strain-rate equation reduces to:

$$\dot{\varepsilon}_{min} = \dot{\varepsilon}_0' \exp\left(-\frac{Q_c}{RT}\right) \sinh\left[\frac{\sigma(1-H^*)}{\sigma_0}\right] \tag{5.27}$$

Taking *logs* of each side gives:

$$\log(\dot{\varepsilon}_{min}) = \log\left(\dot{\varepsilon}_0' \, exp\left(-\frac{Q_c}{RT}\right)\right) + \log\left(sinh\left(\frac{\sigma H^*}{\sigma_0}\right)\right) \tag{5.28}$$

By plotting the graph of $\log(\dot{\varepsilon}_{min})$ against $\log\left(sinh\left(\frac{\sigma H^*}{\sigma_0}\right)\right)$ as shown in Figure 5-1, the y-intercept gives the value of $\log\left(\dot{\varepsilon}_0' \, exp\left(-\frac{Q_c}{RT}\right)\right)$ as shown by equation 5. Therefore, for a known temperature and value of creep activation energy, Q_c the empirical value of $\dot{\varepsilon}_0'$ can be calculated.

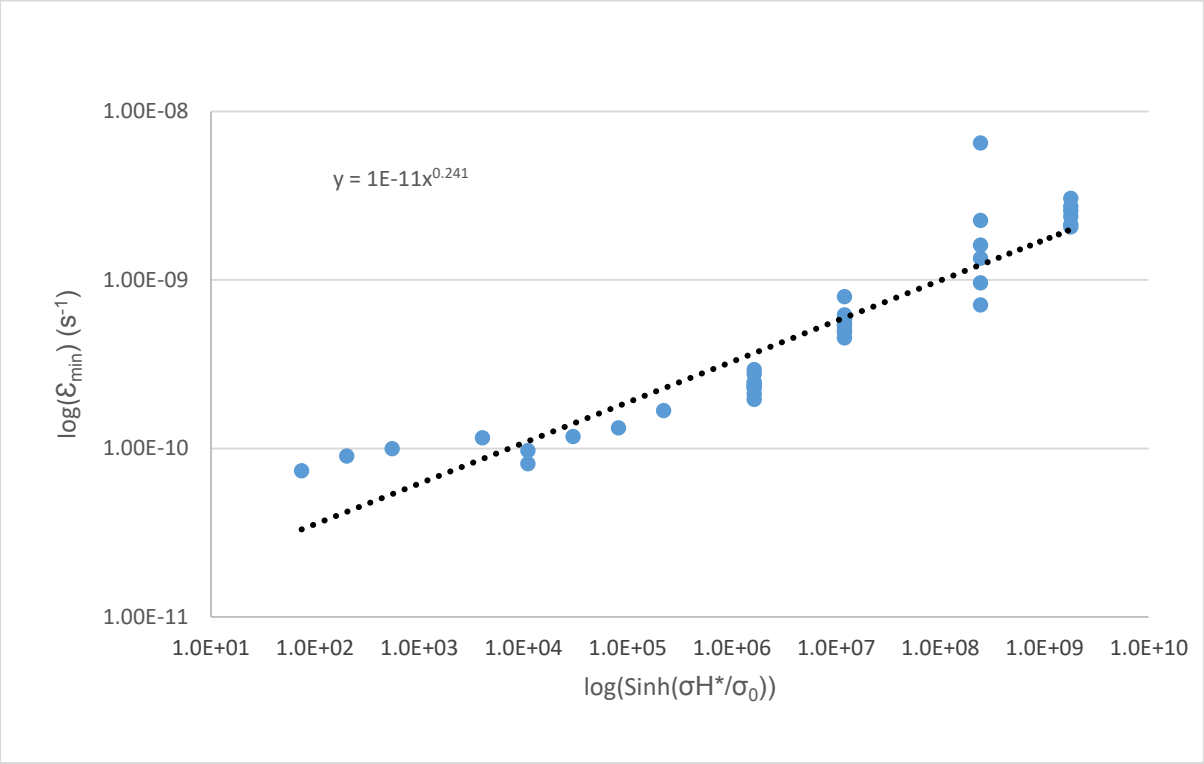

Figure 5-1: *log $\dot{\varepsilon}_{min}$ versus log (sinh ($\sigma H^*/\sigma_0$))* for a set of creep curves of CB8 steel at 650°C

The creep activation energy Q_c is generally taken to be equal to that of lattice self-diffusion plus that of dislocation jog formation. This value can be calculated using thermodynamic software such as *Thermocalc*™ or from minimum creep rate data [1]. This value has generally been found to be in the range of 330 kJmol^{-1} for 9-12% Cr steels [11], [50], [58] . As the value for Q_c has a significant impact on the overall creep life of the material, an attempt was made to obtain an accurate approximation of it using an optimisation routine. In order to do this, an acceptable range of values needed to be specified. According to various studies [8], [45], [47], [50] the value for lattice self-diffusion in 9-12% Cr steels can be as low as 280 kJmol^{-1} and as high as 360 kJmol^{-1}. This range was found to be too large a window in which to search for an optimised value and was therefore incremented to acceptable ranges and the optimised parameter set compared using a Root Mean Squared Error calculation against experimental data (see Figure 5-2). The optimisation range with the lowest RMSE value for CB8 was found to be 290 kJmol^{-1} -340 kJmol^{-1}.

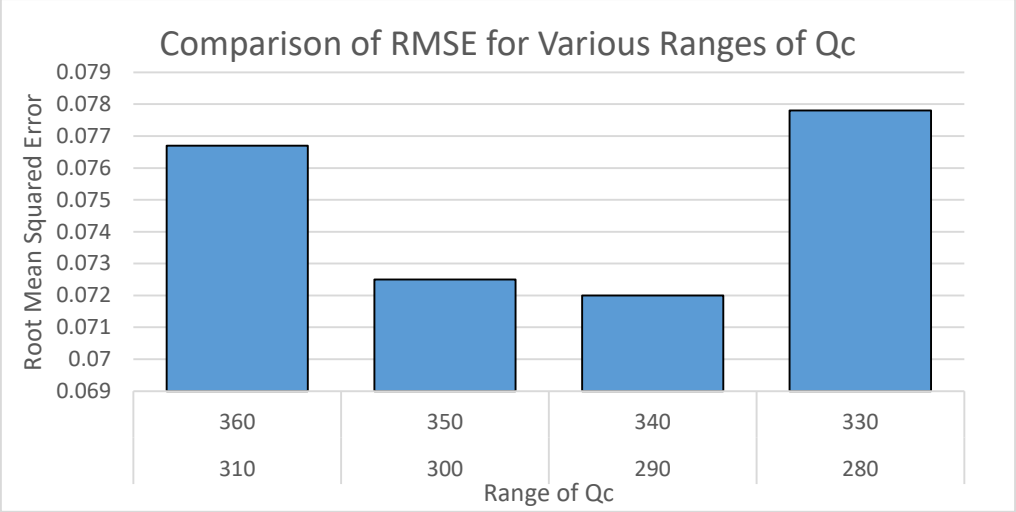

Figure 5-2: Graph comparing the RMSE associated with various optimisation ranges of Qc

5.5.2 *Subgrain Evolution Parameters*

The values of the subgrain constants K_{S1} and Ks_2 as derived in section 5.2 obtained from subgrain coarsening data for CB8 [12]. The value of the subgrain coarsening activation energy Q_s, requires subgrain coarsening data over a range of different temperatures as its value is independent of temperature. However, the value of Q_s has been found to be similar to that of lattice self-diffusion [47], and can therefore be obtained from thermodynamic modelling software such as Matcalc or it can be assumed. For the purpose of this study the value of Q_s was assumed as $330\ kJ/mol$ as determined by *Oruganti et al.* [7]. Once this was done, the value of K_{S2} was calculated from the plot of subgrain size vs strain for a thermally aged sample (Figure 5-3). As the gradient of the plot is equal to $K_{S2}\exp\left(-\frac{Q_s}{RT}\right)$. The value of K_{S1} was then calculated from the plot of subgrain size vs strain for a creep loaded sample. The gradient of this plot being equivalent to, $K_{S1} + K_{S2}\exp\left(-\frac{Q_s}{RT}\right)$

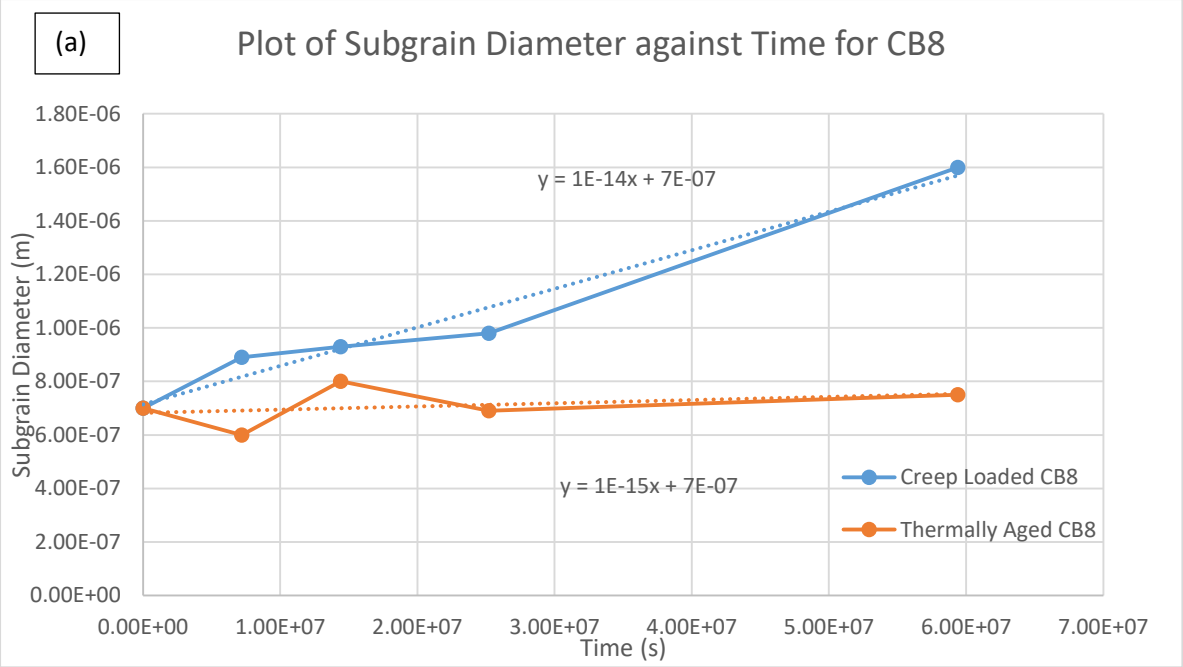

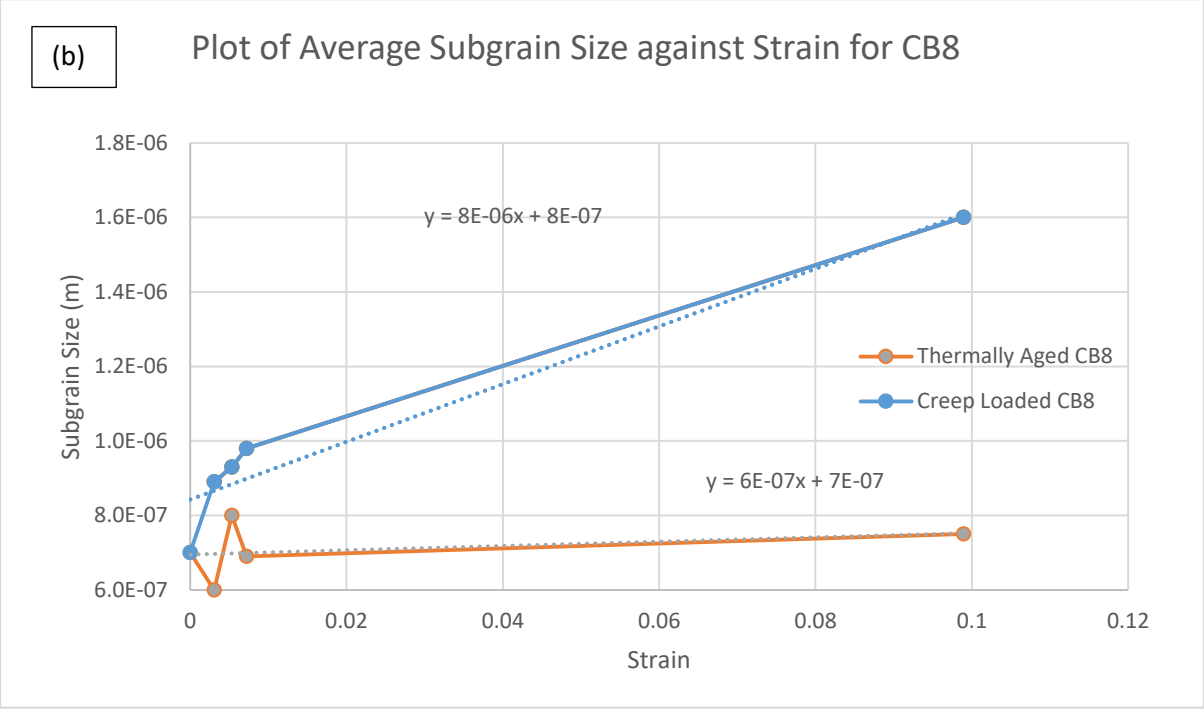

Figure 5-3 Plot of subgrain size against (a) time and (b) strain for CB8 at 75 MPa and 650°C

5.5.3 *Particle Coarsening Paramters*

The empirical value for the precipitate coarsening constant K_p for $M_{23}C_6$ precipitates was obtained from microscopy results of average precipitate diameter in CB8 steel during creep exposure at 75 MPa and 650°C (see Appendix A section 0). K_p was taken as the gradient of the plot of precipitate diameter d^3, against time as per the Ostwald ripening law (equation 2.1). Figure 5-4 shows the diameter-time plot along with a linear best fit approximation.

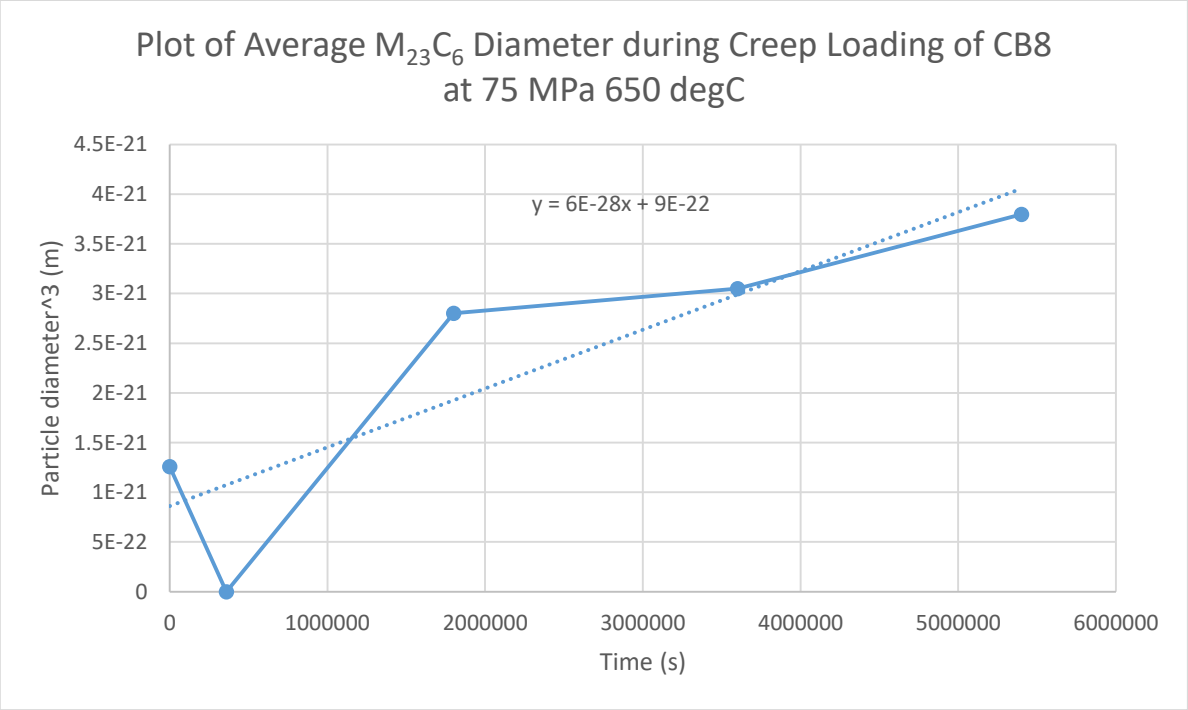

Figure 5-4: Plot of average $M_{23}C_6$ diameter against time for CB8 at 75 MPa and 650°C

The empirically calculated values for the parameters discussed in this chapter are summarised in Table 5-6 for the steel CB8.

Table 5-6: Empirically obtained CDM parameter values for the steel CB8

Parameter	Empirically Calculated Value
$\dot{\varepsilon}_0' \ (s^{-1})$	4.8×10^{7}
$k \ (JK^{-1})$	1.38×10^{-23}
$R \ (Jmol^{-1}K^{-1})$	8.31
$K_{s1} \ (ms^{-1})$	7.4×10^{-6}
$K_{S2} \ (ms^{-1})$	2.9×10^{12}
$K_p \ (m^3s^{-1})$	6×10^{-28}

6 CB8-Model Results

6.1.1 *Parameter Analysis*

In order to develop the current model, a comprehensive understanding and interpretation of the various parameters used was required. This was done by adjusting the values of these parameters within prescribed limits [47] and systematically examining the effects these adjustments have on the strain/time plots as well as on relevant microstructural predictions.

6.1.1.1 Scaling Parameter ε'_0

The parameter ε'_0 is a characteristic strain rate and is usually described as a measure of mobile dislocation density and precipitate volume fraction [7], [46], [58] as explained in section 5.1.

While the relationship described by Equation 4.5 gives some insight into the parameter $\dot{\varepsilon}'_0$, a specific physical relationship between this parameter and the aforementioned quantities without material constants cannot be found in literature. In fact, this parameter is usually estimated using empirical calculations based on minimum creep rate data as outlined in section 5.5.1. Estimates of this parameter were obtained from literature and varied within acceptable limits [47] to analyse its effects on creep predictions using the CDM approach as shown in Figure 6-1.

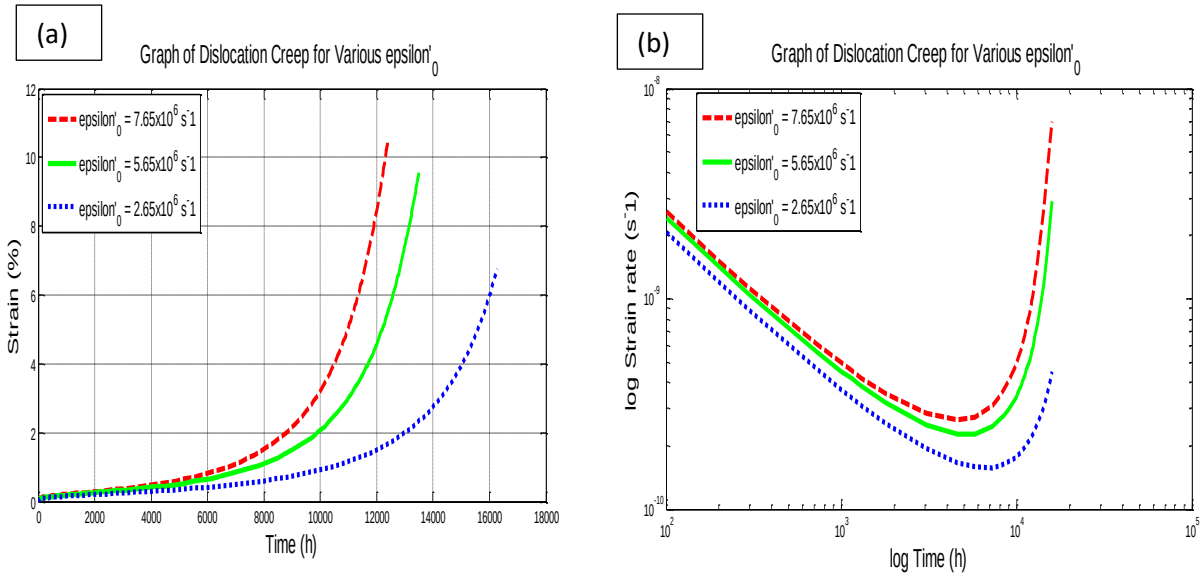

Figure 6-1:(a) Model analysis of (a) strain-time plots and (b) strain rate-time plots until rupture for various values of $\dot{\varepsilon}_0$

Figure 6-1(a) shows that an increase in the value of ε'_0 corresponds to a decrease in time to rupture predicted by the model. Also, the value of ε'_0 affects the entire creep curve proportionally. This justifies the treatment of this parameter as a scaling constant. Figure 6-1(b) shows that the creep rate during each creep stage varies proportionally with $\dot{\varepsilon}'_0$ while the time at which the minimum creep rate occurs varies only slightly. This is once again consistent with the behaviour of a scaling parameter.

*6.1.1.2 Back stress Limiting Value H**

The parameter H^* represents the limiting value of stress distribution between 'hard' and 'soft' regions within the material microstructure. In the context of 9-12% Cr steels these 'hard' regions include subgrain/network dislocation boundaries as well as any prominent precipitate substructure. The 'soft' regions in this context can be taken as the material matrix. As the stress redistribution due to MX and $M_{23}C_6$ is considered in the evaluation of the normalising stress σ_0, only the subgrain structure is considered as a 'hard' region in the evaluation of H^* as shown in section 5.4. However, as the subgrain structure is well known to coarsen during creep exposure, the value of $H^*$is expected to vary as well [14]. Therefore, the value of H^* is coupled to the subgrain coarsening damage parameter D_s by the kinetic rate equation 5.11-4.

The starting value of H^* denoted as H_0^* is calculated from physical relations as explained in section 5.4, has been reported in literature to be in the range of 0.3- 0.45 for 9-12% Cr steels [4, 30, 31, 34]. For the current investigation, three different values of H_0^* were used to examine their effects on the overall strain/time plots as shown in Figure 6-2.

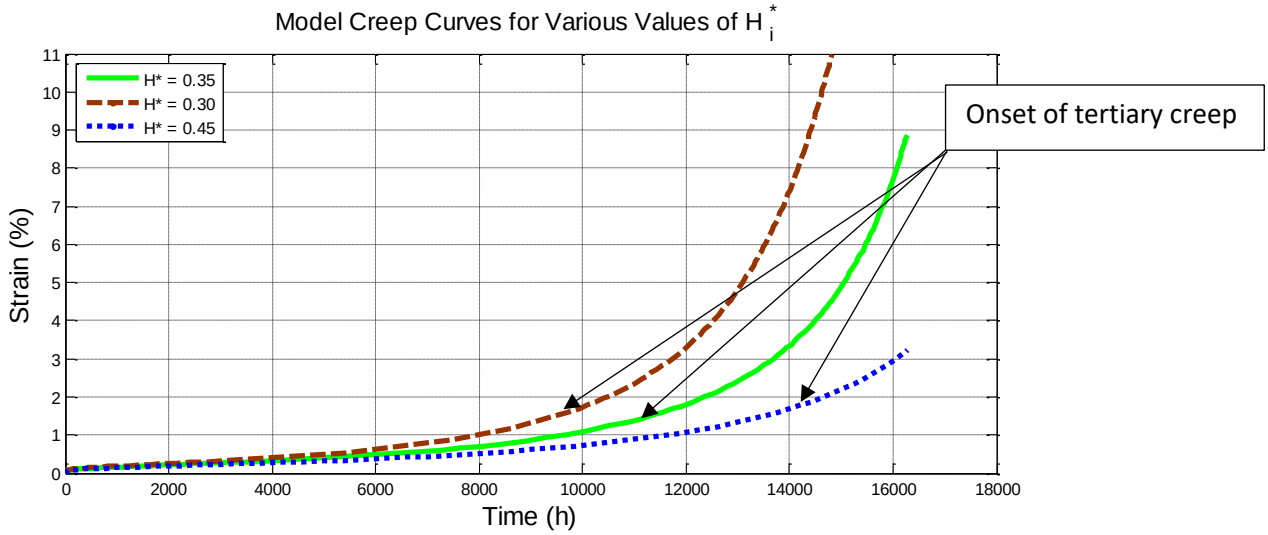

Figure 6-2: Model analysis of strain-time plots for various values of H_0^*

Figure 6-2 displays the effect on the strain/time curve of adjusting the value of H_0^* and as expected there is a marked difference in the model's prediction for the different values. Firstly, the model predicts an increase in creep strength with increasing H_0^* as indicated by an increase in time to rupture for increasing values of H_0^*. Also, the model predicts that the onset of tertiary creep occurs earlier for lower values of H_0^*.For H_0^* values of 0.30, 0.35 and 0.45, the onset of tertiary creep occurs at approximately 8000h, 11000h and 13000h respectively. These observations can be interpreted by considering that the H^* is a measure of stress distribution between subgrain boundaries and matrix. Therefore a higher value of H_0^* implies greater stress distribution and a more prevalent initial subgrain structure and higher creep strength. However, as subgrain coarsening occurs the stress distribution decreases leading to a loss in creep strength resulting in the onset of tertiary creep.

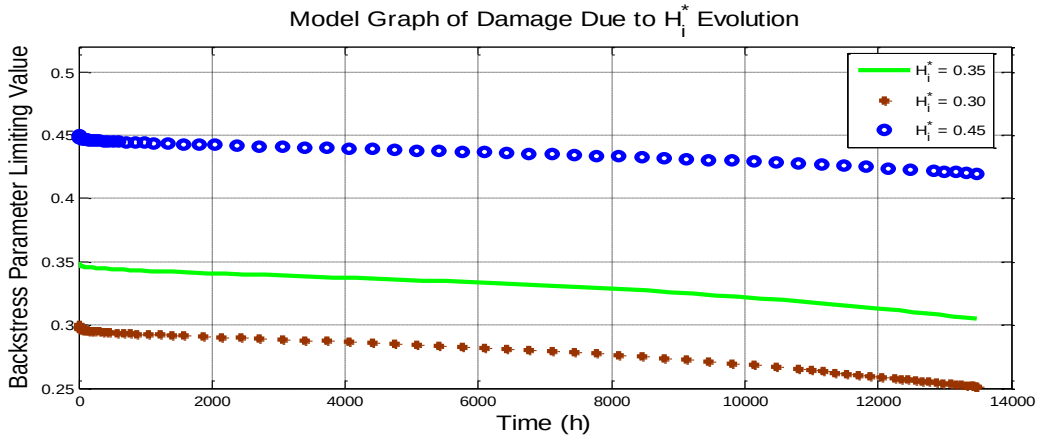

Figure 6-3: Model predictions of limiting Back stress values over time for various initial values of H_0^*

Figure 6-3 displays the change in H^* over time for values of H_0^* of 0.30, 0.35 and 0.45 respectively. The graph shows an initial steady decrease in the value of H^* following by a more accelerated decrease in its value. Also, as the initial value of H^* is reduced, the decrease in its value occurs more rapidly. This observations can be explained by once again considering the physical interpretation of the parameter H^*. Firstly, since this parameter represents the distribution of stress between the subgrain boundaries and the matrix, a decrease in its value indicates a decrease in the stress distribution between these two microstructural features. As subgrains grow and coarsen under creep exposure, there is consequently a loss in subgrain boundary structure. This therefore causes a decrease in the distribution of stress between the subgrain boundaries and the matrix and hence a decrease in the value of H^*.

Primary Creep Constant $\boldsymbol{K_1}$

The primary creep constants K_1 andK_2 describe how the reference stress σ_0 evolves during creep exposure. The reference stress σ_0 is effectively a measure of how the initial mobile dislocation structure evolves to reach equilibrium with the applied stress. This process in 9-12% Cr steels is primarily governed by the interactions between mobile dislocations and precipitates. Once the dislocations are pinned by precipitates, the microstructure effectively moves into equilibrium with the applied stress and the primary creep stage can be assumed to be complete.

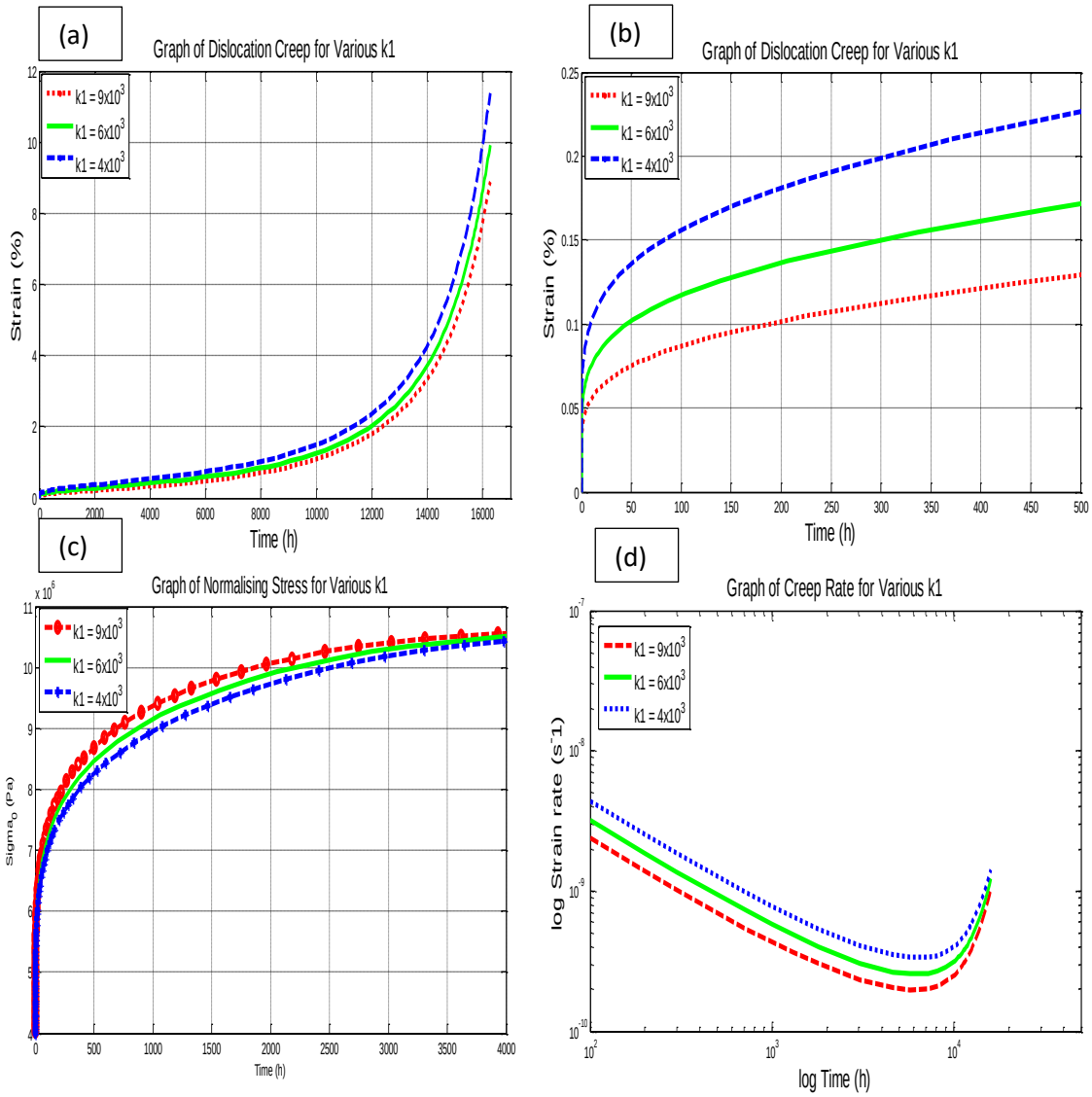

Figure 6-4 (a) Model analysis of strain-time plots until rupture for various values of K_1 (b) Model analysis of strain-time plots during primary creep for various values of K_1 (c) Model analysis of σ_0 during creep for various values of K_1 (d) Model analysis of strain rate-time plots during creep for various values of K_1

Figure 6-4 (a) shows that there is a slight decrease in creep strength with decreasing values of K_1. As shown in Figure 6-4 (b), K_1 only affects the creep rate during the primary creep stage and is a measure of the rate at which primary creep occurs. This parameter therefore has little effect on the later stages of creep.

6.1.1.3 Primary Creep Constant K_2

The primary creep stage constant K_2 is defined as the limiting value of σ_0 and is mainly dependent on the initial precipitate ($M_{23}C_6$ *and* MX) size, inter-particle spacing and type. It is the theoretical maximum stress withstood by the precipitate structure within the steel. The value of K_2 has been reported to be in the range of 10-14 MPa [46], [47].

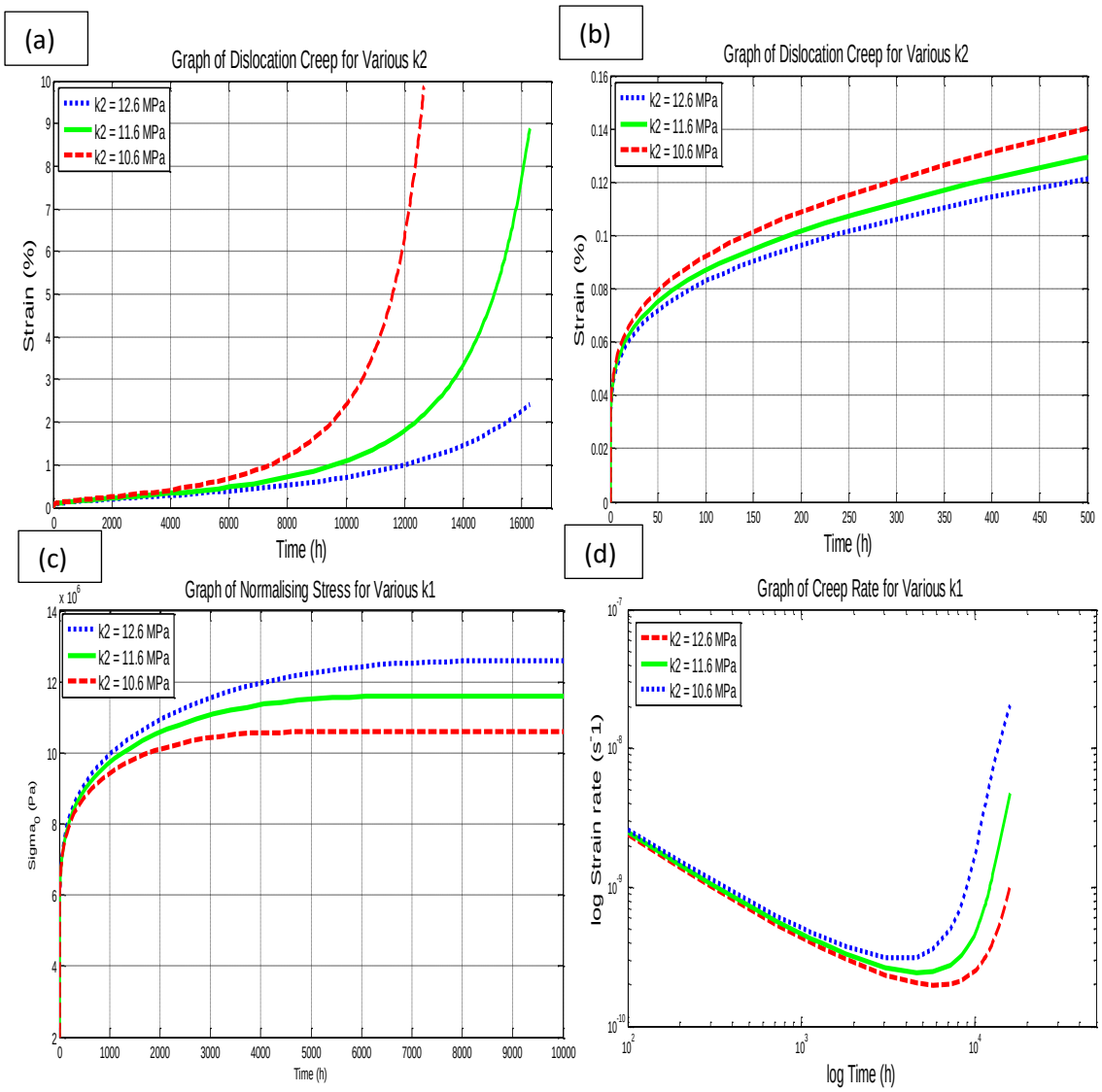

Figure 6-5: (a) Model analysis of strain-time plots until rupture for various values of K_2 (b) Model analysis of strain-time plots during primary creep for various values of K_2 (c) Model analysis of σ_0 during creep for various values of K_2

Figure 6-5 (a) illustrates the impact of the value of K_2 on the model's creep strain time plots. It is clear that K_2 has a significant impact on the entire creep life of a steel and influences the time at which tertiary creep occurs and therefore rupture time. The creep strength of the steel in the model displays a proportional relationship with the value of K_2 as indicated by the increase in time to rupture with increasing values of K_2. A K_2 value of 12.6 MPa results in a 1% creep strain at about 12000 hours whilst a K_2 value of 10.6 results in a 1% creep strain at less than 8000 hours. These results can be interpreted with an understanding of what K_2 represents. As K_2 is a measure of resistance to dislocation motion due to precipitates acting as dislocation obstacles, a higher value of K_2 translates to greater resistance to dislocation motion. Since dislocation motion is fundamentally what drives dislocation creep, a reduction in it essentially provides greater creep strength to the steel. Also, while K_2 is a constant used in describing primary creep and therefore only the initial precipitate structure, it has a significant impact on the later stages of creep as the precipitates play such a pivotal role in limiting dislocation motion throughout the creep life of the steel.

6.1.1.4 *Primary Creep Constant* K_{s1}

The material parameters K_{s1} and K_{s2} describe the temperature independent and temperature dependent aspects of subgrain growth and coarsening as explained in section 5.2.

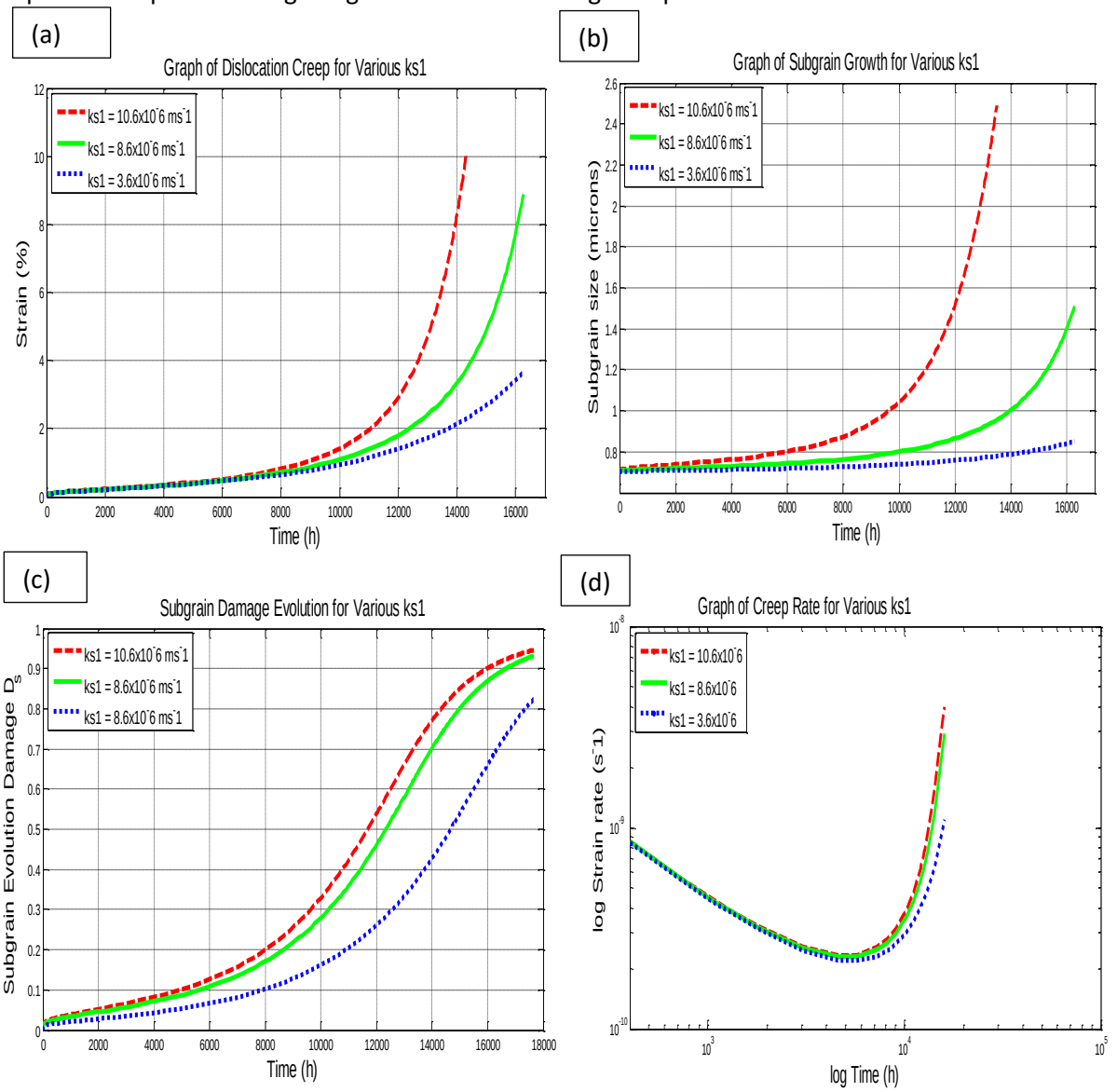

Figure 6-6: (a) Model analysis of strain-time plots for various values of K_{s1} (b) Model analysis of subgrain size plots during creep for various values of K_{s1} (c) Model analysis of D_S during creep for various values of K_{s1}

Figure 6-6 (a) shows the model's creep strain-time plot for various values of K_{s1}. The results show that K_{s1} has a strong influence on when the tertiary creep stage begins, the rate at which it occurs and the time at which rupture occurs. Conversely, the value of K_{s1} has little to no impact on the primary and secondary creep stages (below approx. 10 000h). K_{s1} is a measure of subgrain growth and evolution due to an applied strain. The subgrain structure in 9-12% Cr steels only exhibits significant growth and coarsening towards the end of the secondary and throughout the tertiary creep stages when enough strain has accumulated in the microstructure to drive these changes. Therefore the influence that the value of K_{s2} seems to have almost exclusively on the later stages of dislocation creep agrees with theory [18], [65]. Figure 6-6 (b) displays the model's prediction of subgrain size during creep for different values of ks1. As with the creep-time plots, K_{s1} has a clear impact on the subgrain size especially in the later creep stages. The predicted values of subgrain size during creep show good agreement with reported values in literature particularly below 10 000h. *Bazazi* [17] reported a

subgrain size of approximately 0.9 μm for X20CrMoV12 steel after approximately 10 000h of creep exposure. This agrees well with the results shown in Figure 6-6 (b) especially for K_{s1} values of $10.6 \times 10^{-6} ms^{-6}$ and $8.6 \times 10^{-6} ms^{-6}$ bearing in mind that these values are highly dependent on applied stress and material microstructure. Figure 6-6 (c) shows the change in the subgrain damage parameter D_s during creep for various K_{s1}. As expected the subgrain damage parameter evoluton shows the same trend as the as the subgrain coarsening results with the rate of coarsening increasing with increasing values of K_{s1}. However, the subgrain coarsening damage parameter D_s begins to plateau as it approaches 1. This is due to the fact that the damage in quantified on a scale between 0 and 1 with 1 representing material failure.

Primary Creep Constant $\boldsymbol{K_{s2}}$

The parameter K_{s2} relates to the aspects of subgrain coarsening which are thermally activated. The effects of temperature on subgrain coarsening have been found to be small at typical creep exposure temperatures (550°C-650°C) by researchers [12], [17].

$$\dot{S} = \dot{\varepsilon}\left(K_{S1} + K_{S2}\exp\left(-\frac{Q_s}{RT}\right)\right) \tag{4.21}$$

For constant temperature applications, the above equation can be simplified to:

$$\dot{S} = \dot{\varepsilon}(K_{S1} + K_{S2}') \tag{6.0}$$

Where:

$$K_{S2}' = K_{S2}\exp\left(-\frac{Q_s}{RT}\right) \tag{6.1}$$

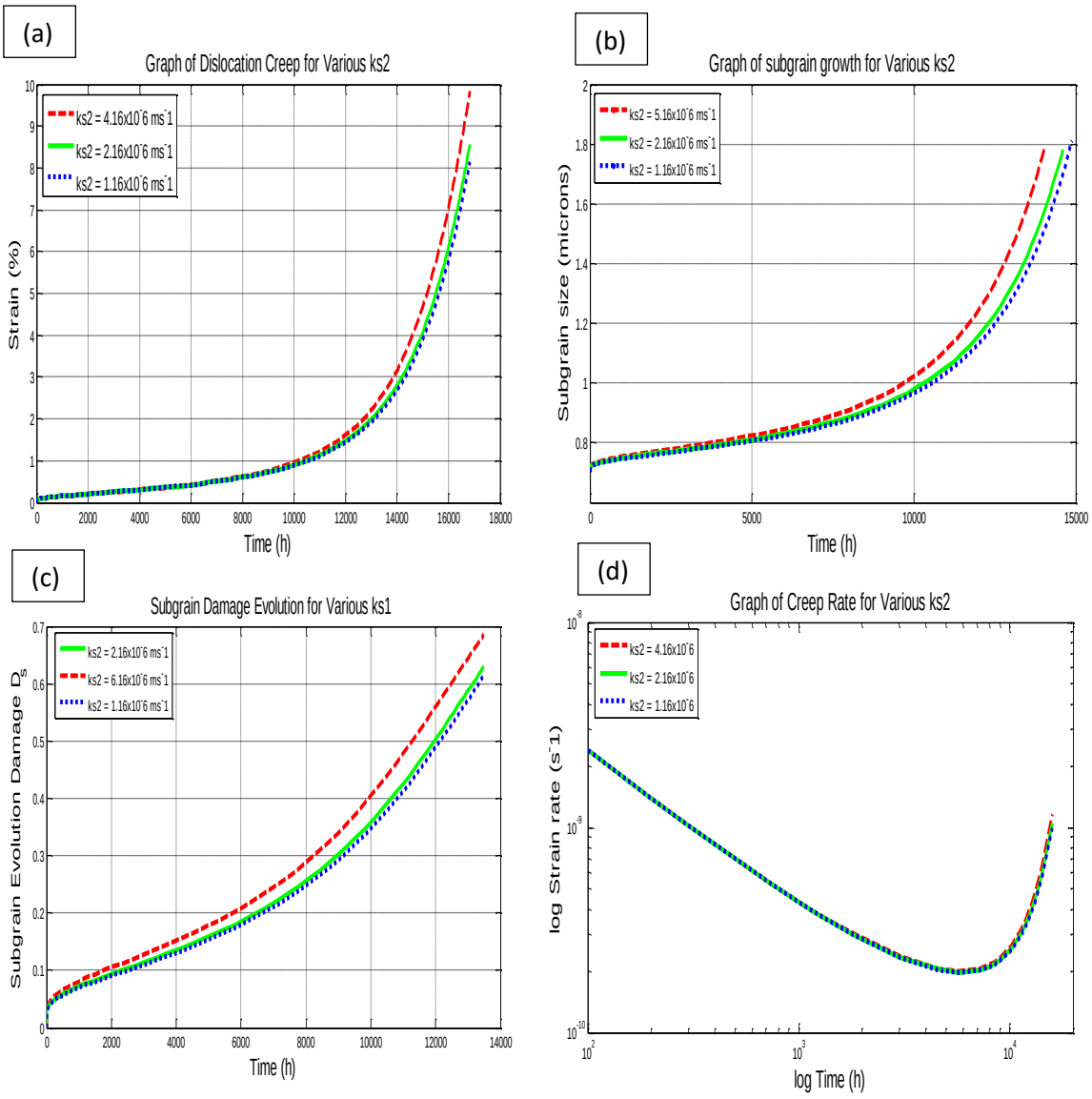

Figure 6-7: (a) Model analysis of strain-time plots for various values of K_{s2} (b) Model analysis of subgrain size plots during creep for various values of K_{s2} (c) Model analysis of D_S during creep for various values of K_{s2}

As with K_{s1}, K_{s2} has an effect almost exclusively on the tertiary creep stage. This effect, albeit slight, increases with increasing values of K_{s2}. An increase in the value of K_{s2} implies a greater dependence of the subgrain coarsening rate on thermal agitation. This is different from the thermal activation energy constant Q_s, which is a measure of the energy required for subgrain growth and coarsening to start, not the rate at which it occurs. Once again, the only slight impact that the value of K_{s2} has on the subgrain coarsening rate (Figure 6-7 (b)) and by extension the creep strain rate (Figure 6-7 (b)) agrees well with reports from literature [12], [17].

6.1.1.5 Coarsening Constant K_P

The coarsening constant K_P describes the rate at which coarsening occurs during creep exposure based on the Ostwald ripening law as described in section 5.3. In 9-12% Cr steels the coarsening of $M_{23}C_6$ has been repeatedly shown to be detrimental to creep strength in numerous studies [8], [15],

[66]. Values of K_P have been found to be in the range of $10^{-29} - 10^{-28} m^3 s^{-1}$ for $M_{23}C_6$ precipitates [12], [64]. Model results for various values of K_P within an acceptable range are shown in Figure 6-8.

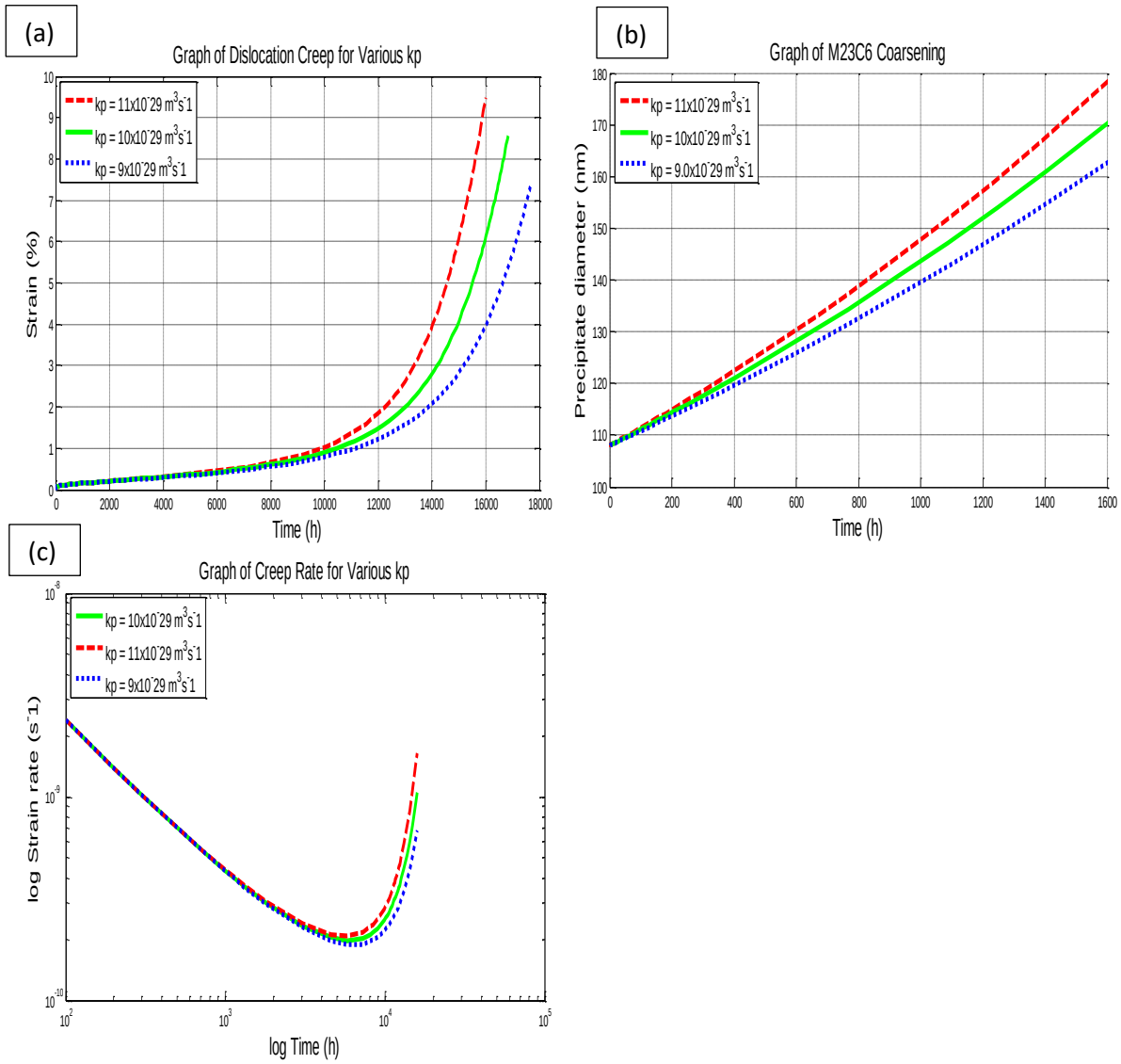

Figure 6-8: (a) Model analysis of strain-time plots for various values of K_P (b) Model analysis of average $M_{23}C_6$ precipitate diameter plots during creep for various values of K_P (c) Model analysis of strain rate-time plots for various values of K_P

Figure 6-8 (a) shows that the value of the $M_{23}C_6$ coarsening constant plays a significant role in the tertiary creep stage especially above 10 000h of creep exposure. The value of Kp influences both the onset of tertiary creep as well as the rate of creep thereafter until rupture. Figure 6-8 (c) shows that the value of K_p' has a very slight impact on the minimum creep rate and the time taken to reach it. The role of $M_{23}C_6$ in creep resistant steels has been well documented as mainly affecting the later stages of creep and the model displays this behaviour well. The coarsening mechanism typically influences the creep rate by causing an increase in inter-particle spacing and allowing dislocations and subgrain boundaries which would otherwise be pinned, to migrate. However, until the inter-particle spacing reaches a critical value such that the Orowan stress is high enough to allow dislocations to move past precipitates, the dislocation motion will still be impeded. Thus the effects of $M_{23}C_6$ coarsening are negligible in the early stages of creep.

6.1.2 *Theoretical Model Predictions for CB8*

The CDM creep model proposed in chapter 5 was set up initially with model parameters based on purely theoretical approximations as outlined in sections 5.1- 5.4. The main model parameters are summarised in Table 6-2. The model was implemented in the numerical solving software *Matlab*^{TM}. The equation set 5.11 was solved and integrated with respect to time using Matlab's *ODE45* function; a Fourth order *Runge-Kutta* routine with an adaptive step size (see appendix B1 for full derivations). The model's strain-time predications were calculated using initial subgrain and $M_{23}C_6$ data for CB8 (see Appendix A1). The predictions for the three stress conditions being analysed were compared to the experimentally obtained data and are shown in Figure 6-9. Full source code with commented descriptions can be found in Appendix C2. Also, a Graphical User Interface (GUI) was created for convenience (see Appendix) C2. The GUI can be launched using the file: *CDM_GUI.m.* The GUI runs the CDM initialisation function: *CDM_Dislocation_creep_Model_function.m.* The CDM differential equation loop is run in the file: *CDM_equation_loop.m.*

Table 6-1: Initial values for CDM parameters

Parameter	Initial Value
$\dot{\boldsymbol{\varepsilon}}\ (\boldsymbol{s^{-1}})$	0
$\dot{\boldsymbol{\sigma}}_{\boldsymbol{0}}\ (\boldsymbol{MPa})$	2
$\dot{\boldsymbol{D}}_{\boldsymbol{s}}$	0
$\dot{\boldsymbol{H}}^{*}$	0.4
$\dot{\boldsymbol{D}}_{\boldsymbol{p}}$	0
$\boldsymbol{S}(\boldsymbol{\mu m})$	0.7
$\boldsymbol{P}(\boldsymbol{nm})$	60

Table 6-2: Summary of theoretically calculated CDM parameters

Parameter	Theoretical Value
$Q_c\ (kJ/mol)$	330
$Q_s\ (kJ/mol)$	303
$\dot{\varepsilon}'_0\ (s^{-1})$	3.78×10^5
$K_1\ (Pa)$	7.14×10^9
$K_2\ (Pa)$	9.5×10^6
$K_{S1}\ (ms^{-1})$	3.9×10^{-6}
$Ks_2\ (ms^{-1})$	7.7×10^{-6}
$K_p\ (m^3 s^{-1})$	4.72×10^{-28}

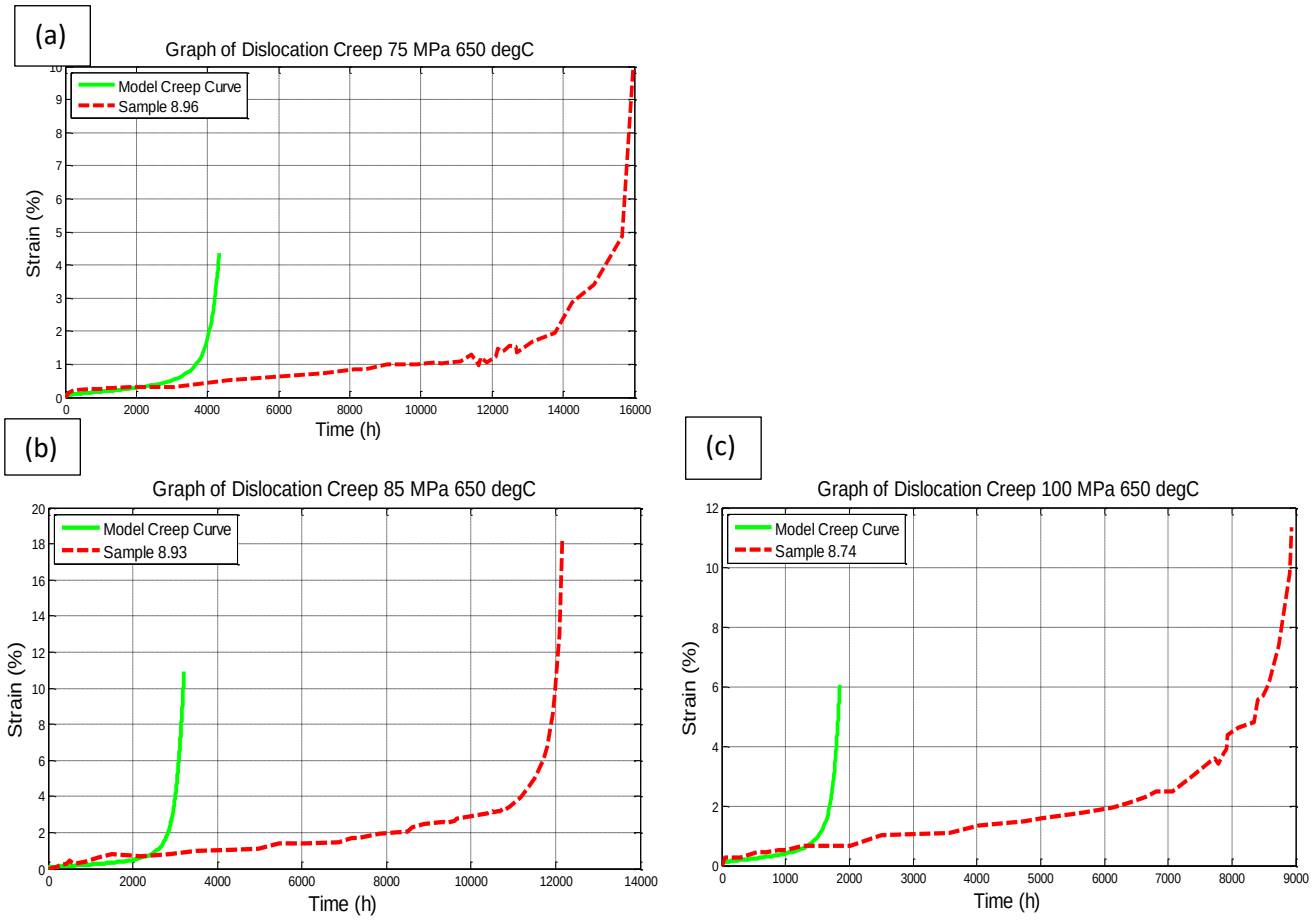

Figure 6-9: (a) Plot of 75 MPa, 650°C creep test for sample 8.96 with model result. (b) Plot of 85 MPa, 650°C creep test for sample 8.93 with model result. (c) Plot of 100 MPa, 650°C creep test for sample 8.74 with model result.

The creep-strain time plots for CB8 shown in Figure 6-9 clearly show that the CDM strain-time predictions for all three stress states grossly underestimate the creep strength of the material

particularly within the secondary and tertiary creep stages. The model predicts creep rupture at approximately 4000h, 3000h and 2000h for stresses of 75, 85 and 100 MPa respectively while rupture only occurred at approximately 16000h, 12000h and 9000h for the same stresses. Conversely, model predictions for the primary creep regions seem to correlate well with the experimental obtained creep curves.

While these results may at first appear to dismiss the CDM approach as being wholly inaccurate, it is important to consider that the results thus far have been based on purely theoretical approaches to obtaining all the model parameters as determined in sections 5.1-5.4. No form of calibration has been used for the model in order to obtain parameter values specific to CB8. Furthermore, some of these parameters have been calculated based on theoretic approximations and are likely to have innate inaccuracies. The CDM modelling approach is generally used in conjunction with some form of parameter optimisation [7], [11], [50]. In light of this, the fact that the model is capable of accurately reflecting the creep properties of the material albeit exclusively for primary creep for each stress state, lends credibility to the approach. It is also apparent that the model results lose accuracy in their predictions of the onset of tertiary creep leading to an early, exponential loss in creep strength. The error therefore lies in the equations/ characteristics or more specifically their parameters which influence tertiary creep. The parameter analysis shown in section 6.1.1 indicate that tertiary creep and its onset is dictated mostly by subgrain and precipitate evolution described by equations 5.11-3 and 5.11-5 respectively.

6.1.3 *Model Callibration and Parameter Optimisation*

In order to produce accurate creep predictions for specific material microstructures using the CDM approach, a parameter optimisation routine was utilised for the various material parameters. This was motivated by the fact that microstructural measurements are often only approximate and have some acceptable scatter associated with them. Therefore optimising the parameters within acceptable limits can be justified. In order to optimise the parameter set, initial parameter guesses; creep test data; and an optimisation merit function are required.

The creep test data for the current study were obtained from the Graz University of Technology for the 11% Cr COST steel designated CB8. This consisted of long-term, constant stress, creep strain-time data for stresses of 75, 85 and 100 MPa at 650°C (see Chapter 4). This data was used to obtain initial parameter guesses as explained in section 5.5.

6.1.3.1 Optimisation Routine

The best way to obtain an optimised parameter set for a given steel, is to run the CDM model with initial guess parameter values and compute the error between experimental and model results. Based on the error calculated, the initial parameter guesses need to be adjusted using a minimisation function and the process repeated until pre-determined error conditions are met. For the current study a Sum of Squared Error (SSE) was used as the merit function to calculate the error between the model and experimental creep strain-time plots. This merit function was then minimised and new parameter guesses produced using a constrained *Nelder-Mead simplex* function (*fminsearchbnd.m*). This iterative process was continued until pre-set tolerance limits were met.

Consider a parameter set p_0 representing the initial model parameter guesses $Q_c, \varepsilon_0', k_1, k_2, k_{s1}\ k_{s2}$ and k_p. The equation set 5.11 in section 5 is solved numerically to give strain time predictions, $\varepsilon(t_i\ p_i)$. The SSE is computed between experimental strain time data $\varepsilon_{exp}(t)$ and the model prediction $\varepsilon(t_i\ p_i)$ as:

$$SSE = \sum_{i=1}^{N} \left[\frac{\varepsilon_{exp}(t) - \varepsilon(t_i\ p_i)}{\varepsilon_{exp}} \right]^2 \tag{6.3}$$

This equation is then minimised in an iterative fashion until an optimised parameter set for the material at the experimental conditions (stress and temperature) is obtained.

In order to obtain a global parameter set to satisfy parameter conditions across a range of temperatures, experimental data at different creep conditions is required. The Universal Sum of Squared Error (USSE) for the material can then be computed as:

$$USSE\ (p) = SSE_1(p) + SSE_2(p) + \cdots + SSE_N(p) \tag{6.4}$$

Where $1,2,N$ represent the SSE at various creep conditions. The $USSE(p)$ is then minimised in the same manner as explained earlier and a new parameter set is generated. Once again this procedure continues iteratively until the tolerance limits are met giving a material specific optimised parameter set across a range of creep conditions.

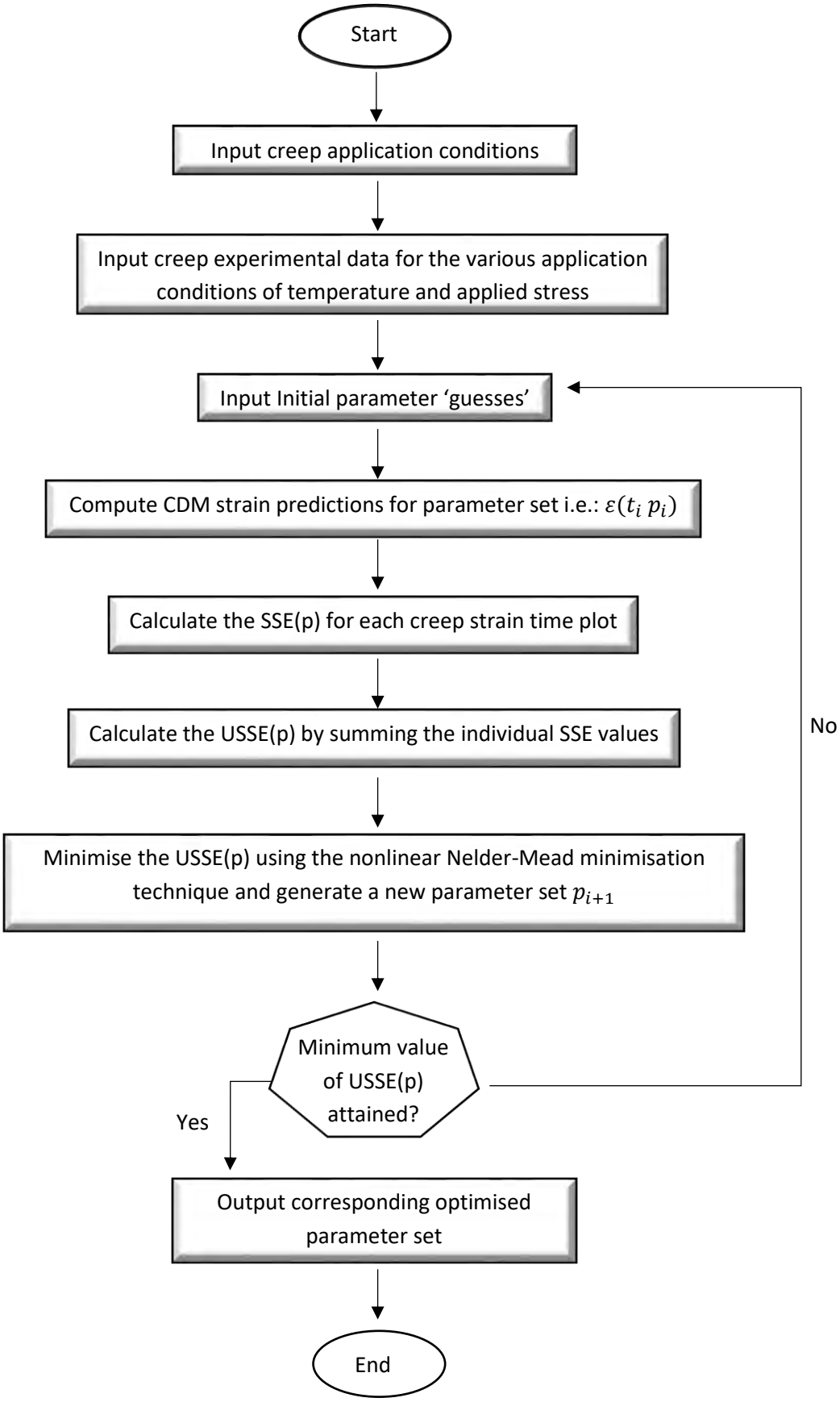

Figure 6-10: Flow chart of material parameter optimisation routine

Parameter optimisation was conducted for three different stress states, 75 MPa, 85MPa and 100 MPa for CB8 steel at a single temperature only. This was due to the availability of results of creep tests conducted at 650°C only (see section 4). These conditions were selected due to availability and reliability of experimental creep curves. Optimisation across stresses (by minimising the USSE(p)) as well as optimisation at a single stress (by minimising the SSE(p)) was conducted and analysed. Full source code can be found in appendix C2. The file: *Optiisation_multiple_stresses_CB8.m* initialises the optimisation routine capturing initial parameter guesses and creep conditions. Thereafter the objective function is calculated by running the CDM model loop (*myodefn_stress.m*) and calculating the SSE for each stress state and USSE for the stress range. The function *fminsearchbnd.m* then produces a new parameter set and the iterative routine continues.

6.1.4 *Accuracy Measurement Techniques*

6.1.4.1 Onset of Tertiary Creep

An important criterion required to measure the effectiveness of creep estimates is the accuracy to which it can predict the onset of tertiary creep. Tertiary creep for most 9-12% Cr steel applications signifies the end of the useful life of the component as material behaviour becomes increasingly unpredictable within this regime (see section 1.4). There exist two main techniques used to determine the onset of tertiary creep [67]:

1. Point of departure of the creep curve from the 'steady-state' secondary creep line (Figure 6-11 (a))
2. Point at which the 0.2% off-set strain intercepts the creep curve (Figure 6-11 (b))

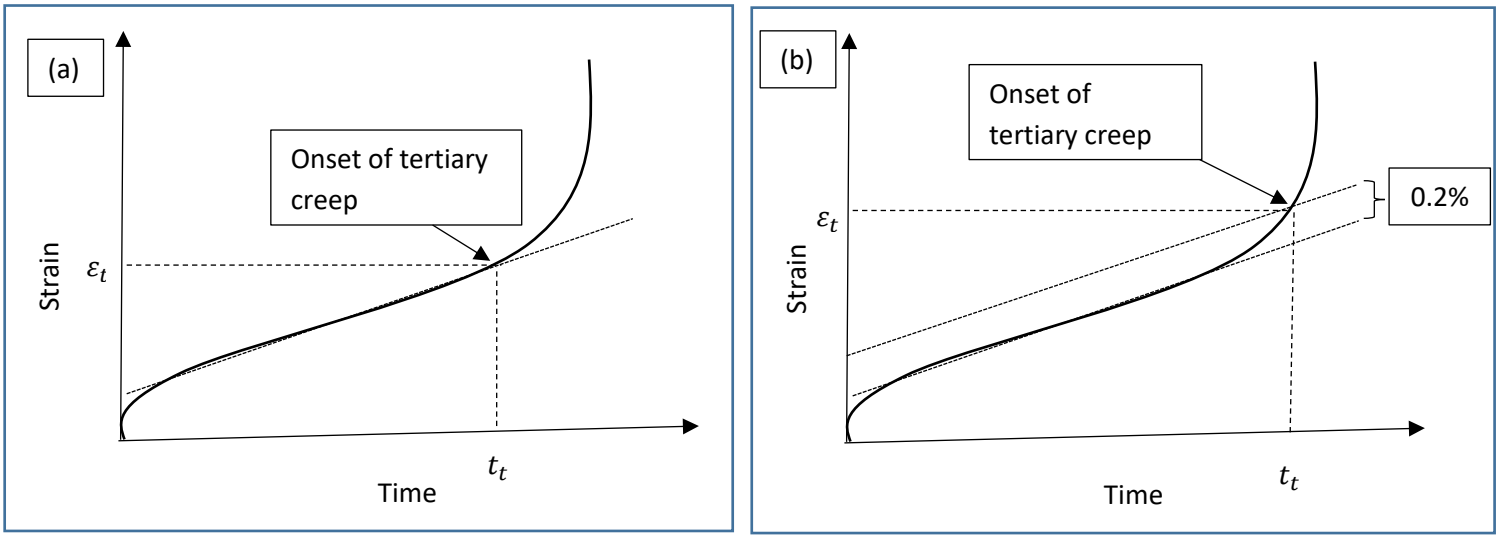

Figure 6-11 Method of determining the onset of tertiary creep using (a) the point of departure from steady state creep line and (b) the point at which the 0.2% off-set strain intercepts the creep curve

According to *Stark et al.* [67] the 0.2% offset method produces more reliable and consistent predictions of the onset of tertiary creep when compared against experimental observations. This approach was used in the current study as a means by which the prediction of the onset of tertiary creep could be compared to the experimentally obtained results. However, the conventional approach in determining the 0.2% offset strain and time (ε_t t_t) was adjusted for the current study in the

following way. Instead of assuming a steady state creep strain rate $\dot{\varepsilon}_{ss}$, the time at which the minimum creep rate $\dot{\varepsilon}_{min}$ occurred was used as the point at which the 0.2% strain was added. As $\dot{\varepsilon}_{ss}$, is an idealisation of secondary creep the preferred use of $\dot{\varepsilon}_{min}$ was based on the grounds of it being a more valid reflection of actual creep phenomena as explained in section 1.4.2.

$$t_t = t(\varepsilon_t) \tag{6.5-1}$$

$$\varepsilon_t = \varepsilon(t(\varepsilon_t)) + 0.2\% \tag{6.5-2}$$

$$t(\varepsilon_t) = t(\dot{\varepsilon}_{min}) \tag{6.5-3}$$

6.1.4.2 Minimum Creep Rate

The minimum creep rate $\dot{\varepsilon}_{min}$ and the time at which it occurs are commonly used measurements for secondary creep. The minimum creep rate represents the peak creep strength of a material and is used for creep life measurements such as the *Monkman-Grant* relationship. The time at which it occurs during creep loading is a direct indication of a material's creep resistance and is often used as a metric of remaining creep life. Figure 6-12 shows how the error between the predicted and experimentally observed time at which the minimum creep rate (Err_t) is obtained. This error is normalised by the time at which fracture occurs (t_f) giving:

$$Err_{min} = \left(\sqrt{\frac{Err_t}{t_f}}\right)^2 \tag{6.6}$$

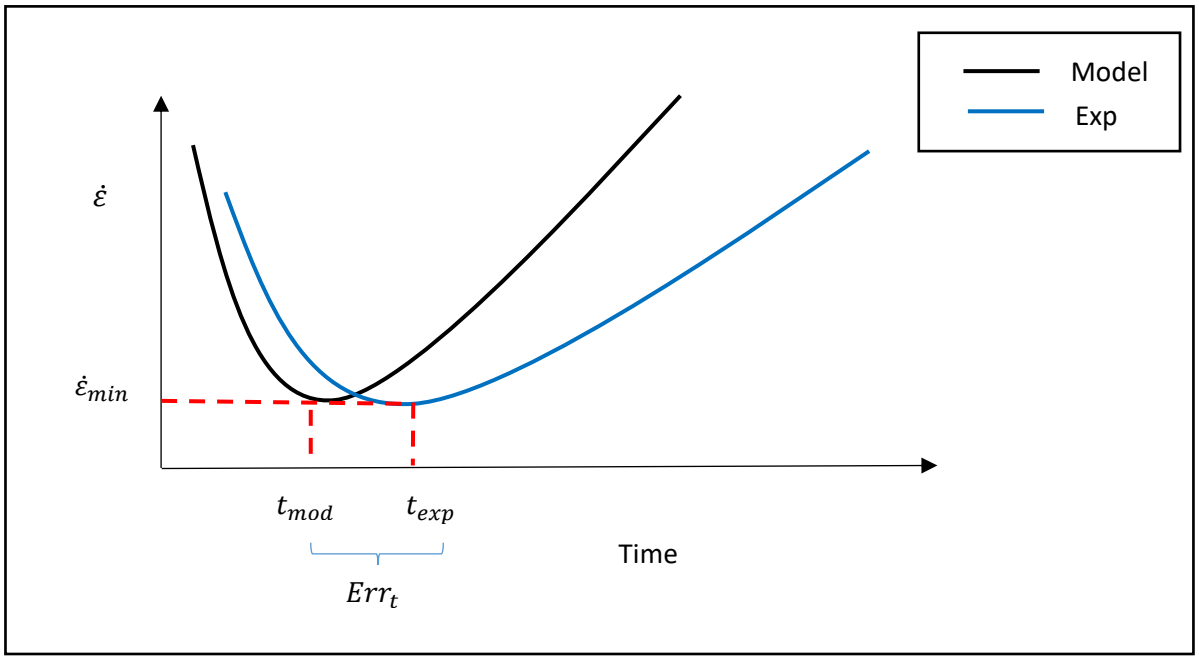

Figure 6-12: Schematic of error calculation between model prediction and experimental obtained creep curves for minimum creep rate

6.1.4.3 Time at 5% Strain

One of the difficulties in measuring creep prediction accuracy lies in the approximation of tertiary creep. While the primary and secondary creep stages exhibit high repeatability during creep tests, the tertiary creep stage can often be random and relatively unpredictable. This makes it difficult to ascertain the reliability of creep predictions of tertiary creep. However, for higher creep stresses (such as those typical of dislocation creep) tertiary creep becomes more predictable and a technique used by *Hore et al* [46] is to measure the accuracy to which the time at 5% strain is predicted. As the current study is focused on high creep stresses (75-104 MPa) this approach was adopted as a measure of tertiary creep prediction accuracy. Figure 6-13 shows how the error in the time at which 5% strain occurs ($Err_{t5\%}$) is determined. This error is normalised by the time at which fracture occurs (t_f) giving:

$$Err_{5\%} = \left(\sqrt{\frac{Err_{t5\%}}{t_f}} \right)^2 \tag{6.7}$$

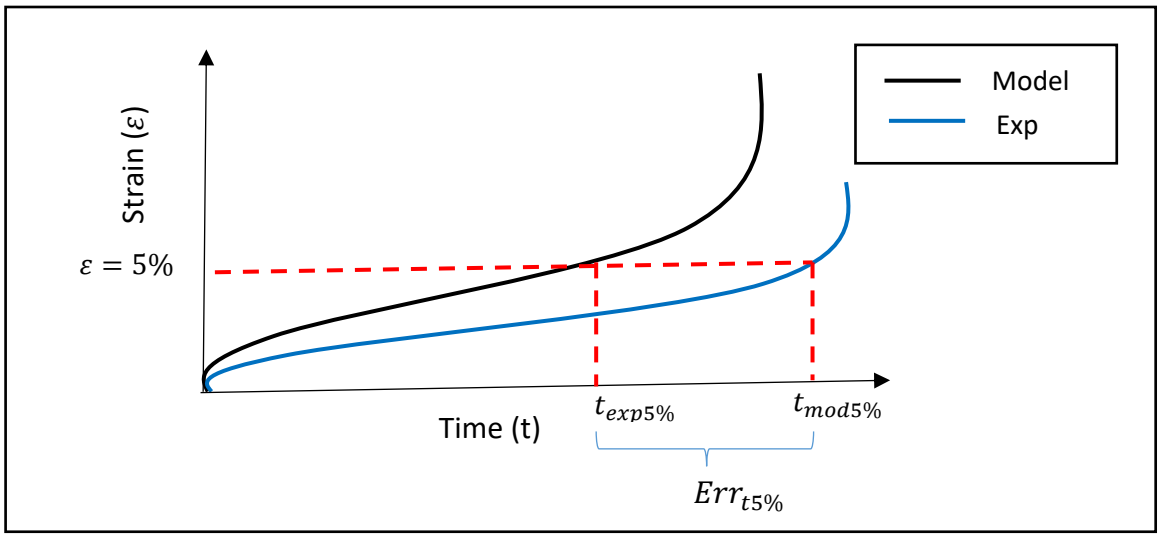

Figure 6-13: Schematic of error calculation between model prediction and experimental obtained creep curves for the time at which 5% strain is reached

6.1.5 *CB8 Optimisation across Stress Range*

The first optimisation attempt was made using creep deformation data (see section 4) at the three stress states (75, 85 and 100 MPa) for CB8 simultaneously until rupture. This was done in order to calculate the USSE(p) that is, the optimum parameter set across the stress range. If the model captures a true representation of the material's creep behaviour this optimisation should produce the 'best case results' across the stress range. Once the optimisation routine was complete, the optimised parameters were used in the CDM creep model for each stress state and the model output was compared with experimental creep data for CB8 at the different stresses.

6.1.5.1 Model Results from Optimisation against samples at stress states of 75, 85 and 100 MPa simultaneously until Rupture

Table 6-3: Table of optimised parameters for model optimisation against samples 8.96 at 75 MPa, 8.93 at 85 MPa, 8.74 at 100 MPa, 650 °C

Optimised Parameter	Recommended Range	Range Used	Initial Guess	Optimised Parameters
$\boldsymbol{Q_c}$ $\boldsymbol{(kJ/mol)}$		$290 - 340$	330.0	325
$\boldsymbol{\dot{\varepsilon}'_0}$ $\boldsymbol{(s^{-1})}$	$5 \times 10^6 - 5 \times 10^7$	$5 \times 10^6 - 5 \times 10^7$	4.84×10^7	1.8×10^7
$\boldsymbol{K_1}$ $\boldsymbol{(Pa)}$	$5 \times 10^9 - 1 \times 10^{10}$	$5 \times 10^9 - 1 \times 10^{10}$	7.14×10^9	5.3×10^9
$\boldsymbol{K_2}$ $\boldsymbol{(Pa)}$	$8 \times 10^6 - 1.5 \times 10^7$	$8 \times 10^6 - 1.5 \times 10^7$	1.17×10^7	1.5×10^7
$\boldsymbol{K_{S1}}$ $\boldsymbol{(ms^{-1})}$	$1 \times 10^{-6} - 1 \times 10^{-5}$	$1 \times 10^{-6} - 1 \times 10^{-5}$	7.1×10^{-6}	6.1×10^{-6}
$\boldsymbol{Ks_2'}$ $\boldsymbol{(ms^{-1})}$	$5 \times 10^{-7} - 5 \times 10^{-6}$	$5 \times 10^{-7} - 5 \times 10^{-6}$	6.0×10^{-6}	1.9×10^{-6}
$\boldsymbol{K_p}$ $\boldsymbol{(m^3 s^{-1})}$	$1 \times 10^{-29} - 1 \times 10^{-28}$	$1 \times 10^{-29} - 1 \times 10^{-28}$	6.0×10^{-29}	1.0×10^{-28}

Table 6-4: Table of Non-optimised parameters

Parameter	Value
$\boldsymbol{R}$ $\boldsymbol{(JK^{-1}mol^{-1})}$	8.314
$\boldsymbol{P_i(nm)}$	108
$\boldsymbol{S_i}$ $\boldsymbol{(\mu m)}$	0.7

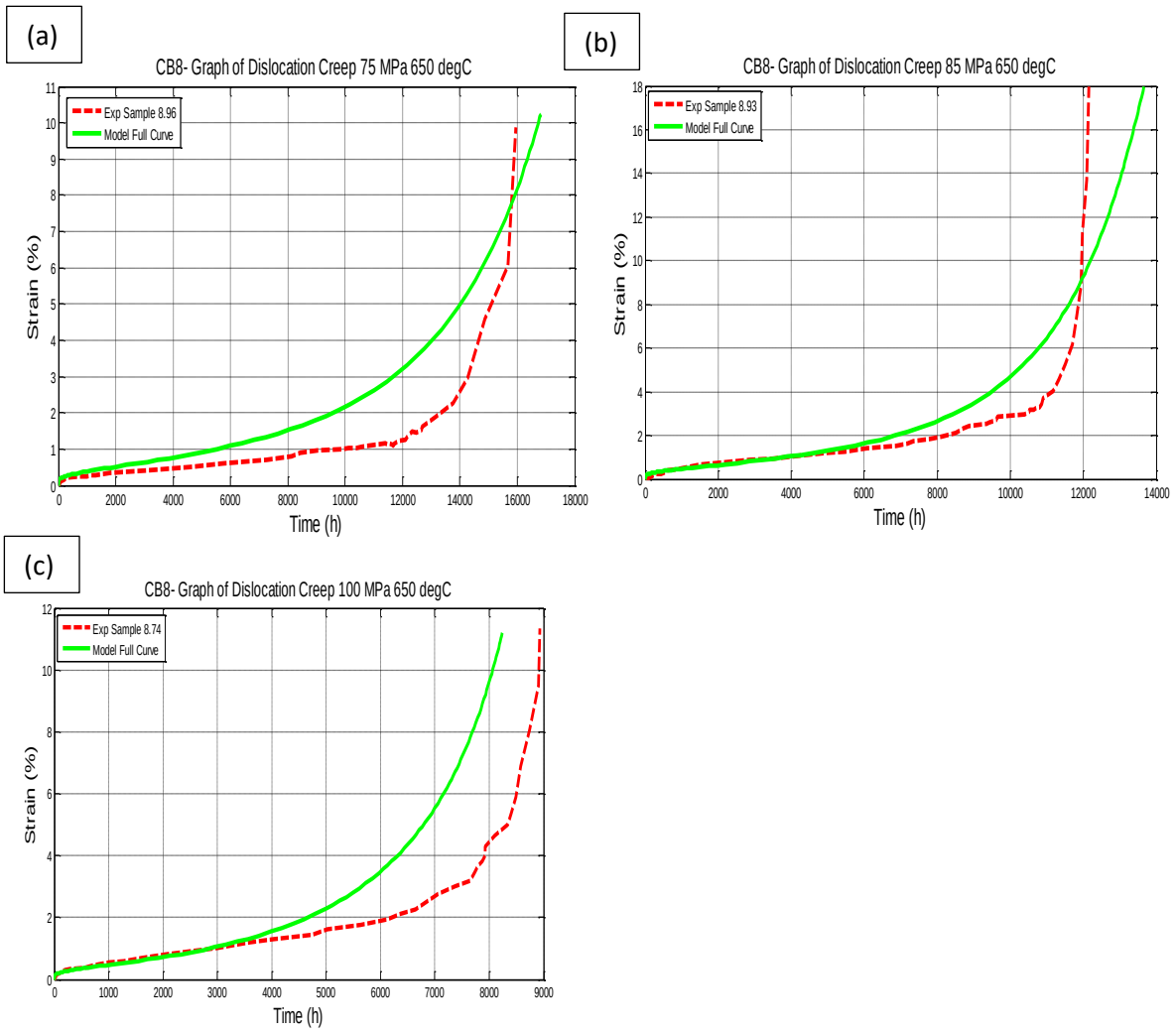

Figure 6-14: (a) Plot of 75 MPa, 650°C creep test for sample 8.96 with model result. Model parameters optimised across stress range (b) Plot of 85 MPa, 650°C creep test for sample 8.89 with optimised model result. Model parameters optimised at multiple stresses (c) Plot of 100 MPa, 650°C creep test for sample 8.74 with model result. Model parameters optimised at multiple stresses

The error between the creep-time model predictions and the experimental data was quantified using the methods outlined in section 6.1.4 for each sample. The results for the three error metrics namely the percentage error in the time at which the minimum creep rate occurs (Err_{min}), the time at which the onset of tertiary creep occurs (Err_{tr}) and the time at which 5% strain is reached (Err_{min}). Figure 6-15 shows a bar plot of the error measurements.

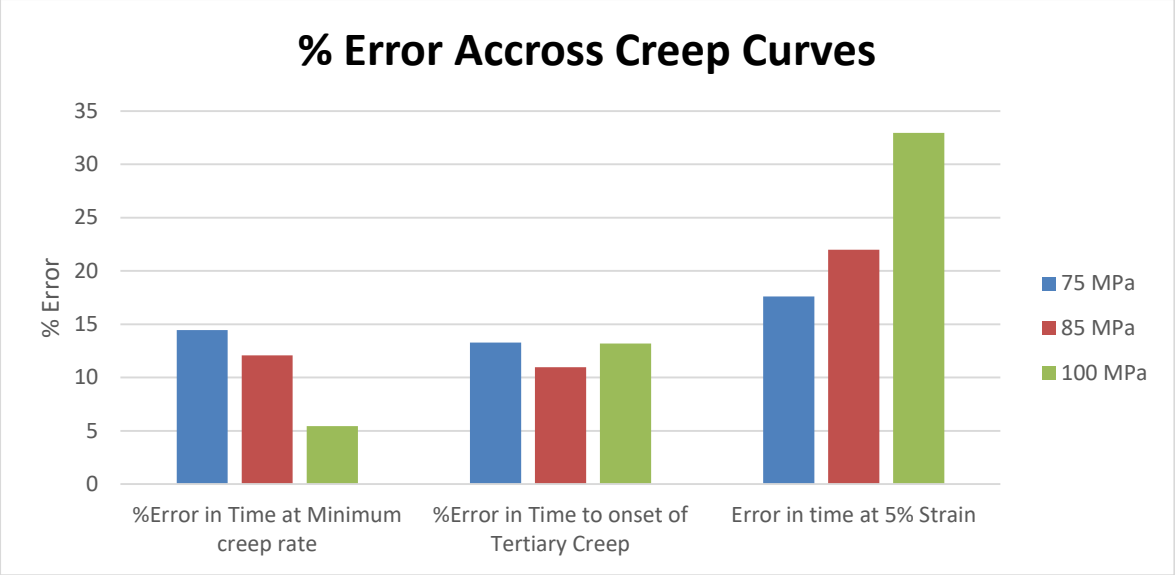

Figure 6-15 Plot of percentage error between model and experimental creep curves at the minimum strain rate, onset of tertiary creep and 5% strain for CB8

From the initial model optimisation against the experimental creep strain-time data at the three different stress states, it is apparent that the model predicts the creep life at all three stressed states relatively well through the primary and early secondary creep regions but loses accuracy in predicting tertiary creep. This is shown by the relatively low percentage error for Err_{min} and Err_{tr} when compared with the error for tertiary creep, $Err_{5\%}$. While values of Err_{min} and Err_{tr} fall below 15% for all stress state, the error values for $Err_{5\%}$ are approximately 17%, 22% and 33% for the stresses 75, 85 and 100 MPa respectively.

Based on the error calculations, it can be deduced that the most significant sources of error in the model's predictions occur in the final stages of creep leading to rupture. A possible cause of this error could be due to macrostructural necking clearly apparent in all the creep specimens and characterised by an almost instantaneous sharp increase in strain (see Figure 6-14). As these effects are not microstructurally based (the CDM approach is fundamentally a microstructural approach) optimising parameters against data which includes necking may distort the model's results.

6.1.6 *Multiple Stress Optimisation- Varying Strain Limit*

To overcome the problem of macrostructural necking distortion during parameter optimisation as explained in section 6.1.5.1, an attempt was made to limit the strains of the experimental creep-time data set against which optimisation was carried out. By limiting the strain of the creep data, the effects of necking could be negated leaving only the aspects of creep present during the creep tests dictating the optimisation of the creep parameters. The onset of necking occurs as a result of insufficient strain hardening causing the localised strain to propagate under higher localised stress. The presence of 'random' inhomogeneities within the specimen microstructure can accelerate the strain propagation leading to necking. Therefore, the onset of necking can be regarded in this context as a 'random' phenomenon. In order to account for the distortion due to necking a range of three different strain limits was used for parameter optimisation. The accumulated strains of 8%, 6% and 4% were chosen as conservative estimates based on observation of the experimental creep curves.

Table 6-5: Optimised parameter sets for various strain limits considered

Optimised Parameter	Full Creep Curve	8% Strain Limit	6% Strain Limit	4% strain Limit
$\boldsymbol{Q_c}\ (\boldsymbol{kJ/mol})$	325	338.0	334.0	340.0
$\boldsymbol{\dot{\varepsilon}'_0}\ (\boldsymbol{s^{-1}})$	1.8×10^{7}	4.2×10^{7}	4.0×10^{7}	5.0×10^{7}
$\boldsymbol{K_1}\ (\boldsymbol{Pa})$	5.3×10^{9}	5.0×10^{9}	7.1×10^{9}	5.0×10^{9}
$\boldsymbol{K_2'}\ (\boldsymbol{Pa})$	1.5×10^{7}	1.4×10^{7}	1.5×10^{7}	1.4×10^{7}
$\boldsymbol{K_{S1}}\ (\boldsymbol{ms^{-1}})$	6.1×10^{-6}	6.1×10^{-6}	6.2×10^{-6}	6.0×10^{-6}
$\boldsymbol{Ks_2}\ (\boldsymbol{ms^{-1}})$	1.9×10^{-6}	8.1×10^{-7}	9.5×10^{-7}	2.6×10^{-6}
$\boldsymbol{K_p'}\ (\boldsymbol{m^3 s^{-1}})$	1.0×10^{-28}	9.5×10^{-29}	9.5×10^{-29}	1.0×10^{-28}

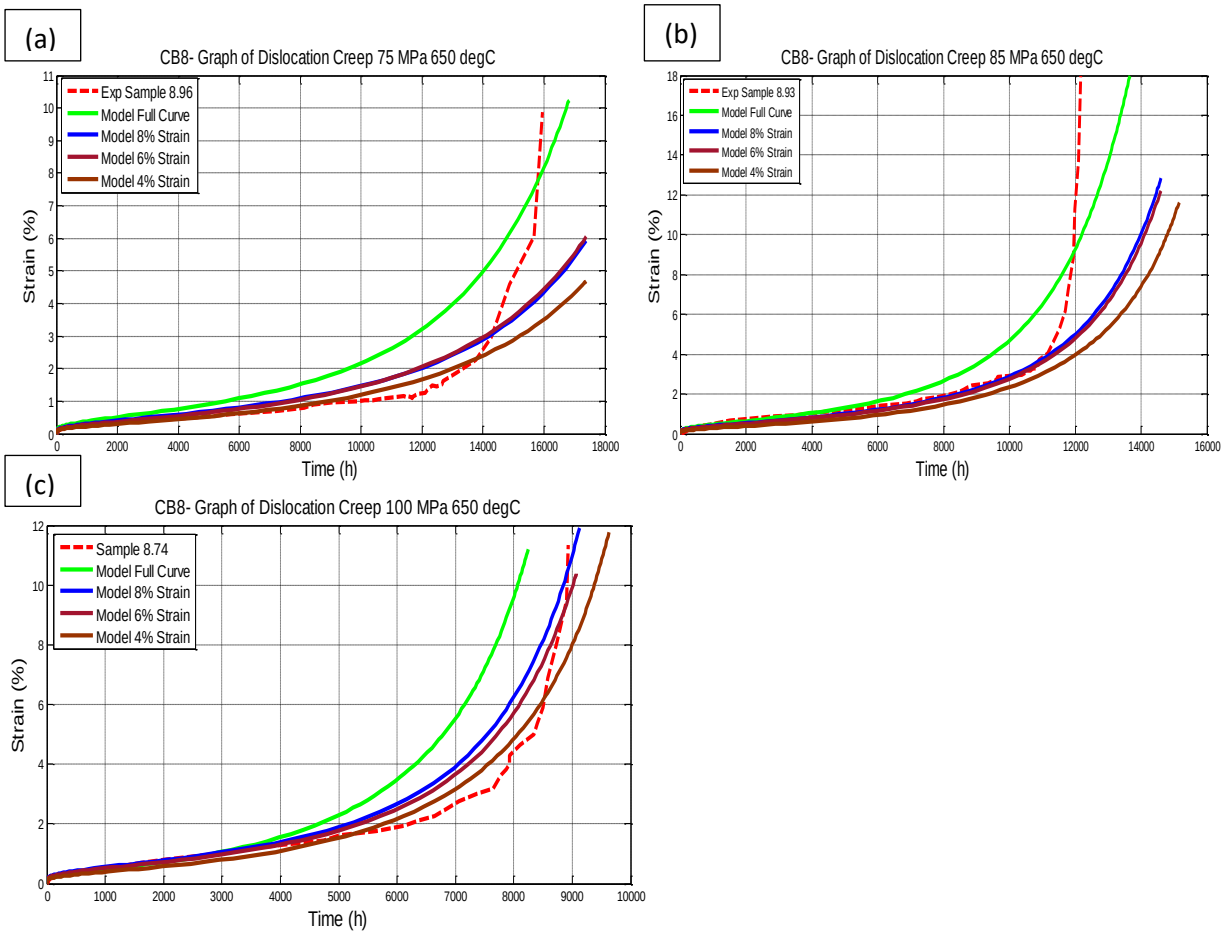

Figure 6-16:(a) Plot of 75 MPa, 650°C creep test for CB8 with model result. Model parameters optimised at multiple stresses up to rupture, 8%, 6% and 5% strain respectively (b) Plot of 85 MPa, 650°C creep test for CB8 with model result. Model parameters optimised at multiple stresses up to rupture, 8%, 6% and 5% strain respectively (c) Plot of 100 MPa, 650°C creep test for CB8 with model result. Model parameters optimised at multiple stresses up to rupture, 8%, 6% and 5% strain respectively

Figure 6-16 shows that adjusting the maximum accumulated strain against which the model is optimised has a profound effect on the model's creep strain predictions for each stress state. The model's results for the 75 MPa and 85 MPa appear to produce improved predictions for the primary and secondary creep stages as the maximum optimisation strain is reduced to 8%, 6% and 4% respectively. This is clearly illustrated in Figure 6-18 where a strain limit of 8% results in a reduction in Err_{min} of approximately 7% for the 75 MPa sample. The error remains approximately constant for the 6% and 4% strain limit conditions with Err_{min} values of 5%, 3% and 4% for the 75, 85 and 100 MPa stress condition respectively.

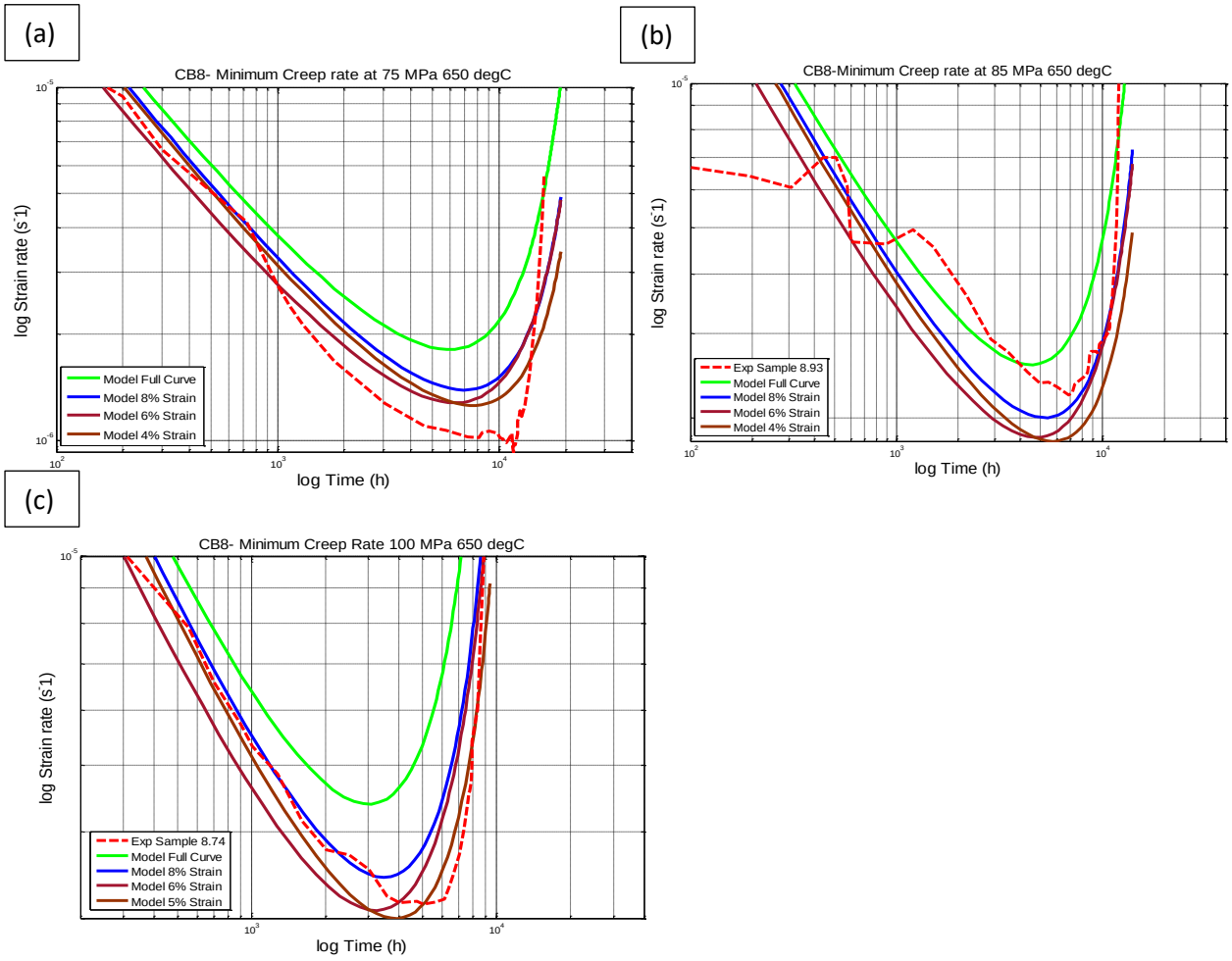

Figure 6-17:(a) Creep rate-time plot for CB8 at 75 MPa, 650°C with model result. Model parameters optimised at multiple stresses up to rupture, 8%, 6% and 5% strain respectively (b) Creep rate plot for CB8 at 85 MPa, 650°C with model result. Model parameters optimised at multiple stresses up to rupture, 8%, 6% and 5% strain respectively (c) Creep rate plot for CB8 at 100 MPa, 650°C with model result. Model parameters optimised at multiple stresses up to rupture, 8%, 6% and 5% strain respectively

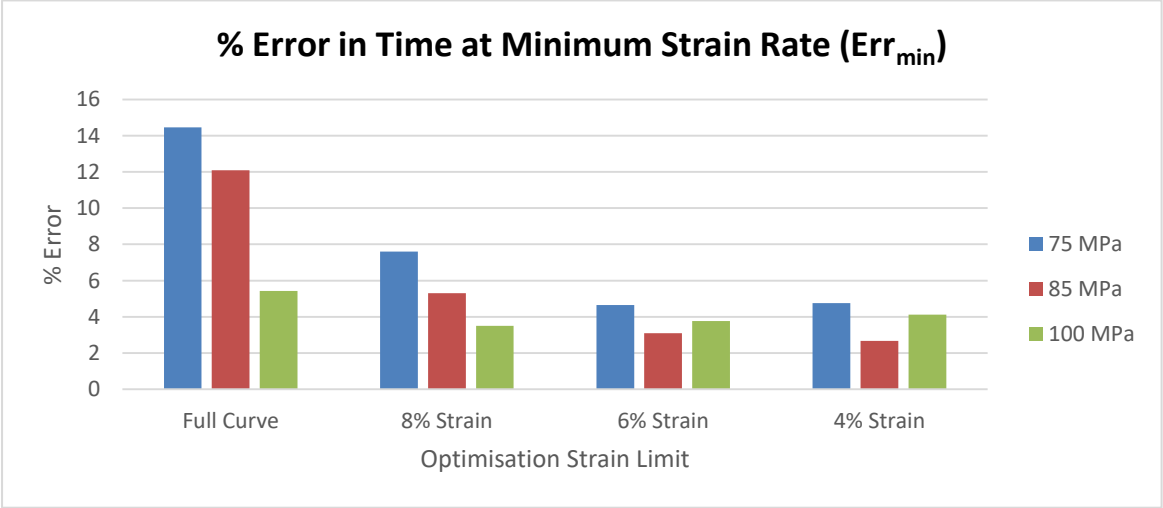

Figure 6-18: Graph illustrating error between experimental and model predictions of time at which the minimum strain rate occurs for various optimisation strain limits

The improvement in the prediction of the primary and secondary stages of creep comes at the expense of reduced accuracy in predicting tertiary creep and rupture time. This is clearly evident in Figure 6-16 (b) at 12 000h of creep exposure at 85 MPa. The predicted creep strain at this time is approximately 5% whereas the experimental creep plot indicates a strain of approximately 10%. Conversely, the predicted creep plots for the 100 MPa condition (Figure 6-16 (c)) shows a continuous improvement in creep prediction for the entire creep curve for decreasing strain optimisation limits.

In order to compare model predictions with experimental results during tertiary creep, the error in the time at 5% strain was compared as explained in section 6.1.4.3.

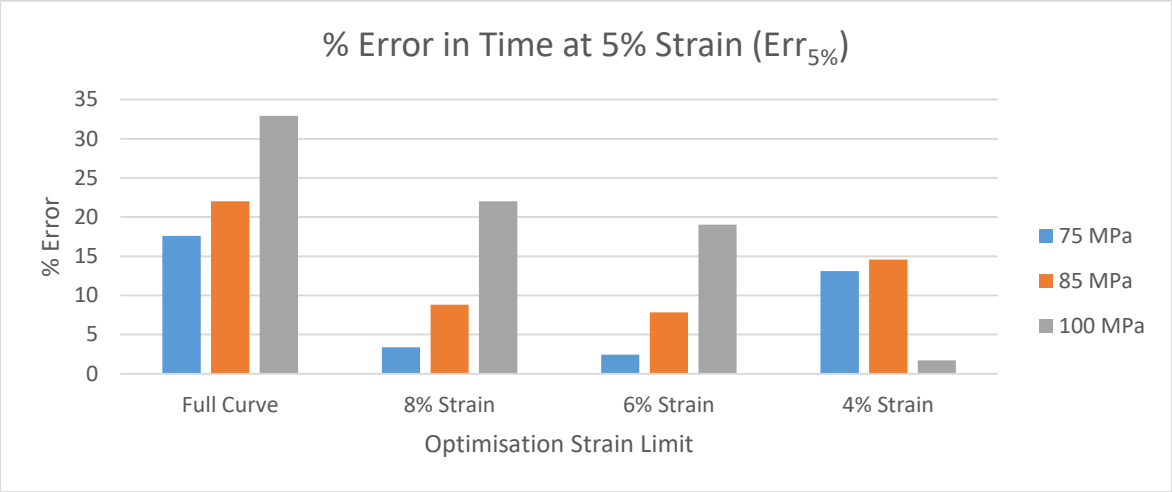

Figure 6-19: Graph illustrating error between experimental and model times to reach 5% strain for various optimisation strain limits

Figure 6-19 displays a clear trend in model accuracy with change in optimisation strain limit. Model predictions at 85 and 75 MPa show a significant improvement in model accuracy from optimisation against the entire creep curve to model predictions from optimisation with a 6% strain limit. As shown in Figure 6-19 the model's creep predictions from optimisation against the entire creep curve for 85 and 75 MPa produce an $Err_{5\%}$ of 22% and 17% respectively. However model predictions for the same stresses but optimised with a 6% strain limit produces $Err_{5\%}$ of 8% and 2% respectively. A clear improvement in model prediction is thus observed by reducing the optimisation strain limit. This trend reverses however once the maximum strain limit is reduced to 4% as indicated by an $Err_{5\%}$ of 13% and 14% for 75 and 85 MPa respectively

The 100 MPa model predictions show a significant increase in accuracy from optimisation against the entire creep curve to optimisation against creep curves with progressively lower strain limits (see Figure 6-19). The $Err_{5\%}$ value for the full creep curve optimisation is 33% and reduces to 2% when optimised with a 4% strain limit. While the accuracy of the model's creep predictions for all applied stresses shows improvement with a decreasing optimisation strain limit, the 100 MPa condition appears to behave anomalously in that it produces a minimum error for the 4% strain limit while the 85 and 75 MPa conditions display a minimum error for the 6% strain limit (see Figure 6-19)

Overall, the improvement in the model's creep prediction results when lower strain limits are used for parameter optimisation confirms that strain-time data towards the end of the creep curve due to macrostructural necking does distort optimisation results. It is also apparent that limiting the

maximum strain during optimisation is a simple and effective method of excluding the distortion effects of necking.

While imposing a limit on the maximum optimisation strain does improve prediction accuracy, the extent to which it does so, seems to depend on the stress conditions being analysed. While the 75 and 85 MPa stress conditions seem to behave similarly in this regard (with an optimal strain limit of 6%) the 100 MPa condition behaves differently. Also, while the 100 MPa stress condition shows improvement in prediction accuracy along the entire creep curve, the 75 and 85 MPa conditions seem to show improvement only until early, tertiary creep (see Figure 6-16). It is therefore, logical to conclude that the discrepancy due to different stress conditions lies in the tertiary creep stage.

6.1.7 *Optimising Parameters for Individual Stress Conditions*

In order to investigate the effects on the various parameters due to the different stress conditions, the parameter optimisation routine was run against experimental data for a single stress condition. That is, the parameter optimisation routine was set to produce a parameter set for a single SSE (see section 6.1.3). This was again done for different strain limits in order to analyse the effects of necking on the model's creep prediction accuracy. With each optimised parameter set the model's creep prediction capabilities were assessed by extrapolating to different stress conditions and comparing its results with the experimental strain-time data. Table 6-6 shows the optimised parameter sets for the various strains at 75 MPa.

6.1.7.1 Parameter Optimisation for CB8 at 75 MPa 650°C

Table 6-6 shows the results of the parameter optimisation carried out against the creep-time data for CB8 sample 8.96 at 75 MPa and 650°C.

Table 6-6: Optimised parameters for the 75 MPa stress condition for various optimisation strain limits

75 MPa Stress Condition				
Optimised Parameter	Full Creep Curve	8% Strain Limit	6% Strain Limit	4% strain Limit
$\boldsymbol{Q_c}$ $\boldsymbol{(kJ/mol)}$	340	339.0	330.0	337.0
$\boldsymbol{\dot{\varepsilon}'_0}$ $\boldsymbol{(s^{-1})}$	3.1×10^{7}	2.5×10^{7}	6.4×10^{6}	7.0×10^{6}
$\boldsymbol{K_1}$ $\boldsymbol{(Pa)}$	7.9×10^{9}	9.7×10^{9}	9.1×10^{9}	7.3×10^{9}
$\boldsymbol{K_2'}$ $\boldsymbol{(Pa)}$	1.2×10^{7}	1.2×10^{7}	1.4×10^{7}	1.3×10^{7}
$\boldsymbol{K_{S1}}$ $\boldsymbol{(ms^{-1})}$	1.1×10^{-6}	2.1×10^{-5}	5.8×10^{-5}	3.9×10^{-5}
$\boldsymbol{Ks_2}$ $\boldsymbol{(ms^{-1})}$	3.2×10^{-6}	5.9×10^{-7}	7.2×10^{-7}	4.5×10^{-6}
$\boldsymbol{K_p'}$ $\boldsymbol{(m^3 s^{-1})}$	9.3×10^{-29}	5.6×10^{-29}	9.6×10^{-29}	1.0×10^{-28}

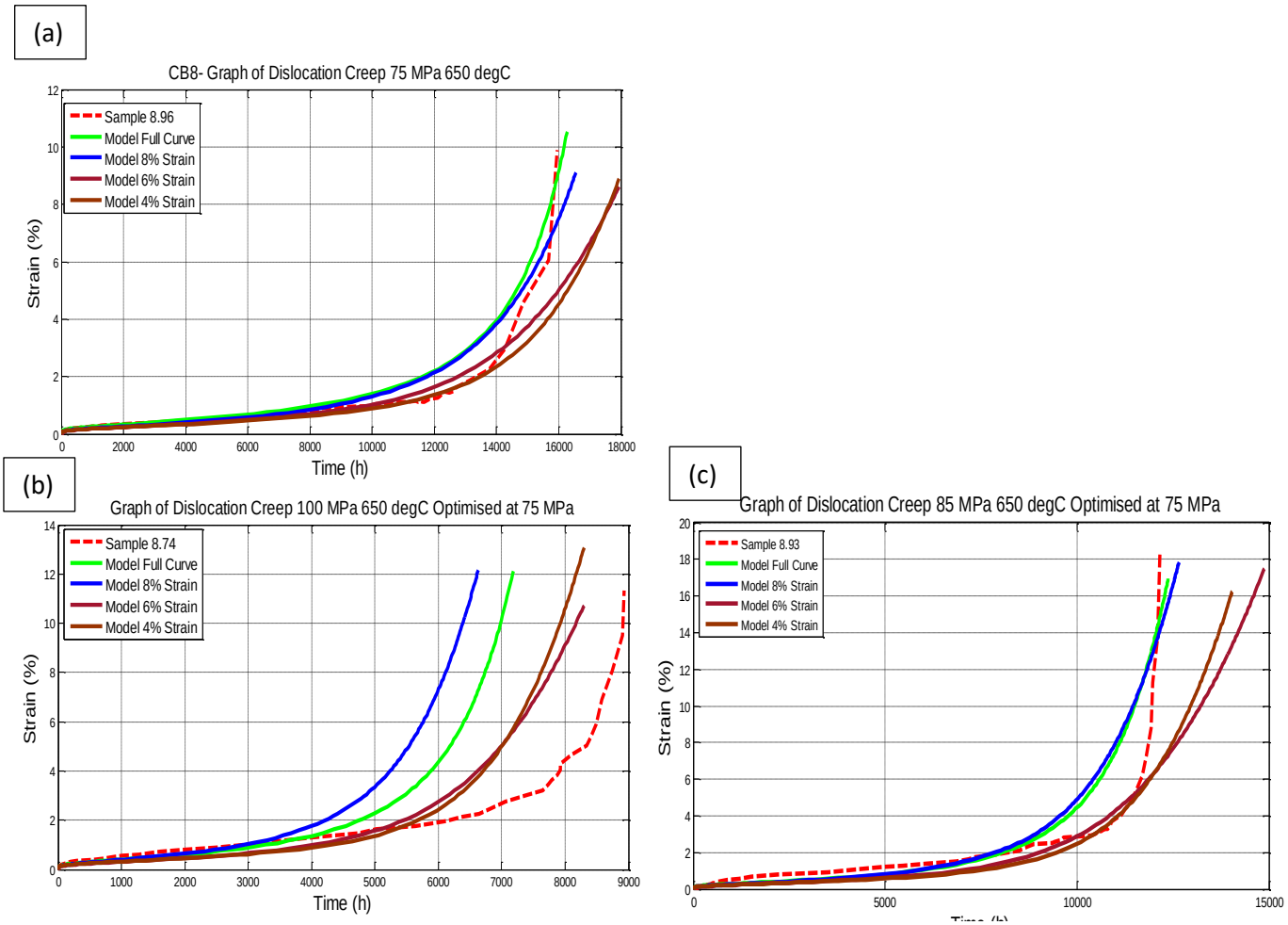

Figure 6-20(a) Plot of model's creep strain-time predictions for CB8 at 75 MPa optimised at 75 MPa against creep data up to various strain limits (b)) Plot of model's creep strain-time predictions for CB8 at 100 MPa optimised at 75 MPa against creep data up to various strain limits (c)) Plot of model's creep strain-time predictions for CB8 at 85 MPa optimised at 75 MPa against creep data up to various strain limits

Figure 6-20 (a) shows that as the strain limit for the parameter optimisation at 75 MPa is decreased to 6%, model predictions for the 75 MPa and 85 MPa (Figure 6-20 (c)) conditions improve for the entire creep curve up to the onset of necking. The 100 MPa stress condition also shows a significant improvement in model accuracy for the primary and secondary creep regions with a decrease in optimisation strain limit. However, even with an optimisation strain limit of 4% the model does not accurately represent the tertiary creep region and underestimates the sample's creep strength (Figure 6-20 (c)).

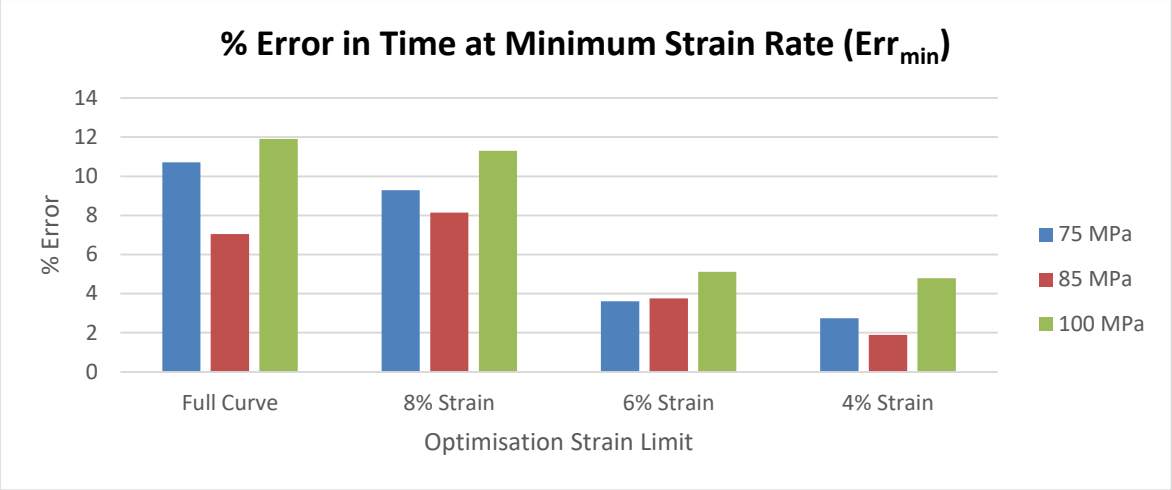

Figure 6-21: Graph illustrating error between experimental and model predictions of time at which the minimum strain rate occurs for various optimisation strain limits. Optimisation at 75 MPa, 650°C

Figure 6-21 illustrates the Err_{min} values for the three stress states with the SEE parameter set obtained from optimising against the 75 MPa test sample. Similarly to the results in section 6.1.6, the Err_{min} values drop significantly with a reduction in optimisation strain limit. The Err_{min} values drop from approximately 11%, 7% and 12% for the Full Curve to 3%, 2% and 5% with a 4% strain limit for the applied stresses of 75, 85 and 100 MPa respectively. This once again demonstrates the significant improvement in the models accuracy by negating any necking effects. Furthermore, the trend in the reduction in Err_{min} values is consistent across the stress range with the highest accuracy obtained for each stress with a 4% strain parameter limit.

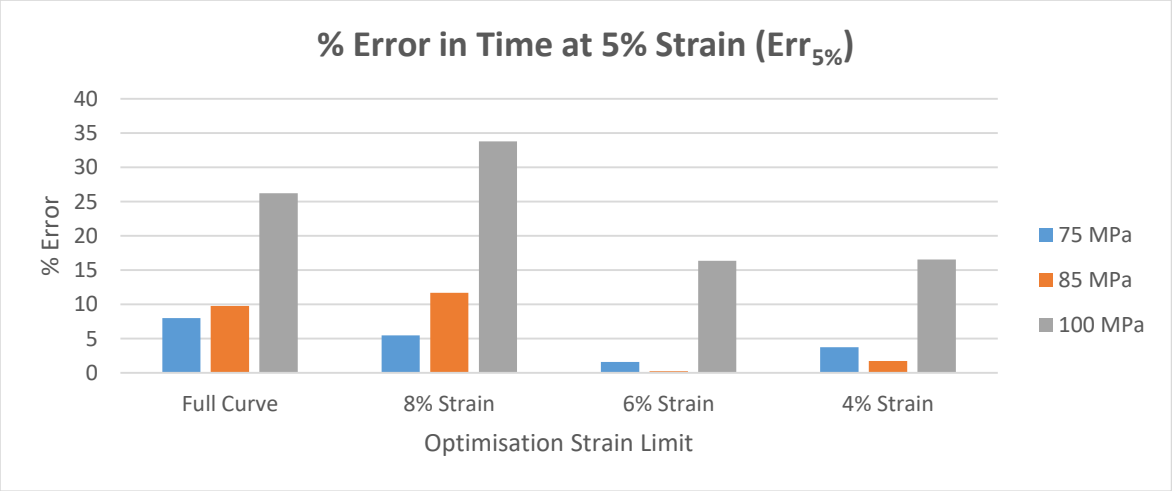

Figure 6-22: Graph illustrating error between experimental and model times to reach 5% strain for various optimisation strain limits. All optimisation carried out at 75 MPa

Figure 6-22 confirms that for the 75 MPa optimisation condition, there is an improvement in model accuracy in the prediction of the time at which 5% strain is reached. This is especially true for the 75 MPa and 85 MPa conditions with a $Err_{5\%}$ value falling well below 5% for the 6% strain limit parameter optimisation (Figure 6-22). While the 100 MPa condition does show a significant improvement in accuracy up to the 6% optimisation strain limit, the percentage error in the time to reach 5% strain does not fall below 15%.

6.1.7.2 Parameter Optimisation for CB8 at 85MPa 650°C

Table 6-7 shows the results of the parameter optimisation carried out against the creep-time data for CB8 sample 8.93 at 85 MPa and 650°C.

Table 6-7: Optimised parameters for the 85 MPa stress condition for various optimisation strain limits

85 MPa Stress Condition				
Optimised Parameter	Full Creep Curve	8% Strain Limit	6% Strain Limit	4% strain Limit
$\boldsymbol{Q_c}$ $\boldsymbol{(kJ/mol)}$	332	335.0	334.0	334.0
$\boldsymbol{\dot{\varepsilon}'_0}$ $\boldsymbol{(s^{-1})}$	4.3×10^{7}	1.2×10^{7}	2.5×10^{7}	4.4×10^{7}
$\boldsymbol{K_1}$ $\boldsymbol{(Pa)}$	7.1×10^{9}	9.3×10^{9}	6.0×10^{9}	5.0×10^{9}
$\boldsymbol{K_2'}$ $\boldsymbol{(Pa)}$	1.4×10^{7}	1.2×10^{7}	1.5×10^{7}	1.5×10^{7}
$\boldsymbol{K_{S1}}$ $\boldsymbol{(ms^{-1})}$	6.9×10^{-6}	1.4×10^{-5}	4.5×10^{-5}	9.2×10^{-6}
$\boldsymbol{Ks_2}$ $\boldsymbol{(ms^{-1})}$	1.0×10^{-6}	8.9×10^{-7}	1.2×10^{-6}	6.9×10^{-7}
$\boldsymbol{K_p'}$ $\boldsymbol{(m^3 s^{-1})}$	9.8×10^{-29}	7.9×10^{-29}	9.4×10^{-29}	7.5×10^{-29}

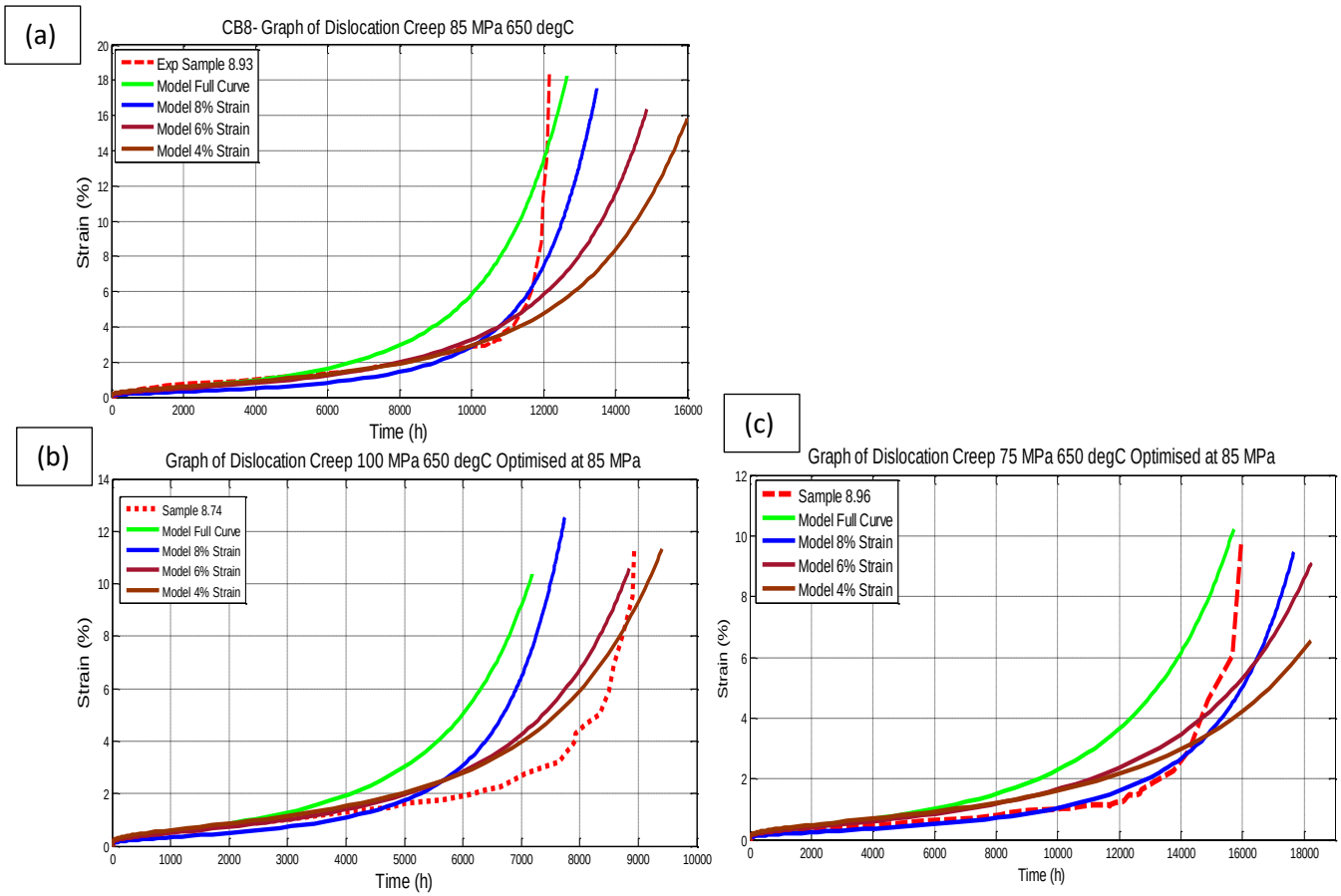

Figure 6-23(a) Plot of model's creep strain-time predictions for CB8 at 85 MPa optimised at 85 MPa against creep data up to various strain limits (b) Plot of model's creep strain-time predictions for CB8 at 100 MPa optimised at 85 MPa against creep data up to various strain limits (c) Plot of model's creep strain-time predictions for CB8 at 75 MPa optimised at 85 MPa against creep data up to various strain limits

The parameter optimisation done against the 85 MPa experimental data displays similar results to that done against the 75 MPa data. Once again, a decrease in strain limit during optimisation produces more reliable results when compared with experimental data. While it does show significant improvement in model accuracy with decreasing optimisation strain limit, the 100 MPa stress condition once again falls short of predicting the tertiary creep region accurately, tending rather to underestimate the creep strength of the material.

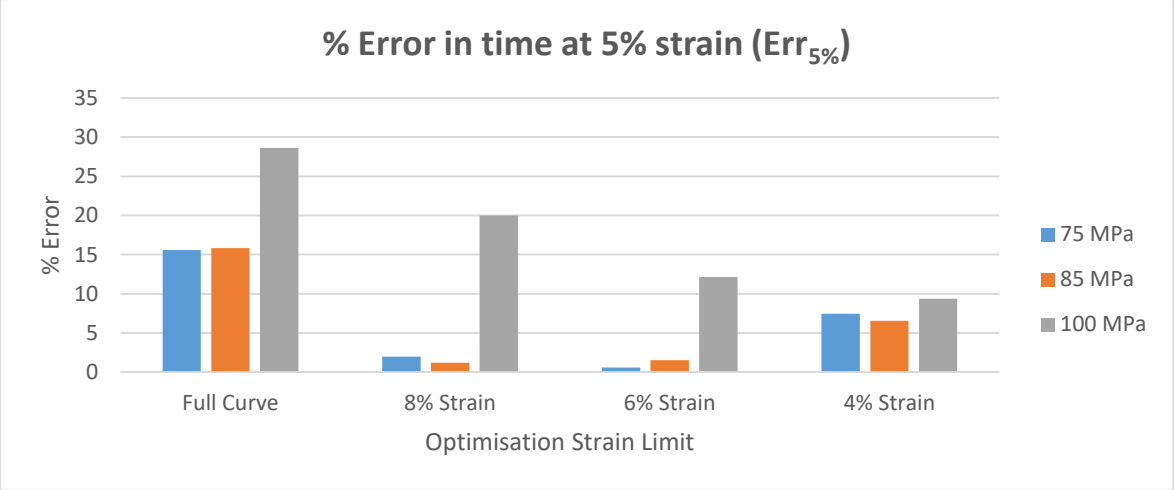

Figure 6-24: Graph illustrating error between experimental and model times to reach 5% strain for various optimisation strain limits. Optimisation carried out at 85 MPa

Figure 6-24 shows that the value of $Err_{5\%}$ decreases with decreasing strain limit for all applied stresses resulting in an increase in model accuracy. The extent to which the $Err_{5\%}$ decreases, differs between the different stress conditions. The 75 MPa and 85 MPa stress conditions behave similarly and display an initial sharp decrease in $Err_{5\%}$ when optimised with decreasing strain limit. The value of $Err_{5\%}$ then plateaus reaching a minimum with a 6% strain limit and $Err_{5\%}$ values of less than 2%. This is then followed by an increase in $Err_{5\%}$ for a strain limit of 4%. Conversely, the 100 MPa stress condition shows a continuous decrease in $Err_{5\%}$ with a minimum $Err_{5\%}$ value of 9% for the 4% strain limit condition.

6.1.7.3 Parameter Optimisation for CB8 at 100 MPa 650°C

Table 6-8 shows the results of the parameter optimisation carried out against the creep-time data for CB8 sample 8.74 at 100 MPa and 650°C.

Table 6-8: Optimised parameters for the 100 MPa stress condition for various optimisation strain limits

100 MPa Stress Condition				
Optimised Parameter	Full Creep Curve	8% Strain Limit	6% Strain Limit	4% strain Limit
$\boldsymbol{Q_c\ (kJ/mol)}$	339	340.0	340.0	340.0
$\boldsymbol{\dot{\varepsilon}'_0\ (s^{-1})}$	4.9×10^{7}	5.0×10^{7}	5.0×10^{7}	5.0×10^{7}
$\boldsymbol{K_1\ (Pa)}$	5.0×10^{9}	5.1×10^{9}	5.0×10^{9}	5.0×10^{9}
$\boldsymbol{K_2'\ (Pa)}$	1.4×10^{7}	1.5×10^{7}	1.5×10^{7}	1.5×10^{7}
$\boldsymbol{K_{S1}\ (ms^{-1})}$	6.1×10^{-6}	7.5×10^{-6}	6.0×10^{-6}	6.0×10^{-6}
$\boldsymbol{Ks_2\ (ms^{-1})}$	3.5×10^{-6}	4.9×10^{-6}	3.1×10^{-6}	2.3×10^{-6}
$\boldsymbol{K_p'\ (m^3 s^{-1})}$	9.9×10^{-29}	9.7×10^{-29}	1.0×10^{-28}	1.0×10^{-28}

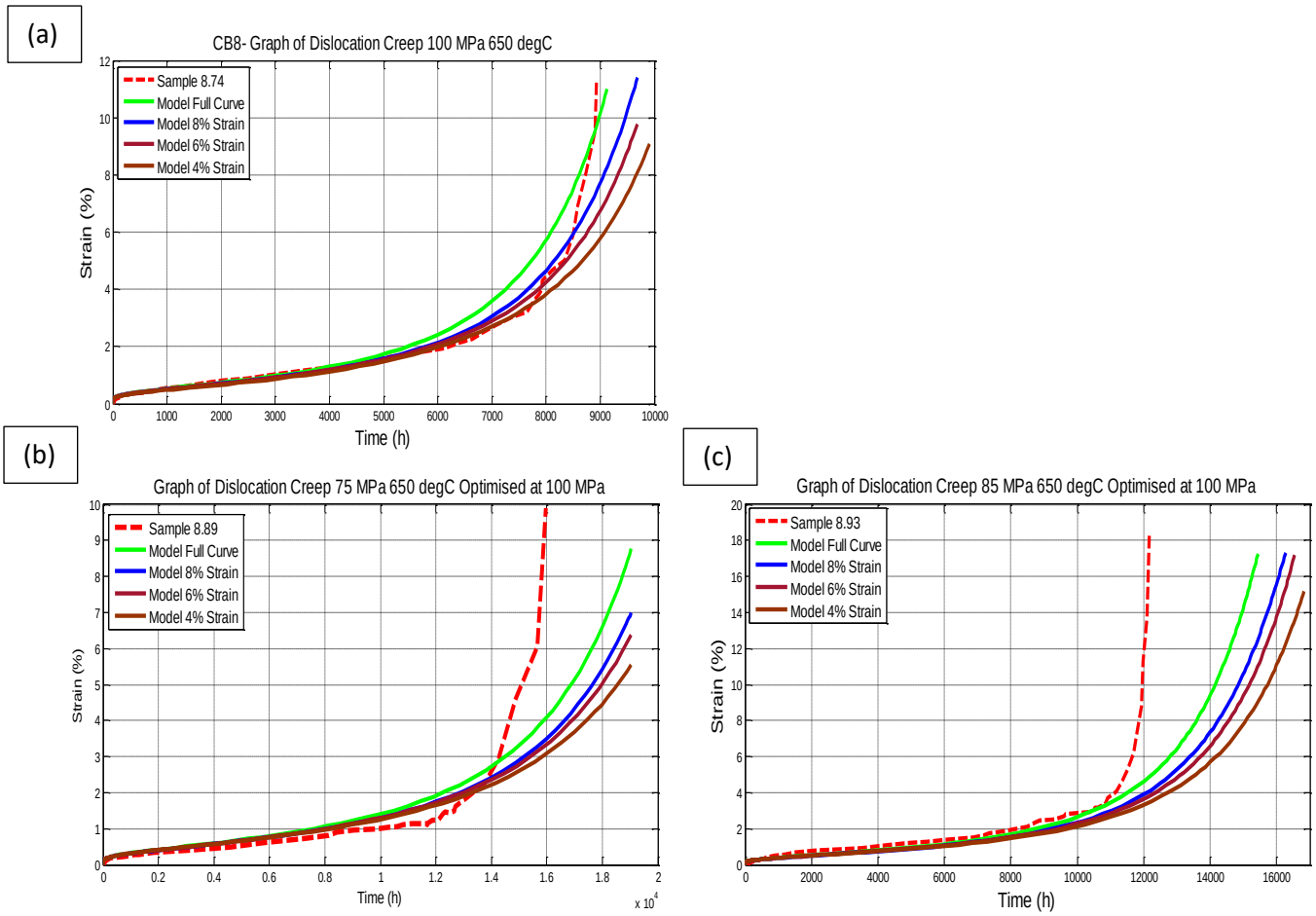

Figure 6-25(a) Plot of model's creep strain-time predictions for CB8 at 100 MPa optimised at 100 MPa against creep data up to various strain limits (b) Plot of model's creep strain-time predictions for CB8 at 75 MPa optimised at 100 MPa against creep data up to various strain limits (c) Plot of model's creep strain-time predictions for CB8 at 85 MPa optimised at 100 MPa against creep data up to various strain limits

Figure 6-25 (a) shows that when the parameter optimisation is carried out against data at 100 MPa, there is once again an improvement in creep prediction accuracy with a decrease in strain albeit slight. Contrary to previous results (optimisation at 75 and 85 MPa), this improvement does not extend to the other stress conditions (Figure 6-25 (b) & (c)). In fact, lowering the strain limit results in a decrease in model accuracy when extrapolated to the 75 and 85 MPa stress conditions.

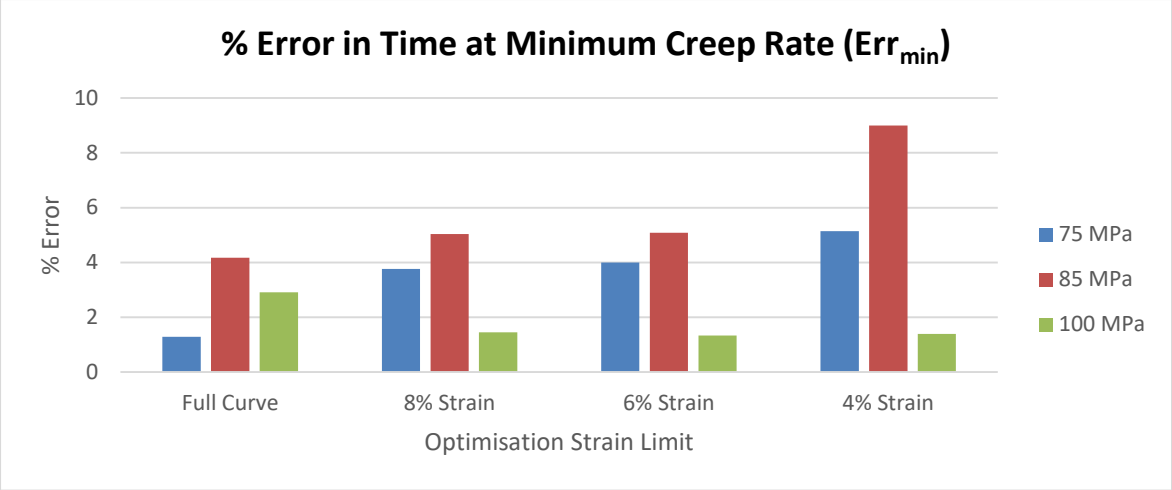

Figure 6-26: Graph illustrating error between experimental and model predictions of time at which the minimum strain rate occurs for various optimisation strain limits. Optimisation at 100 MPa, 650°C

Figure 6-27 shows the Err_{min} values for CB8 with model parameters optimised at 100 MPa. The figure shows that the accuracy behaviour of the various stress condition differs significantly with changes in optimisation strain limit. The 100 MPa condition shows a marked reduction in Err_{min} value from approximately 3% for the Full curve case, to below 2% with strain limits of 8%, 6% and 4%. Conversely, the Err_{min} values for the 75 and 85 MPa stress conditions show an increase in their Err_{min} values with decreasing strain limits.

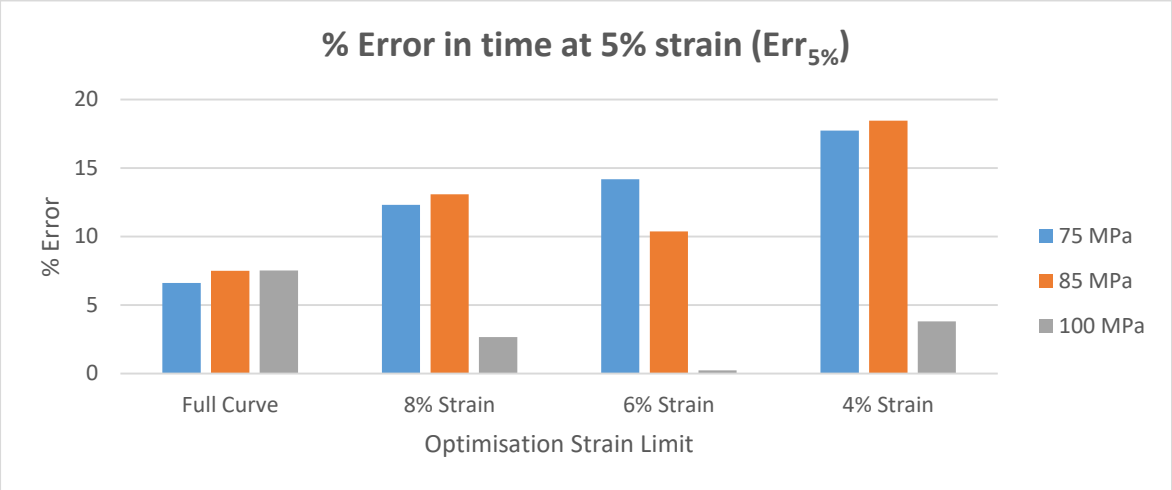

Figure 6-27: Graph illustrating error between experimental and model times to reach 5% strain for various optimisation strain limits. Optimisation carried out at 100 MPa

Figure 6-27 shows that similarly to the Err_{min} results, there is an increase in model accuracy with decreasing strain limit with regards to the $Err_{5\%}$ values for the 100 MPa condition only. This is illustrated by a reduction in the value of Err_{min} for the 100 MPa condition with decreasing strain limit. As the strain limit used for optimisation is decreased from the Full curve case to 6%, the error between the experimental and model prediction (Err_{min}) decreases drastically from approximately 7% to below 1%. However, this behaviour is reversed for the 75 and 85 MPa conditions where the model predictions deviate more from experimental results with decreasing optimisation strain limit. Figure

6-27 shows a large increase in Err_{min} from approximately 7% for the full creep curve condition to approximately 14% and 15% for the 6% strain limit at the 75 MPa and 85 MPa stress conditions respectively.

6.1.8 *Discussion of Individual Stress Optimisation Results*

From the optimisation results thus far it is clear that both the strain limit and stress condition for the experimental data against which parameter optimisation is carried out, have a significant impact in the model's creep-time prediction reliability. The former seems to improve the model's reliability when limited to approximately 6% creep strain. This improvement is most starkly observed when optimisation is carried out at either 75 or 85 MPa and extrapolated to the other (see Figure 6-20 & Figure 6-23). It can therefore be concluded that macrostructural necking observed in creep data does significantly distort the values of the optimised parameters and that its effects can be effectively diminished by reducing the strain limit during parameter optimisation.

Parameter optimisation carried out against the 100 MPa experimental data (section 6.1.7.3) seems to overestimate the material's creep strength when extrapolated downwards to the 75 and 85 MPa stress conditions and does so increasingly with a decrease in optimisation strain limit. Conversely, parameter optimisation carried out against either the 75 MPa (section 6.1.7.1) or 85 MPa (section 6.1.7.2) experimental creep-time data tends to underestimate the material's creep strength when extrapolated upwards to 100 MPa. There is therefore a clear disconnect between predicted and experimental creep results which cannot be attributed to macrostructural necking. Moreover, this inaccuracy seems to exist mostly in the prediction of the tertiary stage of creep and its point of onset. This is clearly illustrated in Figure 6-28 where the results extrapolated between 85 MPa and 75 MPa produce Err_{tr} values of less than 2% whereas the extrapolation to the 100 MPa stress condition results in Err_{tr} values of up to 8%.

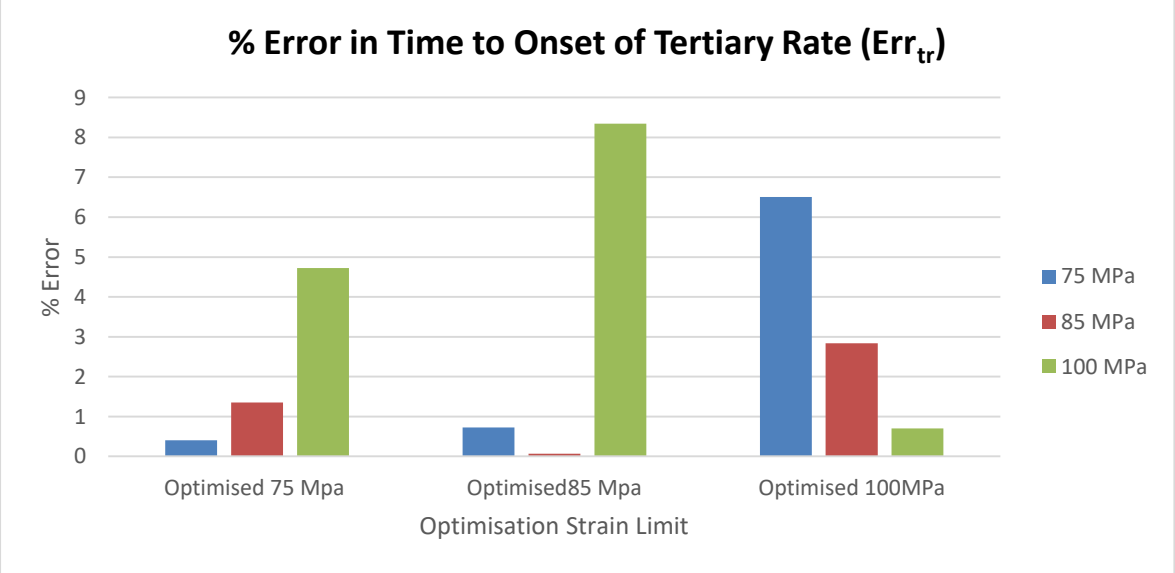

Figure 6-28: Plot of errors between model and experimental predictions for the time of onset of tertiary creep (Err_{tr}) for various optimisation stress conditions

The primary and secondary stages of creep seem to be accurately represented across the stress range by the model when optimisation is carried out at either 75 or 85 MPa with a strain limit of 6%. Once again, optimisation carried out against the 100 MPa sample produces anomalous results as shown in section 6.1.7.3, where a reduction in strain limit results in an increase in Err_{min} when extrapolated to the 75 and 85 MPa stress conditions. As the parameter optimisation in this context can be interpreted as a model calibration, a discrepancy between optimised and extrapolated results can be attributed to differences in material properties at the different stress states. Since the material properties considered in this model are all microstructurally based, it is likely that the microstructural evolution at 100 MPa differs from that at 75 and 85 MPa specifically within the tertiary creep region.

Table 6-9: Summary of individual stress optimisation and extrapolation results

Optimisation Stress	Extrapolated Stress MPa					
	75		85		100	
	Secondary creep (Err_{min})	Tertiary Creep ($Err_{5\%}$)	Secondary creep (Err_{min})	Tertiary Creep ($Err_{5\%}$)	Secondary creep (Err_{min})	Tertiary Creep ($Err_{5\%}$)
75 (6% Strain Limit)	2.7	1.6	1.9	0.3	4.8	16.3 (Underestimate of creep strength)
85 (6% Strain Limit)	1.9	0.6	1.6	1.5	3.3	12.1 (Underestimate of creep strength)
100 (6% Strain Limit)	4.0	14 (Overestimate of creep strength)	5.1	10.3 (Overestimate of creep strength)	1.3	0.2

If it is assumed that a microstructural effect is responsible for the lack of consistency in the results extrapolated to and from the 100 MPa condition, it is then logical to conclude that it only has an effect in the later stages of creep in CB8. Further, since the extrapolation 'downwards' from the 100MPa optimised condition results in an overestimation of creep strength it can be surmised that this microstructural change manifests itself as a loss of creep strength in the long term. This assumption is further reinforced by the underestimation of creep strength observed when parameter optimisation is carried out at 75 or 85 MPa and extrapolated 'upwards' to the 100 MPa condition.

A closer examination of the experimental creep-time plots for the 75, 85 and 100 MPa samples, as shown in Figure 6-29 provides some insight into the possible discrepancy in the observed results. An

important consideration is the rupture times of the respective samples. The 100 MPa sample ruptures after approximately 9000h of creep exposure while the 85 MPa and 75 MPa samples rupture after approximately 12000h and 16000h respectively. The sample set can therefore be divided into two groups; those which rupture prior to 10000h of creep exposure and those which rupture after 10000h. The significance of the 10000h mark lies in its observed correlation with microstructural changes in 9-12% Cr steels and specifically the precipitation of the Modified Z-Phase (see section 2.2.4). In a detailed study by *Danielsen et al.* [29] the precipitation of the Modified Z-phase was only found to occur in 9-12% Cr steels after 10000h of creep exposure at 650°C. Furthermore, the authors reported that this was only the case for steels with a Cr content exceeding approximately 11%. As CB8 has a Cr content of 10.9% (see chapter 4), the precipitation of the Modified Z-phase is likely.

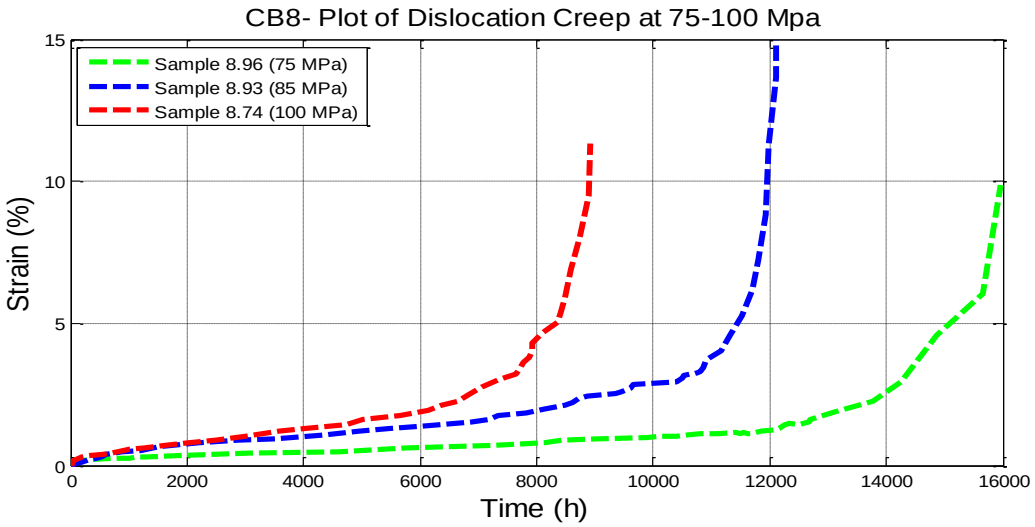

Figure 6-29: Long term creep time plots for CB8 at with applied stresses of 75, 85 and 100 MPa and temperature of 650°C

This seems to offer a credible explanation for the observed results. The apparent loss in creep strength and resulting overestimation of creep strength when model extrapolation is carried out from the 100 MPa calibration condition (rupture time below 10000h) to the 85 and 75 MPa conditions (rupture time above 10000h) seems to agree well with the precipitation of the Modified Z-phase and its resulting effects.

6.1.9 *Microstructure Results*

Along with strain time data, the current CDM model produces microstructural predictions for subgrain and $M_{23}C_6$ precipitate growth and coarsening. These results were compared to experimentally determined results for CB8 (see section 0). The experimental results were obtained from interrupted creep tests at 75 MPa and 650°C. The microstructural results were obtained after parameter optimisation against creep strain-time data. In that way, the model's microstructural predictions are obtained directly from mechanical creep data.

6.1.9.1 Subgrain Coarsening

Figure 6-30 shows model and experimental results of subgrain size during creep. The model results are displayed for parameter optimisation carried out at stresses of 75, 85 and 100 MPa and extrapolated to 75 MPa. The error in the experimental measurements was taken as 200nm based on the spatial resolution of the measurement technique used (see section 4).

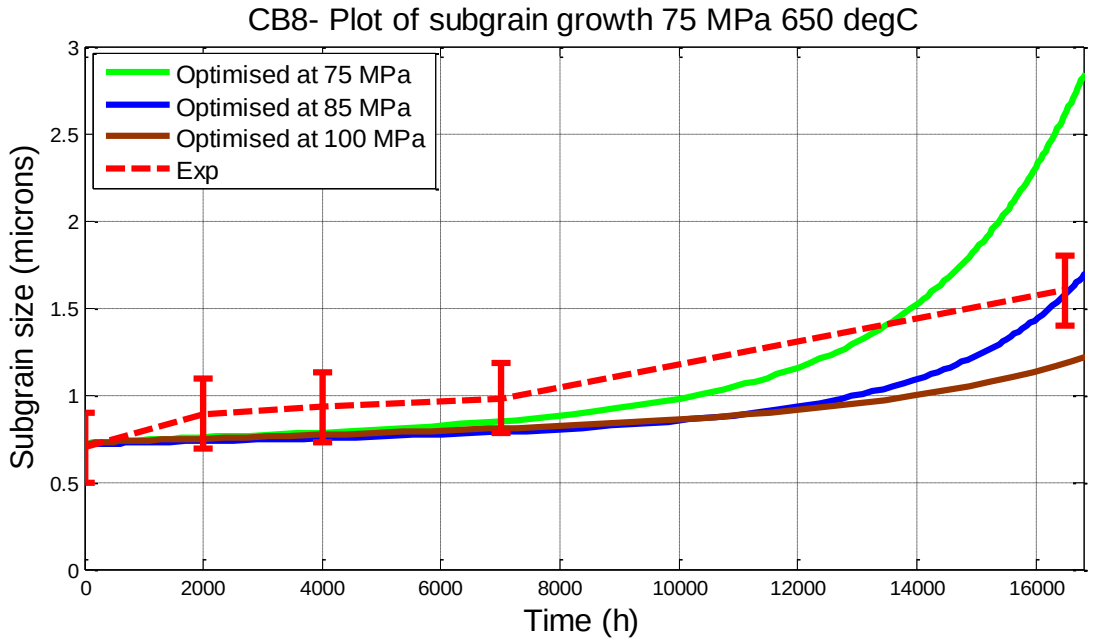

Figure 6-30: Experimental (see Appendix A-1) and model predicted plot of average subgrain diameter for CB8 during creep exposure at 75 MPa 650°C. Model results shown for parameter optimisation carried out at 75, 85 and 100 MPa

The results show that the CDM model is capable of producing predictions of subgrain size during creep within acceptable limits within the primary and secondary creep stages regardless of optimisation stress. The error apparent in the primary and secondary creep stages (up tp appox. 11000h) appears to be constant suggesting that it may be an offset error possibly due to an inaccurate initial reading. This seems to be the case for optimisation carried out at all stresses. The tertiary creep results however appear to lie outside the error margins for both the 75 MPa and 100 MPa optimisations with the former overestimating the coarsening rate and the latter underestimating it. The results optimised at 85 MPa on the other hand lie within the acceptable error even at the later stages of tertiary creep.

6.1.9.2 Discussion of Subgrain Coarsening Results

The subgrain coarsening results appear to produce consistently accurate approximations of subgrain coarsening in CB8 particularly within the primary and secondary creep regime. As subgrain coarsening is a strain dependent phenomenon and has been considered as such in the current model, it is

intrinsically coupled with every other creep property investigated including back stress evolution and $M_{23}C_6$ precipitate coarsening. This makes the results all the more impressive and suggests that the description of subgrain coarsening used as well as its relationship to dislocation creep has been effectively captured by the CDM model.

The error between the model and experimental curves within the tertiary creep stage seems to mirror the errors observed for the creep strain-time curves. In particular the results for the parameter set optimised at 75 MPa overestimate the subgrain size above 14000h.

6.1.9.3 $M_{23}C_6$ Precipitate Coarsening

In addition to subgrain coarsening, the model used in this study also produces predictions of $M_{23}C_6$ precipitate coarsening. These results are expressed as precipitate diameter over time. The model results are essentially precipitate measurements obtained from mechanical creep-time data via the CDM relationships explained in section 5. Figure 6-31 shows the model results as well as experimental $M_{23}C_6$ coarsening data for CB8 at 75 MPa and 650°C. The model results are shown for parameter optimisation carried out at 75, 85 and 100 MPa.

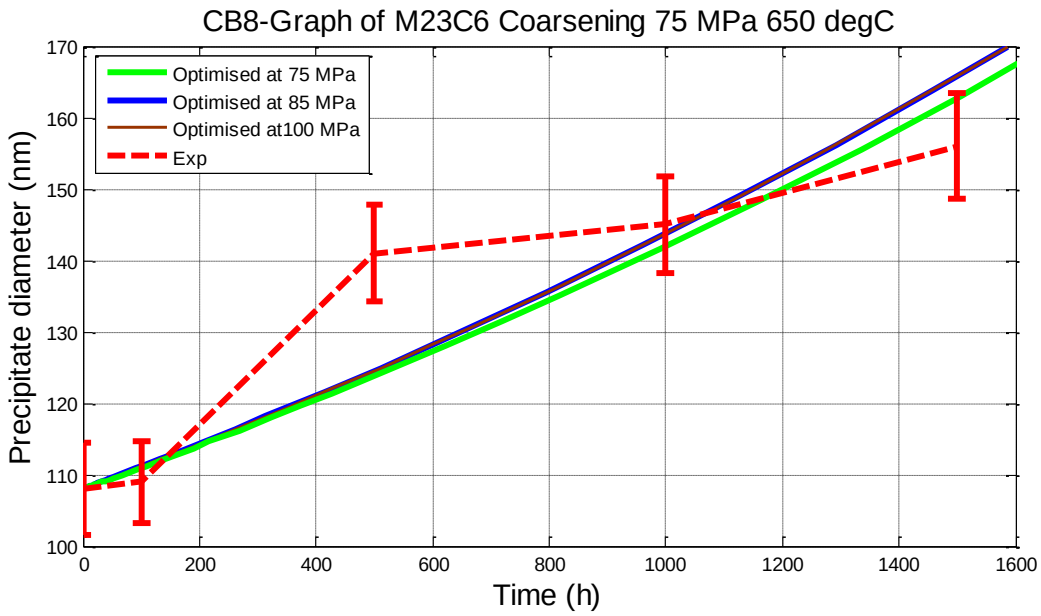

Figure 6-31: Experimental and model predicted plot of $M_{23}C_6$ average diameter for CB8 during creep exposure at 75 MPa 650°C. Model results shown for parameter optimisation carried out at 75, 85 and 100 MPa

7 P92-Model Results

One of the aims of this project is to produce a physically based dislocation creep model for 9-12% Cr steels. While it is impossible to verify unconditionally that this model can be applied to all 9-12% Cr steels, it can be substantiated by application to more than one type of 9-12% Cr steel. The model's applicability to different 9-12% Cr steels can then to some extent be validated.

After producing successful strain-time results for the steel CB8 with 11% Cr content, the CDM model used in this study was applied to the 9% Cr steel P92. The model results were optimised at 92 MPa and 104 MPa stress conditions at a temperature of 650°C. The optimised parameters used for CB8 were used as initial parameter guesses. This was done to assess the degree to which initial parameter guesses could be applied to different types of 9-12% Cr steels. The initial subgrain size S_i and $M_{23}C_6$diameter P_i were obtained from *Ennis et al*.[54] for P92.

Table 7-1: Optimised Parameter set for P92 Steel

Optimised Parameter	Full Creep Curve	11% Strain Limit	8% Strain Limit	6% strain Limit
$\boldsymbol{Q_c\ (kJ/mol)}$	331	328	340	314
$\boldsymbol{\dot{\varepsilon}'_0\ (s^{-1})}$	4.9×10^{7}	5.4×10^{6}	4.2×10^{7}	1.1×10^{7}
$\boldsymbol{K_1\ (Pa)}$	1.0×10^{10}	5.0×10^{9}	5.2×10^{9}	5.1×10^{9}
$\boldsymbol{K_2'\ (Pa)}$	1.5×10^{7}	1.0×10^{7}	1.1×10^{7}	1.5×10^{7}
$\boldsymbol{K_{S1}\ (ms^{-1})}$	5.9×10^{-5}	9.5×10^{-6}	7.5×10^{-6}	6.5×10^{-6}
$\boldsymbol{Ks_2\ (ms^{-1})}$	1.9×10^{-6}	9.4×10^{-7}	2.0×10^{-6}	5.1×10^{-6}
$\boldsymbol{K_p'\ (m^3s^{-1})}$	1.0×10^{-29}	1.1×10^{-29}	1.0×10^{-29}	1.0×10^{-28}

Table 7-2: Initial parameter values for P92 steel

Parameter	Initial Value
$\boldsymbol{\dot{\varepsilon}\ (s^{-1})}$	0
$\boldsymbol{\dot{\sigma}_0\ (MPa)}$	2
$\boldsymbol{\dot{D}_s}$	0
$\boldsymbol{\dot{H}^*}$	0.4
$\boldsymbol{\dot{D}_p}$	0
$\boldsymbol{S(\mu m)}$	0.79 Ref. [54]
$\boldsymbol{P(nm)}$	95 Ref. [54]

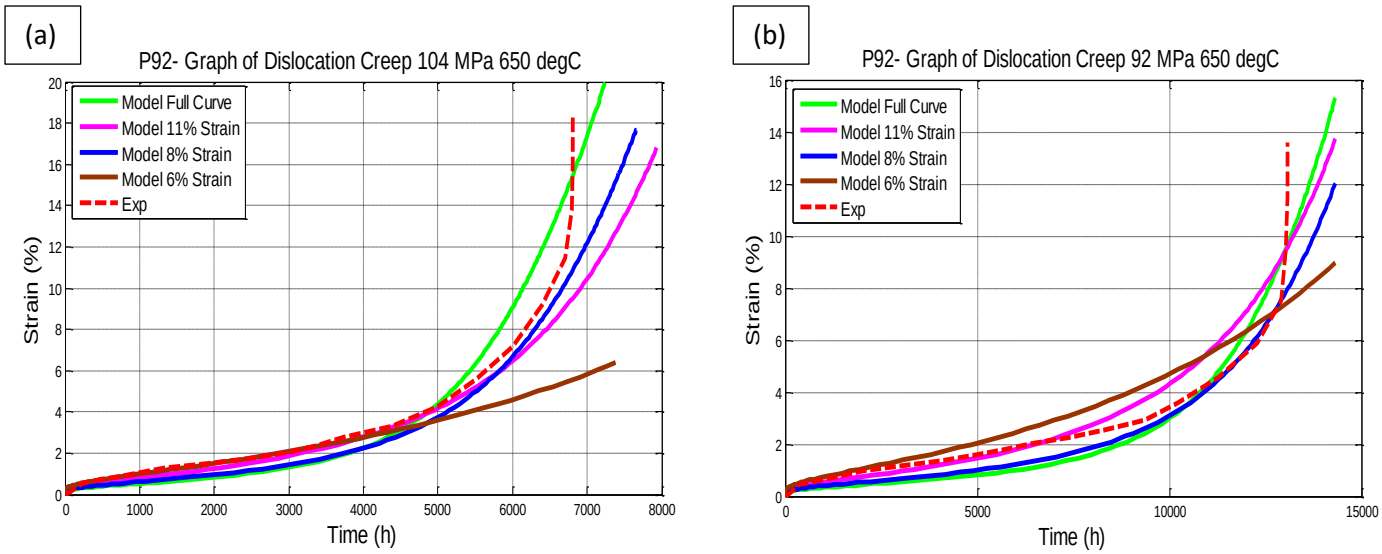

Figure 7-1 (a) Plot of creep strain-at 104 MPa, 650°C for various optimisation strain limits. (b) Plot of creep strain-time for P92 at 92 MPa, 650°C for various optimisation strain limits. All parameter optimisation carried out at 92 MPa and 104 MPa simultaneously

Figure 7-1 shows that the CDM model produces accurate predictions of creep strain-time data for both the 92 and 104 MPa stress conditions for the primary and secondary creep stages when compared with experimental creep curves. It also produces accurate predictions of tertiary creep which improves in accuracy with a decrease in optimisation strain limit at 8% and 6%.

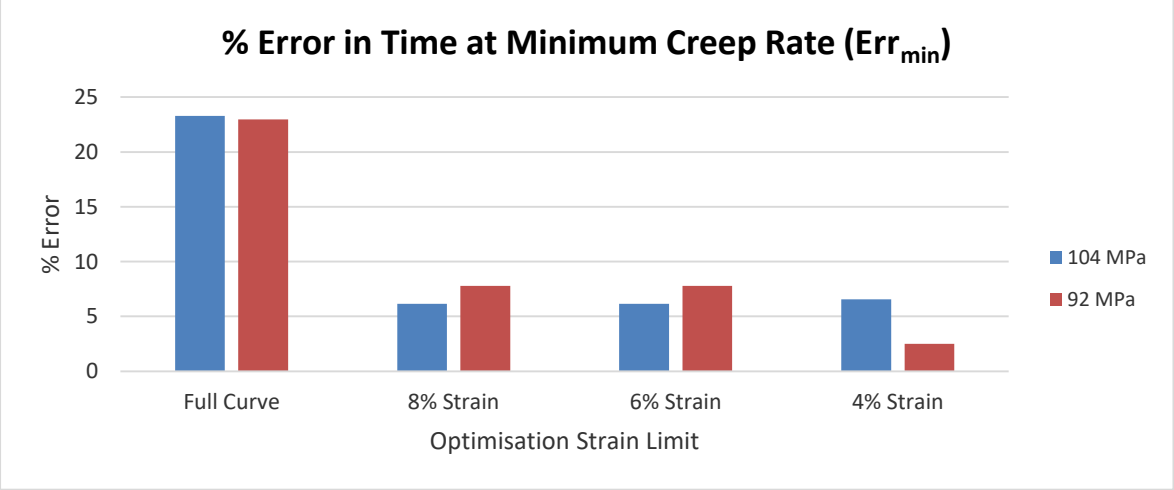

Figure 7-2: Graph illustrating error between experimental and model time at minimum creep rate for various optimisation strain limits. Optimisation carried out at 92 MPa and 104 MPa simultaneously

Figure 7-2 shows that the Err_{min} value decreases significantly when a strain limit for parameter optimisation is used. The Err_{min} value decreases from approximately 25 to 7 and from 33 to 17 for the 104 MPa and 92 MPa stress conditions respectively when the optimisation strain limit is decreased to 8%. The percentage error thereafter remains almost constant for both stress conditions as the strain limit is decreased further to 6% and 4%.

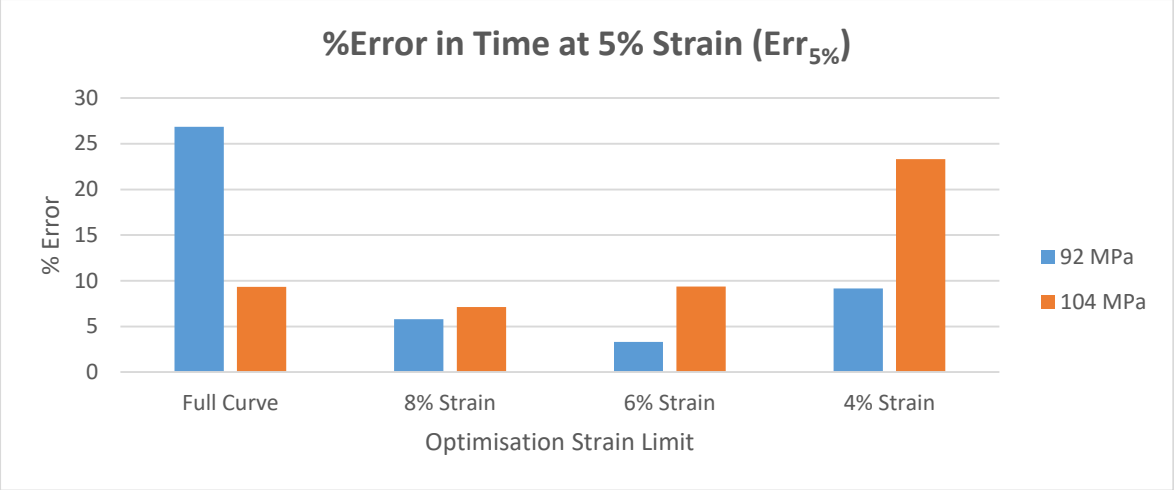

Figure 7-3: Graph illustrating error between experimental and model times to reach 5% strain for various optimisation strain limits. Optimisation carried out at 92 MPa and 104 MPa simultaneously

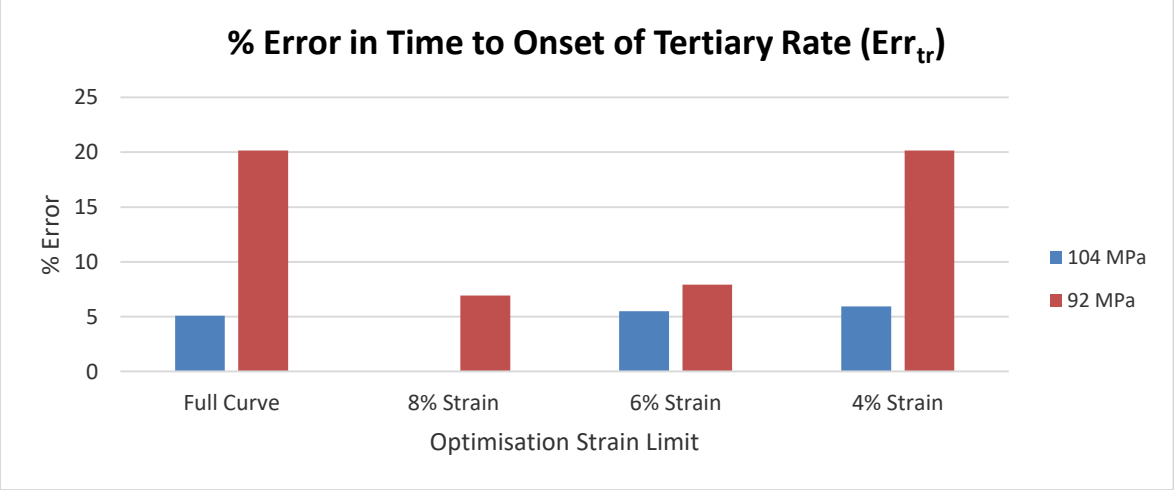

Figure 7-4: Graph illustrating error between experimental and model time at onset of tertiary creep for various optimisation strain limits. Optimisation carried out at 92 MPa and 104 MPa simultaneously

Figure 7-3 shows the percentage error between experimental and model times to reach 5% creep strain ($Err_{5\%}$). As this is a measure of the accuracy of tertiary creep predictions, the results show quantitatively the improvement in tertiary creep approximation when parameters are optimised with 8% and 6% strain limits for both stress. Furthermore, Figure 7-3 shows a clear trend in the behaviour of the model at both stress states. This similarly applies to Figure 7-4 which displays the percentage error in the model's approximation of the onset of tertiary creep. Both stress approach a minimum error using the 8% strain limit with the 104 MPa stress condition approaching a 0% error.

7.1 Discussion of P92 Results

The P92 model results overall responded well to parameter optimisation and produced creep strain-time predictions for the entire creep curve at stresses of both 92 MPa and 104 MPa. The parameter optimisation was successfully run at the two stresses simultaneously in order to obtain the *USSE(p)* and thus calibrate the CDM model for P92 across the entire stress range considered.

The optimised parameter set obtained from the CB8 calibration was used as initial guesses for the P92 optimisation routine. This was done to analyse the flexibility of the CDM approach when applied to similar grades of steel but which exhibit significantly different creep strengths. In this regard the model responded very well as illustrated by the relatively large degree of accuracy in predicting creep life for both stresses considered.

The various strain limits set for the parameter optimisation were once again implemented in order to negate the optimisation distortive effects due to macrostructural necking as was done for CB8. This method showed to improve the model's creep strain-time predictions for secondary as well as tertiary creep. For the secondary creep case this was illustrated by the decrease in error in the prediction of the minimum creep rate (Err_{min}) a metric of secondary creep deformation. The results showed little improvement in accuracy when the strain limit was reduced to below 8% suggesting that the distortion effects on the secondary creep stage had been effectively removed and not further improvement in accuracy could be obtained. The time at which the onset of tertiary creep was predicted by the model also showed a decrease in percentage error (Err_{tr}) when optimised with a strain limit and a minimum error achieved for the 6% strain limit. This behaviour was then reversed for lower strain limits with a progressive increase in error observed for the 6% and 4% strain limits compared to the 8% case. This can be interpreted as an initial improvement in the model's approximation of the onset of tertiary creep due to the negation of necking followed by an increase in error due to loss of tertiary creep microstructural data at lower strain limit optimisation once again resulting in parameter distortion. It is therefore crucial to remove any distortion effects of necking while at the same time retaining adequate strain-time information in describing tertiary creep. Thus a parameter optimisation strain limit which satisfies these conditions needs to be selected which for P92 is approximately 6% strain.

Another point of interest is the correlation in the model's results for the two stresses with significantly different creep lives of approximately 7000h and 12000h for the 104 MPa and 92 MPa stress conditions respectively. While the absolute values may differ, the two sets of results show similar trends in the error associated with the minimum creep rate, onset of tertiary creep and time at 5% strain. This suggests that the microstructural features associated with creep at the two conditions are similar and have been accurately captured by the model's calibration approach i.e. parameter optimisation.

7.2 A Comparison of CB8 and P92 Results

The CDM approach proposed in this study was applied to two grades of 9-12% creep resistant steels namely CB8 and P92. While the model's performance for both steels was mostly successful, some crucial similarities and differences in creep strain-time predictions were observed.

Firstly, parameter optimisation was carried out over the entire creep curve for the two steels over stress ranges of 75-100 MPa and 92-104 MPa for CB8 and P92 respectively. The initial results had large associated error for the secondary and tertiary creep stages when compared with long term experimental creep data. This error was hypothesised as being due to macrostructural necking distorting parameter optimisation. As a result strain limits of 8%, 6% and 4% were each implemented during optimisation in order to preclude these distortive effects. This approach was found to improve creep-strain results for secondary and tertiary creep for both steels across the stress ranges considered although the extent to which it did so varied for the two steels. The P92 steel showed a clear trend in the reduction of error for both stress conditions with minimum error observed for with a strain limit of 6%. The results for CB8 on the other hand showed a trend for the 85 MPa and 75 MPa stress conditions but not for the 100 MPa stress condition. By conducting the parameter optimisation at the three strains individually, it was found that results for the 85 MPa 75 MPa conditions could not be accurately predicted if the parameter optimisation was conducted at the 100 MPa stress condition and vice-versa.

Predictions for the 85 and 75 MPa stress conditions when parameters were optimised at 100 MPa tended to overestimate creep strength while the opposite occurred at 100 MPa for parameter optimisation carried out at 75 or 85 MPa. A key difference in creep deformation between the three stress conditions was identified as the length of time for which the sample was under creep exposure. While the 75 and 85 MPa samples only failed after approximately 17000h and 12000h respectively, the 100 MPa sample failed after less than 9000h. The significance of this is that the Modified Z-phase has been reported in literature as forming only after 10000h of creep exposure at 650°C [32]. The acceleration of the creep process apparent for samples only after 10000h of creep exposure was thus attributed to the precipitation of the Modified Z-phase and its detrimental effects on creep strength.

Conversely, the model results for the P92 steel did not show any obvious discrepancies between the 92 MPa and 104 MPa stress conditions even though these two samples were exposed to creep conditions for approximately 13000h and 7000h respectively. In fact, the creep-time results obtained for creep exposure on either side of the 10000h mark produced good results when compared against experimental data. The question arises as to why these two similar grades of steels behave so differently during long term creep exposure. A possible explanation is that the CB8 and P92 steel grades are not as similar as assumed upon initial inspection especially with regards to their respective chemical compositions. A key difference is in their Cr content. While CB8 has a Cr content of approximately 11 wt%, P92 has a Cr content of 9wt%. This seemingly minor difference in Cr content may not affect the initial microstructure of the steel and by extension the initial stages of creep, but after 10000h of exposure to high temperature and stress conditions it may influence creep properties significantly. Studies undertaken by *Danielsen et al* [29], [31] strongly indicate that the precipitation of the Modified Z-phase is almost undetectable for Cr contents of less than 11% even after exposure times of 31000h at 650°C. The loss of creep strength in CB8 after 10000h of creep exposure but not in P92 can be attributed to the precipitation of the Modified Z-phase in the former but not in the latter.

Figure 7-5 shows a comparison of the model's creep strain-time predictions for both CB8 and P92 at stresses of 104 MPa and 92 MPa and a temperature 650°C.

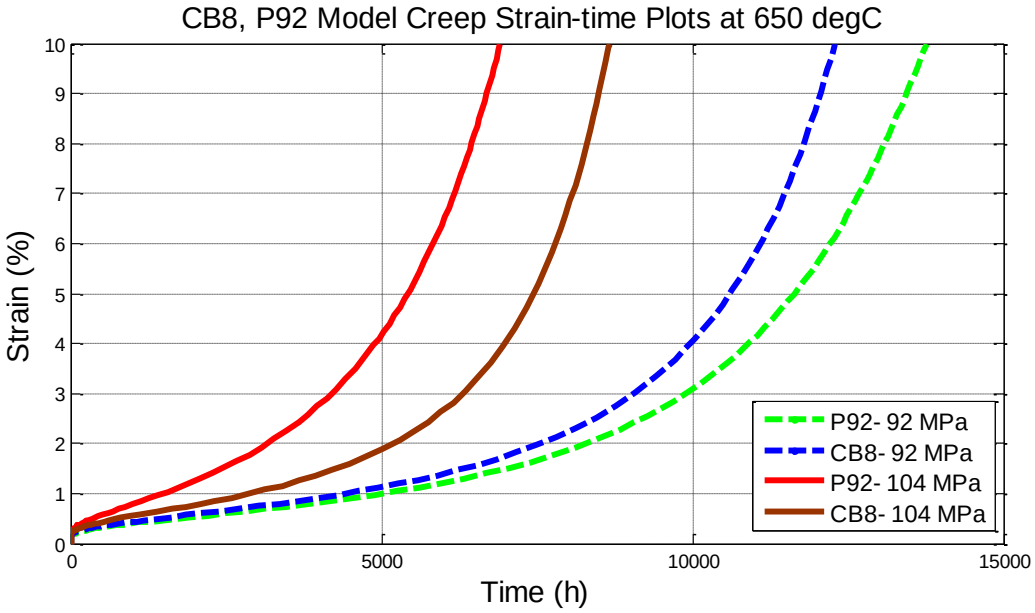

Figure 7-5: A comparison of creep strain-time model predictions for CB8 and P92 at stresses of 104 MPa and 92 MPa at 650°C

The relative creep strength of CB8 and P92 seems to be strongly dependent on stress and thereby creep exposure time. Figure 7-5 illustrates that at 104 MPa CB8 displays apparent higher creep strength as indicated by its lower gradient during secondary creep compared to P92 as well as the time at 5% strain. Conversely at 92 MPa, P92 appears to display higher creep strength. A possible explanation for this change in behaviour could be that P92 has lower tensile strength properties but is more resistant to long-term microstructural changes i.e. it maintains its initial microstructure to a greater extent than does CB8. Another possible explanation is that the Modified Z-phase begins to precipitate for the 92 MPa condition in CB8 as it begins to approach the 10000 exposure time resulting in a loss of creep strength. As P92 is not susceptible to Modified Z-phase precipitation it does not experience these adverse effects and thus maintains greater long-term creep resistance.

8 Conclusions

The aim of this MSc research project was to investigate the modelling of dislocation creep in 9-12% Cr steels using the Continuum Damage Mechanics approach. The key conclusions of this investigation are summarised below:

- A CDM model was successfully constructed based on existing dislocation creep theory as well as experimental observations for 9-12% Cr steels. The model included considerations of mobile dislocation motion, primary creep microstructure, back stress evolution, subgrain coarsening and $M_{23}C_6$ precipitate coarsening.

- The various model parameters were analysed and interpreted based on physical phenomena and shown to agree with observations and reports in literature. An optimisation routine was set up in order to calibrate the parameters to specific steels. A procedure to obtain initial parameter guesses was introduced and described in detail.
- A method to compare model accuracy against experimental long-term creep strain-time data was proposed as:
    1. Percentage error between model and experimental time at minimum creep rate (Err_{min}) as a measure of secondary creep accuracy.
    2. Percentage error between model and experimental time at onset of tertiary creep (Err_{tr}).
    3. Percentage error between model and experimental time at 5% creep strain as a measure of tertiary creep accuracy ($Err_{5\%}$).

- Parameter optimisation was conducted for the 11% Cr CB8 across stress ranges as well as at individual stresses. The following conclusions were made:
    1. Macrostructural necking in experimental samples significantly distorts parameter optimisation particularly within the secondary and tertiary creep regimes. This is effectively overcome by running optimisation up to a maximum strain of 6% so as to preclude to effects of necking.
    2. Parameter optimisation carried out across the stress range considered (75-100 MPa) produces inaccurate results due to varying microstructural features within the stress range. After optimisation for individual stress states, it was found that a significant change in microstructure occurs at approximately 10 000h of creep exposure. Based on reports in literature, this change in microstructure is due to the formation of the Modified Z-phase – a feature not considered in the current creep model.
    3. The model's microstructural predictions of subgrain coarsening as well as $M_{23}C_6$ coarsening were found to coincide well with experimental data as well as reports from literature.

- Parameter optimisation was carried out for the 9% Cr steel, P92. Macrostructural necking was once again found to distort model strain-time accuracy which was overcome by limiting the optimisation strain limit to 6% as with CB8. However, unlike CB8, creep strain results were found to produce accurate results even beyond 10000h of creep exposure.

- The difference in the strain-time behaviour between the CB8 and P92 model results with regards to the 10000h of creep exposure was attributed to the precipitation of the Modified Z-phase in CB8 but not in P92. The difference in the Cr content of each steel was concluded as the underpinning root cause of the formation of the Modified Z-phase in one steel but not the other.

- Overall, the CDM model proved to be an accurate tool in predicting creep behaviour based on microstructural features as well as a useful tool in analysing microstructural evolution. However, the use of CDM in this context comes with a number of caveats. Firstly, an accurate description and understanding of material microstructure is required in order to calibrate the model. Also as illustrated with the CB8 results, the data against which the model is optimised plays a significant role in its prediction accuracy. Finally, caution must be taken in using experimental data with significant macrostructural distortion such as necking.

9 Recommendations

The key recommendations made in this study based on the conclusions are:

- Investigate the applicability of the developed CDM model to more grades of 9-12% Cr. The CDM method used in this study has only been applied and analysed for two 9-12% Cr steels. This has been mostly due to a lack of long term creep test data for other steels. However, as more data becomes available, it can be used to evaluate the extent to which the developed model can make creep life and microstructural predictions over the full range of 9-12% Cr steels.
- Incorporate the Modified Z-phase as a damage parameter in the developed model. A major finding of the current study was the identification of the Modified Z-phase and its influence on model calibration. Hence the consideration of it will improve the model's capabilities. A possible method of capturing the complex kinetics of the modified Z-phase is to use thermodynamic modelling software such as *Matcalc*^{TM}.
- Expand the current model to include multiaxial loading effects rather than only the purely uniaxial case. This can be achieved by modifying the current strain-time differential equation to incorporate a Von Mises effective stress such as:

$$\dot{\varepsilon}_{ij} = \frac{3}{2}\left(\frac{\bar{S}_{ij}}{\sigma_e}\right)\dot{\varepsilon}_0 \sinh\left[\frac{\sigma_e\left(1 - H^*(1 - D_s)\right)}{\sigma_0(1 - D_P)}\right]$$

Where :

σ_e is the Von Mises effective stress; $\dot{\varepsilon}_{ij}$ the deviatoric strain rate tensor and $\bar{S}_{ij}$ the deviatoric stress tensor

- Apply the model to complex, critical components used in high temperature and high stress regions in power plants. This can be achieved by incorporating a Finite Element Analysis approach.
- Explore the application of the model and required modifications to simulate the creep behaviour of the Heat Affected Zone (HAZ) created by welds.
- Explore the use of creep compression as opposed to tensile test results to optimise parameter sets. This will remove any distortion caused by necking giving a 'true' representation of creep strain.
- Implement the developed CDM model within a Finite Element framework of the creep specimen. This can be used to further account for the effects of macrostructural necking.

10 References

1] IEA, “Recent Energy Trends in OECD Excerpt from: Energy Balances of OECD Countries 2015,” London, 2015.

[2] K. H. Mayer and F. Masuyama, “Development of creep-resistant steels,” in *Creep-resistant steels*, F. Abe, T.-U. Kern, and R. Viswanathan, Eds. Cambridge: Woodhead Publishing Limited, 2008, pp. 16–38.

[3] IEA, “Life extension of coal-fired power plants,” London, 2005.

[4] I. Holzer, “Modelling and Simulation of Strengthening in Complex Martensitic 9-12 % Cr Steel and a Binary Fe-Cu Alloy,” GRAZ UNIVERSITY OF TECHNOLOGY, 2010.

[5] M. Sibanda, “Design of a Ferritic / Martensitic Creep-Resistant Steel,” University of Cambridge, 2013.

[6] M. Saber, “Experimental and Finite Element Studies of Creep and Creep Crack Growth in P91 and P92 Weldments,” University of Nottingham, 2011.

[7] R. Oruganti, M. Karadge, and S. Swaminathan, “Damage mechanics-based creep model for 9–10%Cr ferritic steels,” *Acta Mater.*, vol. 59, no. 5, pp. 2145–2155, Mar. 2011.

[8] W. Blum, “Mechanisms of creep deformation in steel,” in *Creep-resistant steels*, F. Abe, T.-I. Kern, and R. Viswanathan, Eds. Cambridge: Woodhead Publishing Limited, 2008, pp. 365–400.

[9] F. Abe, “Creep-resistant steels,” in *Creep-resistant steels*, F. Abe, R. Viswanathan, and T. Kern, Eds. Cambridge: Woodhead Publishing Limited, 2008, pp. 3–14.

[10] J. Hald, E. E. E. Ipl-mpt, and K. Lyngby, “Microstructure and Long-Term Creep Properties of 9-12 % Cr Steels,” no. September, pp. 12–14, 2005.

[11] H. Semba, B. Dyson, and M. Mclean, “Microstructure-based Creep Modelling of a 9 % Cr Martensitic Steel,” 2005, no. September, pp. 12–14.

[12] B. Sonderegger, “Characterisation of the Substructure of Modern Power Plant Steels using the EBSD-Method,” PhD Thesis, Graz University of Technology, 2005.

[13] J. Hald, “Microstructure and long-term creep properties of 9-12% Cr steels,” *Int. J. Press. Vessel. Pip.*, vol. 85, pp. 30–37, 2008.

[14] C. G. Panait, A. Zielińska-Lipiec, T. Koziel, A. Czyrska-Filemonowicz, A.-F. Gourgues-Lorenzon, and W. Bendick, “Evolution of dislocation density, size of subgrains and MX-type precipitates in a P91 steel during creep and during thermal ageing at 600C for more than 100,000h,” *Mater. Sci. Eng. A*, vol. 527, pp. 4062–4069, 2010.

[15] H. Cerjak, I. Holzer, P. Mayr, C. Pein, B. Sonderegger, and E. Kozeschnik, “The relation between microstructure and creep properties of martensitic 9-12 % Cr steels,” *New Dev. Metall. Appl. High Strength Steels, 26.-28.5.2008*, pp. 247–263, 2008.

[16] A. Kostka, K. G. Tak, R. J. Hellmig, Y. Estrin, and G. Eggeler, “On the contribution of carbides and micrograin boundaries to the creep strength of tempered martensite ferritic steels,” *Acta Mater.*, vol. 55, no. 2, pp. 539–550, 2007.

[17] A. Bazazi, “Evolution of Microstructure during Long -term Creep of a Tempered Martensite Ferritic Steel,” Ruhr-Universitat Bochum, 2009.

[18] F. Abe, S. Nakazawa, H. Araki, and T. Noda, “On, The role of microstructural instability creep behavior of a low radio-activation martensitic 9Cr–2W steel,” *Trans, Met.*, no. 23A, pp. 469–477, 1992.

[19] A. Czyrska-filemonowicz, A. Zielińska-lipiec, and P. J. Ennis, “Modified 9 % Cr Steels for Advanced Power Generation : Microstructure and Properties,” *J. Achiev. Mater. Manuf. Eng.*, vol. 19, no. 2, pp. 43–48, 2006.

[20] X. Hu, L. Li, X. Wu, and M. Zhang, “Coarsening behavior of M23C6 carbides after ageing or thermal fatigue in AISI H13 steel with niobium,” *Int. J. Fatigue*, vol. 28, pp. 175–182, 2006.

[21] A. Aghajani, F. Richter, C. Somsen, S. G. Fries, I. Steinbach, and G. Eggeler, “On the formation and growth of Mo-rich Laves phase particles during long-term creep of a 12% chromium tempered martensite ferritic steel,” *Scr. Mater.*, vol. 61, no. 11, pp. 1068–1071, 2009.

[22] Y. Xu, M. Wang, Y. Wang, T. Gu, L. Chen, X. Zhou, Q. Ma, Y. Liu, and J. Huang, “Study on the nucleation and growth of Laves phase in a 10% Cr martensite ferritic steel after long-term aging,” *J. Alloys Compd.*, vol. 621, pp. 93–98, 2015.

[23] H. K. Danielsen, “Z-phase in 9-12 % Cr Steels,” Technical University of Denmark, 2007.

[24] W. O. Binder, “symposium on sigma-phase,” *ASTM*, p. 146, 1950.

[25] A. Henjered, H. Norden, T. Thorvaldsson, and H. Andren, “The composition of the chromium depleted zone in an austenitic stainless steel, an atom-probe study,” *Scr. Mater.*, vol. 17, no. 11, pp. 91–96, 1983.

[26] A. Strang and V. Vodarek, “Z phase formation in martensitic 12CrMoVNb steel,” *Mater. Sci. Technol.*, vol. 12, pp. 552– 556, 1996.

[27] A. Strang and V. Vodarek, *Microstructural Development and Stability in High Chromium Ferritic Power Plant Steels*, 1st ed. London: Cambridge, 1996.

[28] V. Vodarek and A. Strang, “Effect of nickel on the precipitation processes in 12CrMoV steel during creep at 550°C’,” *Scr. Mater.*, vol. 1, no. 38, pp. 101–6, 1998.

[29] H. K. Danielsen and J. Hald, “Influence of Z-phase on Long-term Creep Stability of Martensitic 9 to 12 % Cr Steels,” *VGB PowerTech*, vol. 5, pp. 68–73, 2009.

[30] E. Schnabel, P. Schwaab, and H. Weber, “E. Schnabel, P. Schwaab, H. Weber,” *Stahl Eisen*, vol. 107, pp. 691–696, 1987.

[31] H. K. Danielsen, P. E. Di Nunzio, and J. Hald, “Kinetics of Z-phase precipitation in 9 to 12 pct Cr steels,” *Metall. Mater. Trans. A Phys. Metall. Mater. Sci.*, vol. 44, no. May, pp. 2445–2452, 2013.

[32] H. K. Danielsen and J. Hald, “Behaviour of Z phase in 9–12% Cr steels,” *Energy Mater.*, vol. 1, no. 1, pp. 49–57, 2006.

[33] D. C. and J. Martin, *Thermally Activated Mechanisms in Crystal Plasticity*. Oxford: Elsevier, 2003.

[34] E. Orowan, “No Title,” in *Proc. Phys.Soc*, 1940, vol. 52, no. 8.

[35] K. Maruyama, K. Sawada, and J. Koike, “Advances in Physical Metallurgy and Processing of Steels. Strengthening Mechanisms of Creep Resistant Tempered Martensitic Steel.,” *ISIJ International*, vol. 41. pp. 641–653, 2001.

[36] M. Mclean, “On the threshold stress for dislocation creep in particle strengthened alloys,” *Acta Metall.*, vol. 33, pp. 545–556, 1985.

[37] B. Ilschner, “Hochtemperatur-Plastizität,” *Springer-Verlag*, 1973.

[38] M. R. Ahmadi, E. Povoden-Karadeniz, B. Sonderegger, K. I. Öksüz, a. Falahati, and E. Kozeschnik, “A model for coherency strengthening of large precipitates,” *Scr. Mater.*, pp. 1–4, Apr. 2014.

[39] B. Sonderegger, E. Kozeschnik, I. Holzer, and C. Sommitsch, “Particle Distance Distributions and their Effect on Precipitation Strengthening,” *Comput. Methods Mater. Sci.*, vol. 11, no. 1, pp. 148–153, 2011.

[40] U. Kocks, A. Argon, and M. Ashby, “Thermodynamics of slip,” *Prog. Mat. Sci.*, vol. 19, p. 1, 1975.

[41] P. Bons, “Kristallingeologie,” *Universitat Tuebingen*, 2008. [Online]. Available: http://homepages.uni-tuebingen.de/paul.bons/paul/lectures/kristallingeologie/kristallin_03.pdf. [Accessed: 01-Jun-2014].

[42] J. Weertman, “Steady-state creep of crystals,” *J. Appl. Phys.*, vol. 28, pp. 1185–1189, 1957.

[43] F. R. Nabarro, “Do we have an acceptable model of power-law creep?,” *Mater. Sci. Eng. A*, vol. 387–389, no. 1–2 SPEC. ISS., pp. 659–664, 2004.

[44] Kimura and Kazuhiro, “Proceedings of the ECCC Creep Conference,” 2005, pp. 1009–1022.

[45] M. McLean and B. F. Dyson, “Modeling the Effects of Damage and Microstructural Evolution on the Creep Behavior of Engineering Alloys,” *Journal of Engineering Materials and Technology*, vol. 122. p. 273, 2000.

[46] S. Hore and R. N. Ghosh, “Computer simulation of the high temperature creep behaviour of Cr–Mo steels,” *Mater. Sci. Eng. A*, vol. 528, no. 19–20, pp. 6095–6102, Jul. 2011.

[47] R. Oruganti, M. Karadge, and S. Swaminathan, “A Comprehensive Creep Model for Advanced 9-10% Cr Ferritic Steels,” *Procedia Eng.*, vol. 55, pp. 727–734, Jan. 2013.

[48] P. M. Kelly, “The effect of particle shape on dispersion hardening,” *Scr. Mater.*, vol. 6, no. 8, pp. 647–656, 1972.

[49] S. Takeuchi and A. Argon, “No Title,” *Acta Mater.*, vol. 29, pp. 1877–1884, 1981.

[50] J. Christopher, G. Sainath, V. S. Srinivasan, E. I. Samuel, B. K. Choudhary, M. D. Mathew, and T. Jayakumar, “Continuum Damage Mechanics Approach to Predict Creep Behaviour of Modified 9Cr-1Mo Ferritic Steel at 873K,” *Procedia Eng.*, vol. 55, pp. 798–804, Jan. 2013.

[51] Y. Estrin and H. Mecking, “A unified phenomenological description of work hardening and creep based on one-parameter models,” *Acta Metallurgica*, vol. 32. pp. 57–70, 1984.

[52] Y. F. Yin and R. G. Faulkner, “Continuum damage mechanics modelling based on simulations of microstructural evolution kinetics,” *Mater. Sci. Technol.*, vol. 22, no. 8, pp. 929–936, 2006.

[53] R. G. and Y. F. Y. Faulkner, “Simulation of Precipitation in Ferritic Steels,” *Materials Science and Technology*, vol. 19. pp. 91–98, 2003.

[54] P. J. Ennis, a. Zielinska-Lipiec, O. Wachter, and a. Czyrska-Filemonowicz, “Microstructural stability and creep rupture strength of the martensitic steel P92 for advanced power plant,” *Acta Mater.*, vol. 45, no. 12, pp. 4901–4907, 1997.

[55] B.F.Dyson, S.Osgerby, “Modelling and analysis of creep deformation and fracture in a 1Cr1/2Mo Ferritic Steel.,” *Rep. DMA*, vol. A116, no. NPL, 1993.

[56] F. Abe, “Strengthening mechanisms in steel for creep and creep rupture,” in *Creep-resistant steels*, Cambridge: Woodhead Publishing Limited, 2008, pp. 281–282.

[57] J. P. Hirth and J. Lothe, “Diffusive climb and glide process,” in *Theory of Dislocations*, 1st ed., M. Bever, M. . Shank, and C. Wert, Eds. New York: McGraw-Hill. Inc., 1967, pp. 484–498.

[58] S. Nandi, K. Vikrant, P. Ahv, K. Singh, and R. N. Ghosh, “Creep Modelling of P91 Steel for High Temperature Power Plant Applications,” *Procedia Eng.*, vol. 55, pp. 751–755, Jan. 2013.

[59] Y. F. Yin and R. G. Faulkner, “Modelling the effects of alloying elements on precipitation in ferritic steels,” *Mater. Sci. Eng. A*, vol. 344, pp. 92–102, 2003.

[60] I. Holzer, E. Kozeschnik, and H. Cerjak, “Transactions of The Indian Institute of Metals New approach to predict the long-term creep behaviour and evolution of precipitate back-stress of 9-12 % chromium steels,” vol. 9, 2008.

[61] J. Ro, “Back-stress calculation for dislocation climb past non-interacting particles,” vol. 339, pp. 334–339, 2003.

[62] T. Barkar and J. Ågren, “Creep simulation of 9-12% Cr steels using the composite model with thermodynamically calculated input,” *Mater. Sci. Eng. A*, vol. 395, pp. 110–115, 2005.

[63] J. Hald and L. Korcakova, “Precipitate Stability in Creep Resistant Ferritic Steels-Experimental Investigations and Modelling.,” *ISIJ Int.*, vol. 43, no. 3, pp. 420–427, 2003.

[64] H. Chilukuru, “On the microstructural basis of creep strength and creep-fatigue interaction in 9-12 % Cr steels for application in power plants,” 2007.

[65] S. Straub, M. Meier, J. Ostermann, and W. Blum, “Development of microstructure and strengthening in ferritic steel X20 CrMoV 12 1 at 823K during long-term creep tests and during annealing,” *VGB Kraftwerkstechnik*, no. 73, pp. 646–653, 1993.

[66] N. Zhu, Y. He, W. Liu, S. Huang, J. Vleugels, and O. van der Biest, “Modelling of nucleation and growth of M23C6 carbide in multicomponent Fe-based alloy,” *J. Mater. Sci. Technol.*, vol. 27, no. 8, pp. 725–728, 2011.

[67] E. Stärk, C. Picker, and M. F. Felsen, “Evaluation of the onset of tertiary creep for types 304 and 316 stainless steels,” Luxembourg, 1989.

[68] J. D’Errico, “MathWorks-fminsearchbnd.” [Online]. Available: https://www.mathworks.com/matlabcentral/fileexchange/8277-fminsearchbnd--fminsearchcon. [Accessed: 17-Jun-2016].

[69] D. R. Askeland, “The Science and Engineering of Materials,” *Mater. Sci. Eng. A*, vol. 212, pp. 186–187, 1996.

Appendix A1– Experimental creep data

CB8 – $M_{23}C_6$ Coarsening Data

Table 10-1: Particle size data for $M_{23}C_6$ precipitates in CB8 in as received state

As recieved			
Particle size class (nm)	**Frequency**	**Midpoint**	**fx**
0	**0**		
25	0	12.5	0
50	0.12	37.5	4.5
75	0.23	62.5	14.375
100	0.21	87.5	18.375
125	0.12	112.5	13.5
150	0.13	137.5	17.875
175	0.051	162.5	8.2875
200	0.05	187.5	9.375
225	0.025	212.5	5.3125
250	0.03	237.5	7.125
275	0.01	262.5	2.625
300	0.001	287.5	0.2875
325	0.005	312.5	1.5625
350	0	337.5	0
375	0	362.5	0
400	0	387.5	0
425	0	412.5	0
450	0	437.5	0
475	0	462.5	0
	0.982		103.2
Mean	105.0916497		
Variance	39.51232514		
Standard Deviation	6.285883004		

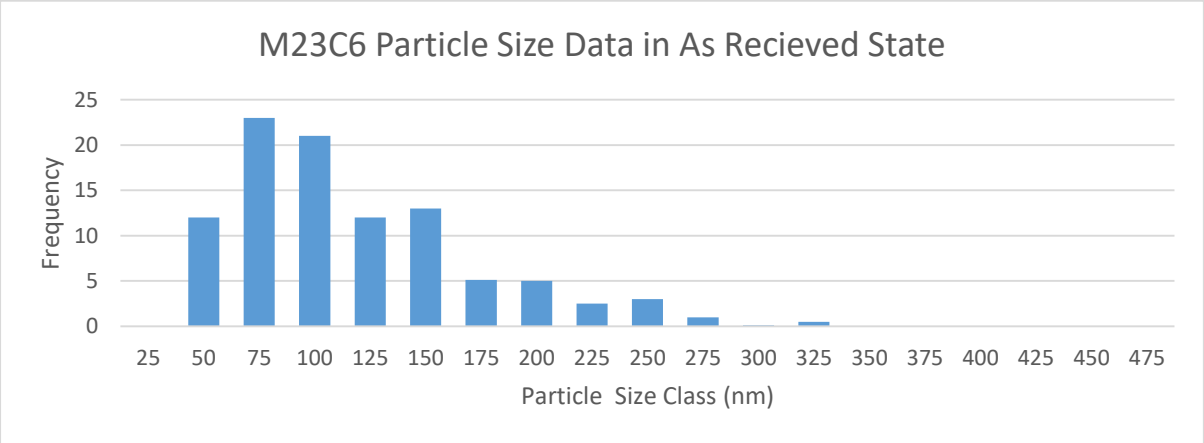

Figure 10-1: Plot of particle size data for $M_{23}C_6$ precipitates in CB8 in as received state

Table 10-2: Particle size data for $M_{23}C_6$ precipitates in CB8 after 2000h of creep exposure at 75 MPa and 650°C

2000 h			
Particle size class (nm)	**Frequency**	**Midpoint**	**fx**
0	**0**		
25	0.035	12.5	0.4375
50	0.32	37.5	12
75	0.245	62.5	15.3125
100	0.16	87.5	14
125	0.145	112.5	16.3125
150	0.035	137.5	4.8125
175	0.035	162.5	5.6875
200	0.015	187.5	2.8125
225	0	212.5	0
250	0.02	237.5	4.75
275	0	262.5	0
300	0	287.5	0
325	0	312.5	0
350	0	337.5	0
375	0	362.5	0
400	0	387.5	0
425	0	412.5	0
450	0	437.5	0
475	0	462.5	0
Total	**1.01**		76.125
Mean	75.37128713		
Variance	32.72322974		
Standard Deviation	5.720422165		

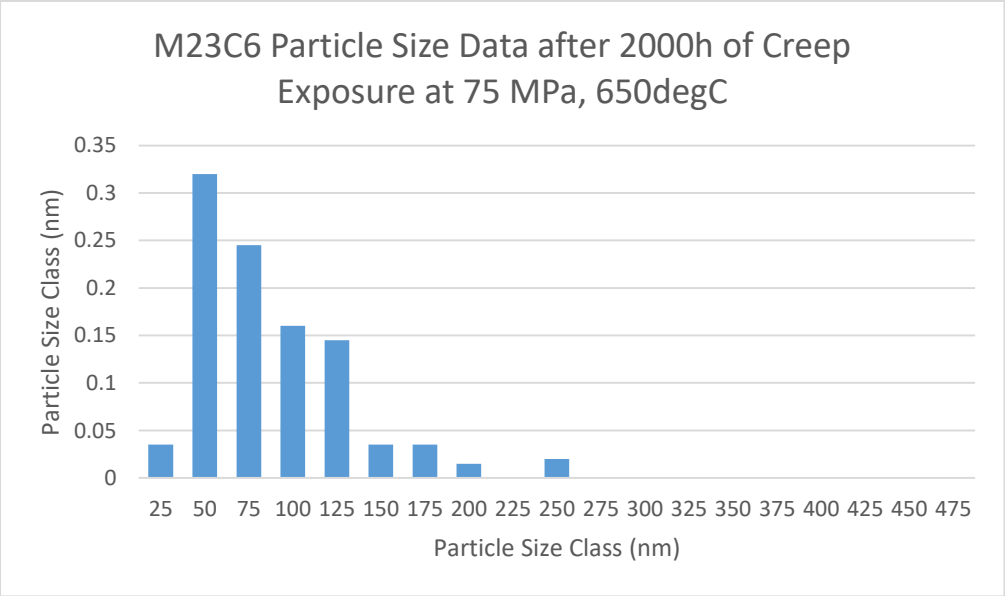

Figure 10-2: Plot of particle size data for $M_{23}C_6$ precipitates in CB8 after 2000h of creep exposure at 75 MPa and 650°C

Table 10-3: Particle size data for $M_{23}C_6$ precipitates in CB8 after 4031h of creep exposure at 75 MPa and 650°C

4031 h			
Particle size class (nm)	**Frequency**	**Midpoint**	**fx**
0	**0**		
25	0.015	12.5	0.1875
50	0.05	37.5	1.875
75	0.145	62.5	9.0625
100	0.22	87.5	19.25
125	0.2	112.5	22.5
150	0.11	137.5	15.125
175	0.07	162.5	11.375
200	0.03	187.5	5.625
225	0.06	212.5	12.75
250	0.03	237.5	7.125
275	0.03	262.5	7.875
300	0.01	287.5	2.875
325	0.005	312.5	1.5625
350	0	337.5	0
375	0.005	362.5	1.8125
400	0	387.5	0
425	0	412.5	0
450	0	437.5	0
475	0	462.5	0
Total	**0.98**		119
Mean	121.42857		
Variance	47.174169		
Standard Deviation	6.8683454		

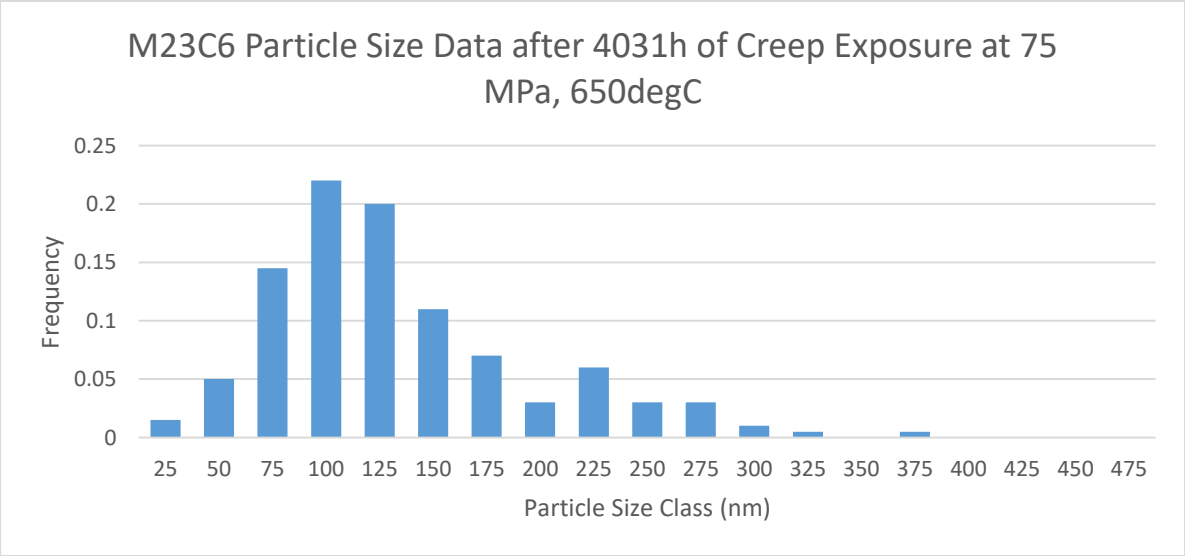

Figure 10-3: Plot of particle size data for $M_{23}C_6$ precipitates in CB8 after 4031h of creep exposure at 75 MPa and 650°C

Table 10-4: Particle size data for $M_{23}C_6$ precipitates in CB8 after 7063h of creep exposure at 75 MPa and 650°C

7063 h			
Particle size class (nm)	**Frequency**	**Midpoint**	**fx**
0	**0**		
25	0	12.5	0
50	0.055	37.5	2.0625
75	0.1	62.5	6.25
100	0.17	87.5	14.875
125	0.22	112.5	24.75
150	0.13	137.5	17.875
175	0.07	162.5	11.375
200	0.02	187.5	3.75
225	0.05	212.5	10.625
250	0.04	237.5	9.5
275	0.045	262.5	11.8125
300	0.015	287.5	4.3125
325	0.02	312.5	6.25
350	0.005	337.5	1.6875
375	0	362.5	0
400	0.002	387.5	0.775
425	0.005	412.5	2.0625
450	0.001	437.5	0.4375
475	0	462.5	0
Total	**0.948**		128.4
Mean	135.443038		
Variance	46.34890149		
Standard Deviation	6.808002753		

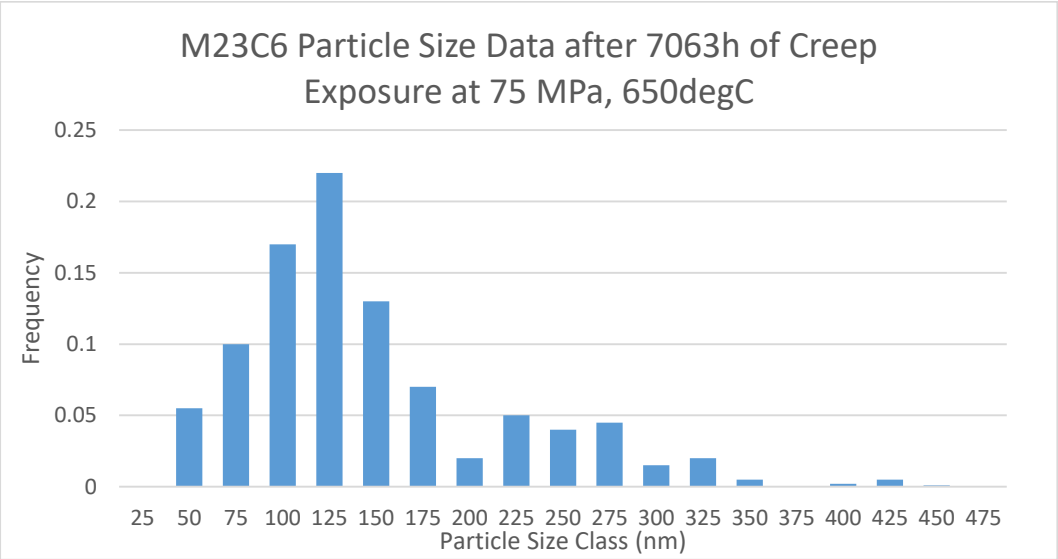

Figure 10-4: Plot of particle size data for $M_{23}C_6$ precipitates in CB8 after 7063h of creep exposure at 75 MPa and 650°C

Table 10-5: Particle size data for $M_{23}C_6$ precipitates in CB8 after 16564h of creep exposure at 75 MPa and 650°C

16564 h			
Particle size class (nm)	**Frequency**	**Midpoint**	**fx**
0	**0**		
25	0	12.5	0
50	0.07	37.5	2.625
75	0.15	62.5	9.375
100	0.145	87.5	12.6875
125	0.26	112.5	29.25
150	0.13	137.5	17.875
175	0.06	162.5	9.75
200	0.035	187.5	6.5625
225	0.05	212.5	10.625
250	0.02	237.5	4.75
275	0.005	262.5	1.3125
300	0.01	287.5	2.875
325	0.02	312.5	6.25
350	0.001	337.5	0.3375
375	0	362.5	0
400	0	387.5	0
425	0.001	412.5	0.4125
450	0.001	437.5	0.4375
475	0	462.5	0
Total	**0.958**		115.125
Mean	120.1722338		
Variance	55.59861582		
Standard Deviation	7.456447936		

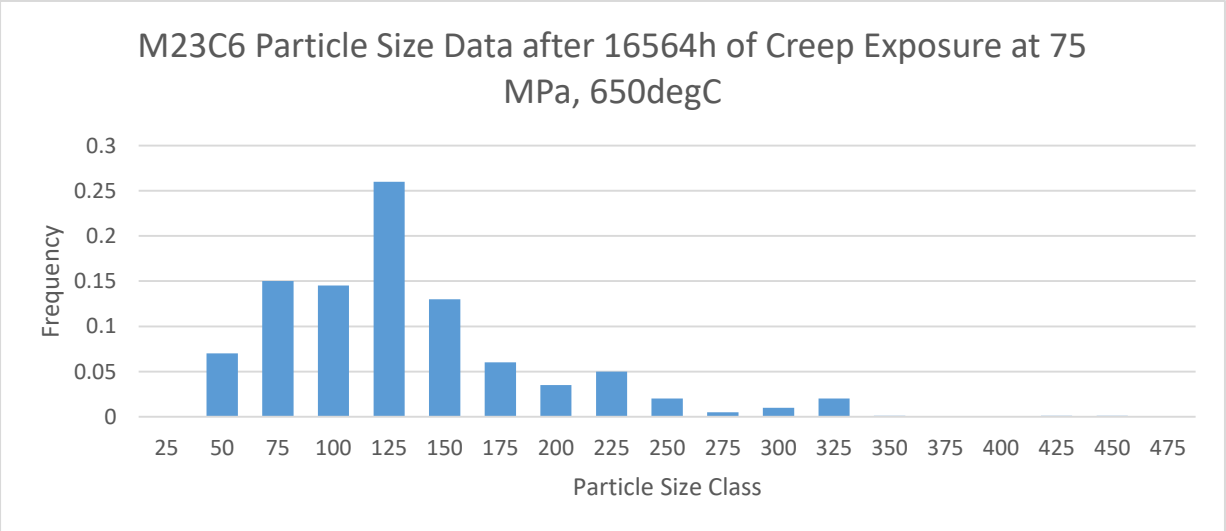

Figure 10-5: Plot of particle size data for $M_{23}C_6$ precipitates in CB8 after 16564h of creep exposure at 75 MPa and 650°C

CB8- Subgrain Coarsening data

Table 10-6: Subgrain diameter measurements during creep exposure and thermal aging. Creep testing carried out at 75 MPa and 650°C and thermal ageing at 650°C

CB8- Subgrain Coarsening Data			
Creep Loaded		Thermally aged	
Subgrain diameter (µm)	time (h)	Subgrain diameter (µm)	time (h)
0.7	0	0.7	0
0.89	2000	0.6	2000
0.93	4000	0.8	4000
0.98	7000	0.69	7000
1.6	16500	0.75	16500

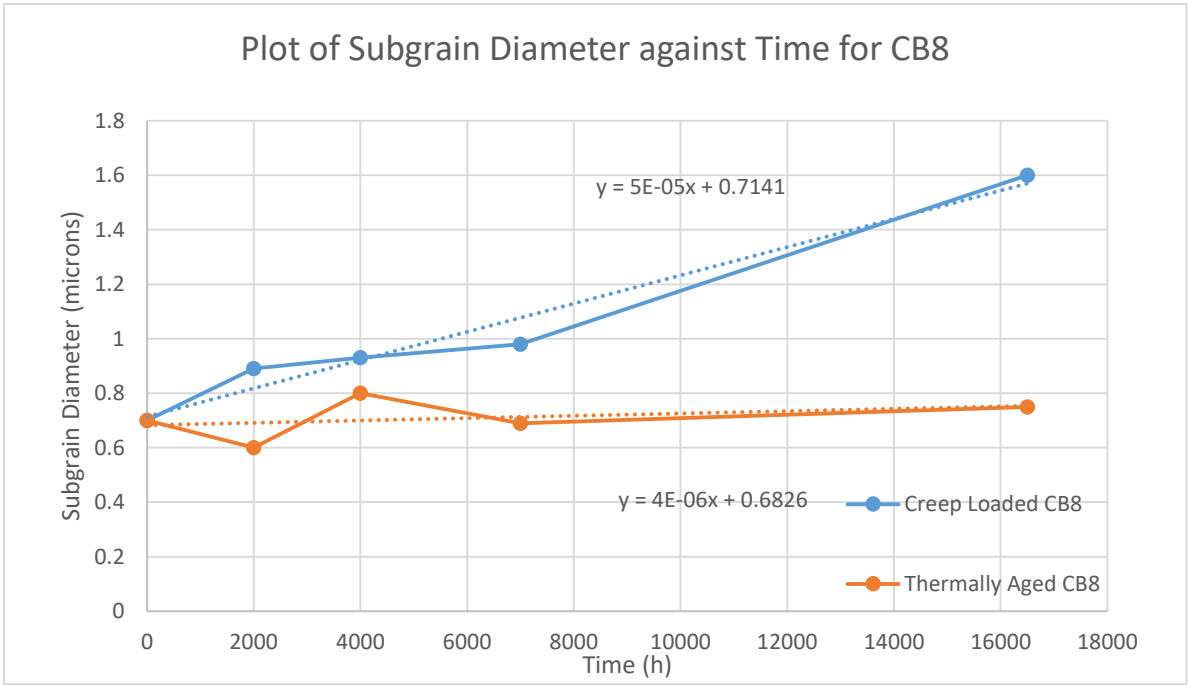

CB8- Creep-time data

Table 10-7: Long term creep-time data until rupture for CB8 at applied stress of 75, 85 and 100 MPa and 650°C

Sample 8.93 Stress = 75 MPa			Sample 8.96 Stress = 85 MPa			Sample 8.74 Stress = 100 MPa	
Strain	**Time (h)**		**Strain**	**Time (h)**		**Strain**	**Time (h)**
0.0000	0		0.0000	0		0.0000	0
0.0012	100		0.0006	77		0.0026	50
0.0019	200		0.0010	193		0.0026	100
0.0021	300		0.0021	307		0.0027	200
0.0024	723		0.0026	442		0.0028	300
0.0026	1000		0.0045	511		0.0044	555
0.0027	1140		0.0031	578		0.0045	700
0.0029	1301		0.0026	604		0.0050	900
0.0031	1800		0.0040	892		0.0053	1007
0.0032	3051		0.0062	1204		0.0065	1274
0.0053	4606		0.0078	1512		0.0066	1609
0.0061	5752		0.0067	2204		0.0067	2016
0.0072	7251		0.0082	2874		0.0104	2498
0.0084	8138		0.0101	3499		0.0104	3002
0.0086	8426		0.0106	4339		0.0108	3574
0.0101	9043		0.0109	4964		0.0133	4031
0.0101	9887		0.0139	5462		0.0147	4739
0.0103	10128		0.0140	6079		0.0160	5026
0.0106	10404		0.0146	6869		0.0178	5643
0.0106	10573		0.0168	7176		0.0195	6131
0.0107	10819		0.0168	7337		0.0209	6372
0.0108	11124		0.0191	7818		0.0231	6648
0.0110	11409		0.0198	8133		0.0248	6817
0.0113	11488		0.0205	8491		0.0249	7063
0.0117	11539		0.0227	8605		0.0300	7368
0.0117	11629		0.0237	8720		0.0349	7653
0.0117	11679		0.0246	8867		0.0360	7732
0.0120	11680		0.0258	9347		0.0342	7783
0.0126	11862		0.0256	9419		0.0378	7873
0.0127	12102		0.0262	9605		0.0391	7923
0.0147	12157		0.0275	9652		0.0436	7924
0.0147	12252		0.0308	10387		0.0463	8106
0.0151	12332		0.0317	10502		0.0482	8346
0.0157	12493		0.0314	10525		0.0556	8401
0.0157	12658		0.0320	10638		0.0571	8496
0.0166	12685		0.0319	10681		0.0608	8576
0.0167	13134		0.0328	10746		0.0737	8737
0.0195	13759		0.0325	10796		0.0980	8902
0.0288	14257		0.0339	10865		0.1133	8929
0.0342	14874		0.0341	10905			
0.0487	15666		0.0396	11165			

Table 10-7 continued							
Stress = 75 MPa			**Stress = 85 MPa**			**Stress = 100 MPa**	
0.0800	15886		0.0446	11327			
			0.0504	11512			
			0.0604	11705			
			0.0676	11796			
			0.0859	11935			
			0.0969	11982			
			0.1298	12098			
			0.1835	12165			

Table 10-8:Long term creep-time data up to 8% strain for CB8 at applied stress of 75, 85 and 100 MPa and 650°C

CB8 Experimental Creep Data until 8% Strain							
Sample 8.93 Stress = 75 MPa			**Sample 8.96 Stress = 85 MPa**			**Sample 8.74 Stress = 100 MPa**	
Strain	Time (h)		Strain	Time (h)		Strain	Time (h)
0.0000	0		0.0000	0		0.0000	0
0.0012	100		0.0006	77		0.0026	50
0.0019	200		0.0010	193		0.0026	100
0.0021	300		0.0021	307		0.0027	200
0.0024	723		0.0026	442		0.0028	300
0.0026	1000		0.0045	511		0.0044	555
0.0027	1140		0.0031	578		0.0045	700
0.0029	1301		0.0026	604		0.0050	900
0.0031	1800		0.0040	892		0.0053	1007
0.0032	3051		0.0062	1204		0.0065	1274
0.0053	4606		0.0078	1512		0.0066	1609
0.0061	5752		0.0067	2204		0.0067	2016
0.0072	7251		0.0082	2874		0.0104	2498
0.0084	8138		0.0101	3499		0.0104	3002
0.0086	8426		0.0106	4339		0.0108	3574
0.0101	9043		0.0109	4964		0.0133	4031
0.0101	9887		0.0139	5462		0.0147	4739
0.0103	10128		0.0140	6079		0.0160	5026
0.0106	10404		0.0146	6869		0.0178	5643
0.0106	10573		0.0168	7176		0.0195	6131
0.0107	10819		0.0168	7337		0.0209	6372
0.0108	11124		0.0191	7818		0.0231	6648
0.0110	11409		0.0198	8133		0.0248	6817
0.0113	11488		0.0205	8491		0.0249	7063
0.0117	11539		0.0227	8605		0.0300	7368
0.0117	11629		0.0237	8720		0.0349	7653
0.0117	11679		0.0246	8867		0.0360	7732
0.0120	11680		0.0258	9347		0.0342	7783
0.0126	11862		0.0256	9419		0.0378	7873
0.0127	12102		0.0262	9605		0.0391	7923
0.0147	12157		0.0275	9652		0.0436	7924
0.0147	12252		0.0308	10387		0.0463	8106
0.0151	12332		0.0317	10502		0.0482	8346
0.0157	12493		0.0314	10525		0.0556	8401
0.0157	12658		0.0320	10638		0.0571	8496
0.0166	12685		0.0319	10681		0.0608	8576
0.0167	13134		0.0328	10746		0.0737	8737
0.0195	13759		0.0325	10796		0.0807	8877
0.0288	14257		0.0339	10865			
0.0342	14874		0.0341	10905			
0.0487	15666		0.0396	11165			
0.0800	15886		0.0446	11327			
			0.0504	11512			
			0.0604	11705			

Table 10-8 Continued

			0.0676	11796			
			0.0809	11855			

Table 10-9:Long term creep-time data up to 6% strain for CB8 at applied stress of 75, 85 and 100 MPa and 650°C

CB8 Experimental Creep Data until 6% Strain							
Sample 8.93 Stress = 75 MPa			**Sample 8.96 Stress = 85 MPa**			**Sample 8.74 Stress = 100 MPa**	
Strain	Time (h)		Strain	Time (h)		Strain	Time (h)
0.0000	0		0.0000	0		0.0000	0
0.0012	100		0.0006	77		0.0026	50
0.0019	200		0.0010	193		0.0026	100
0.0021	300		0.0021	307		0.0027	200
0.0024	723		0.0026	442		0.0028	300
0.0026	1000		0.0045	511		0.0044	555
0.0027	1140		0.0031	578		0.0045	700
0.0029	1301		0.0026	604		0.0050	900
0.0031	1800		0.0040	892		0.0053	1007
0.0032	3051		0.0062	1204		0.0065	1274
0.0053	4606		0.0078	1512		0.0066	1609
0.0061	5752		0.0067	2204		0.0067	2016
0.0072	7251		0.0082	2874		0.0104	2498
0.0084	8138		0.0101	3499		0.0104	3002
0.0086	8426		0.0106	4339		0.0108	3574
0.0101	9043		0.0109	4964		0.0133	4031
0.0101	9887		0.0139	5462		0.0147	4739
0.0103	10128		0.0140	6079		0.0160	5026
0.0106	10404		0.0146	6869		0.0178	5643
0.0104	10573		0.0168	7176		0.0195	6131
0.0107	10819		0.0168	7337		0.0209	6372
0.0108	11124		0.0191	7818		0.0231	6648
0.0128	11409		0.0198	8133		0.0248	6817
0.0117	11488		0.0205	8491		0.0249	7063
0.0113	11539		0.0227	8605		0.0300	7368
0.0098	11629		0.0237	8720		0.0349	7653
0.0117	11679		0.0246	8867		0.0360	7732
0.0120	11680		0.0258	9347		0.0342	7783
0.0106	11862		0.0256	9419		0.0378	7873
0.0125	12102		0.0262	9605		0.0391	7923
0.0147	12157		0.0275	9652		0.0436	7924
0.0137	12252		0.0308	10387		0.0463	8106
0.0141	12332		0.0317	10502		0.0482	8346
0.0157	12493		0.0314	10525		0.0556	8401
0.0153	12658		0.0320	10638		0.0571	8496
0.0136	12685		0.0319	10681		0.0608	8576
0.0167	13134		0.0328	10746			
0.0195	13759		0.0325	10796			
0.0288	14257		0.0339	10865			

Table 10-9 Continued							
0.0342	14874		0.0341	10905			
0.0487	15666		0.0396	11165			
0.0600	15963		0.0446	11327			
			0.0504	11512			
			0.0604	11705			

Table 10-10:Long term creep-time data up to 4% strain for CB8 at applied stress of 75, 85 and 100 MPa and 650°C

CB8 Experimental Creep Data until 4% Strain							
Sample 8.93 Stress = 75 MPa			**Sample 8.96 Stress = 85 MPa**			**Sample 8.74 Stress = 100 MPa**	
Strain	Time (h)		Strain	Time (h)		Strain	Time (h)
0	0		0.0000	0		0.0000	0
0.0012	100		0.0006	77		0.0026	50
0.0019	200		0.0010	193		0.0026	100
0.0021	300		0.0021	307		0.0027	200
0.0024	723		0.0026	442		0.0028	300
0.0026	1000		0.0045	511		0.0044	555
0.0027	1140		0.0031	578		0.0045	700
0.0029	1301		0.0026	604		0.0050	900
0.0031	1800		0.0040	892		0.0053	1007
0.0032	3051		0.0062	1204		0.0065	1274
0.0053	4606		0.0078	1512		0.0066	1609
0.0061	5752		0.0067	2204		0.0067	2016
0.0072	7251		0.0082	2874		0.0104	2498
0.0084	8138		0.0101	3499		0.0104	3002
0.0086	8426		0.0106	4339		0.0108	3574
0.0101	9043		0.0109	4964		0.0133	4031
0.0101	9887		0.0139	5462		0.0147	4739
0.0103	10128		0.0140	6079		0.0160	5026
0.0106	10404		0.0146	6869		0.0178	5643
0.0104	10573		0.0168	7176		0.0195	6131
0.0107	10819		0.0168	7337		0.0209	6372
0.0108	11124		0.0191	7818		0.0231	6648
0.0128	11409		0.0198	8133		0.0248	6817
0.0117	11488		0.0205	8491		0.0249	7063
0.0113	11539		0.0227	8605		0.0300	7368
0.0098	11629		0.0237	8720		0.0349	7653
0.0117	11679		0.0246	8867		0.0360	7732
0.012	11680		0.0258	9347		0.0342	7783
0.0106	11862		0.0256	9419		0.0378	7873
0.0125	12102		0.0262	9605		0.0391	7923
0.0147	12157		0.0275	9652			
0.0137	12252		0.0308	10387			
0.0141	12332		0.0317	10502			
0.0157	12493		0.0314	10525			
0.0153	12658		0.0320	10638			
0.0136	12685		0.0319	10681			

Table 10-10 Continued							
0.0167	13134		0.0328	10746			
0.0195	13759		0.0325	10796			
0.0288	14257		0.0339	10865			
0.0342	14874		0.0341	10905			
			0.0396	11165			

P92- Creep-time Data

Table 10-11: Long term creep-time data until rupture for P92 at applied stress of 92 and 104 MPa and 650°C

P92 Experimental Creep Data until Rupture				
Stress = 92 MPa			**Stress = 104 MPa**	
Strain	Time (h)		Strain	Time (h)
0.0000	0		0.0000	0
0.0049	377		0.0080	248
0.0083	1155		0.0098	810
0.0092	2018		0.0129	1328
0.0117	3011		0.0148	1976
0.0143	4048		0.0172	2494
0.0160	4998		0.0202	3013
0.0177	5688		0.0240	3359
0.0193	6422		0.0261	3732
0.0219	7416		0.0308	4379
0.0253	8322		0.0381	5001
0.0278	9359		0.0471	5501
0.0329	10222		0.0701	6000
0.0397	11259		0.0931	6400
0.0532	12296		0.1115	6700
0.0735	12901		0.1368	6800
0.0938	13031		0.1622	6801
0.1149	13075		0.1842	6802
0.1360	13076			

Table 10-12: Long term creep-time data up to 11% strain for P92 at applied stress of 92 and 104 MPa and 650°C

P92 Experimental Creep Data until 11% Strain				
Stress = 92 MPa			**Stress = 104 MPa**	
Strain	Time (h)		Strain	Time (h)
0.0000	0		0	0
0.0049	377		0.0080	248
0.0083	1155		0.0158	810
0.0092	2018		0.0199	1328
0.0117	3011		0.0238	1976
0.0143	4048		0.0272	2494
0.0160	4998		0.0302	3013
0.0177	5688		0.0330	3359
0.0193	6422		0.0351	3732
0.0219	7416		0.0418	4379
0.0253	8322		0.0471	5001
0.0278	9359		0.0531	5501
0.0329	10222		0.0701	6000
0.0397	11259		0.0931	6400
0.0532	12296		0.1115	6700
0.0635	12501			
0.0735	12901			
0.0800	12951			
0.0938	13031			
0.1149	13075			

Table 10-13:Long term creep-time data up to 4% strain for P92 at applied stress of 92 and 104 MPa and 650°C

P92 Experimental Creep Data until 4% Strain				
Stress = 92 MPa			**Stress = 104 MPa**	
Strain	Time (h)		Strain	Time (h)
0.0000	0		0.0000	0
0.0049	377		0.0080	248
0.0083	1155		0.0158	810
0.0092	2018		0.0199	1328
0.0117	3011		0.0238	1976
0.0143	4048		0.0272	2494
0.0160	4998		0.0302	3013
0.0177	5688		0.0330	3359
0.0193	6422		0.0351	3732
0.0219	7416		0.0418	4379
0.0253	8322			
0.0278	9359			
0.0329				
0.0397				

Appendix A2 CB8 Model Result Values

Parameters Optimised at 100 MPa 650°C

Table 10-14: Model and experimental creep time results for CB8 after parameter optimisation at 100 MPa 650°C

Full Curve Model Results						
Stress (Mpa)	MinRate (s^-1)	Time at min creep rate (h)	Time at failure (h)	Tertiary creep onset strain (%)	Time at onset of tertiary creep (h)	Time at 5% strain
75	1.31E-06	7344	19046	1.18	8572	16700
85	1.88E-06	5576	14046	1.66	8034	12175
100	3.20E-06	3834	9182	1.28	4004	7718
8% Creep Curve						
Stress (Mpa)	MinRate (s^-1)	Time at min creep rate (h)	Time at failure (h)	Tertiary creep onset strain (%)	Time at onset of tertiary creep (h)	Time at 5% strain
75	1.24E-06	7739	19046	1.18	9167	17595
85	1.77E-06	5682	14046	1.66	8491	12807
100	2.98E-06	3704	9407	1.28	4274	8123
6% Creep Curve						
Stress (Mpa)	MinRate (s^-1)	Time at min creep rate (h)	Time at failure (h)	Tertiary creep onset strain (%)	Time at onset of tertiary creep (h)	Time at 5% strain
75	1.24E-06	7777	19046	1.18	9205	17885
85	1.77E-06	5687	14046	1.66	8496	12502
100	2.97E-06	3693	9407	1.28	4363	8365
4% Creep Curve						
Stress (Mpa)	MinRate (s^-1)	Time at min creep rate (h)	Time at failure (h)	Tertiary creep onset strain (%)	Time at onset of tertiary creep (h)	Time at 5% strain
75	1.22E-06	7959	19046	1.18	9387	18443
85	1.73E-06	6163	14046	1.66	8621	13417
100	2.88E-06	3698	9407	1.28	4468	8663
Experimental Results						
Stress (Mpa)	MinRate (s^-1)	Time at min creep rate (h)	Time at failure (h)	Tertiary creep onset strain (%)	Time at onset of tertiary creep (h)	Time at 5% strain
75	8.43E-07	7138	15963	1.18	10426	15666
85	2.12E-06	5069	12165	1.66	8276	11327
100	3.02E-06	3574	8929	1.28	4531	8346

Table 10-15: Model and experimental creep time error values for CB8 after parameter optimisation at 100 MPa 650°C

% Error in Time at onset of Tertiary Creep				
75	11.61	7.88	7.65	6.51
85	1.99	1.77	1.81	2.84
100	5.90	2.88	1.88	0.70
% Error in Time at Minimum creep rate				
75	1.29	3.76	4.00	5.14
85	4.17	5.04	5.08	9.00
100	2.91	1.46	1.33	1.39
% Error in Time at 5% strain				
75	6.60	12.31	14.16	17.73
85	7.49	13.07	10.37	18.45
100	7.52	2.67	0.23	3.81

Parameters Optimised at 85 MPa 650°C

Table 10-16: Model and experimental creep time results after for CB8 after parameter optimisation at 85 MPa 650°C

Full Curve Model Results						
Stress (Mpa)	MinRate (s^-1)	Time at min creep rate (h)	Time at failure (h)	Tertiary creep onset strain (%)	Time at onset of tertiary creep (h)	Time at 5% strain
75	1.66E-06	4834	15607	1.18	6739	13227
85	2.41E-06	3874	12662	1.66	5981	9535
100	4.19E-06	2564	7315	1.28	3026	5956
8% Creep Curve						
Stress (Mpa)	MinRate (s^-1)	Time at min creep rate (h)	Time at failure (h)	Tertiary creep onset strain (%)	Time at onset of tertiary creep (h)	Time at 5% strain
75	8.40E-07	6003	17776	1.18	10541	15976
85	1.28E-06	4346	13567	1.66	8384	11189
100	2.41E-06	2565	7634	1.28	4286	6676
6% Creep Curve						
Stress (Mpa)	MinRate (s^-1)	Time at min creep rate (h)	Time at failure (h)	Tertiary creep onset strain (%)	Time at onset of tertiary creep (h)	Time at 5% strain
75	1.41E-06	6112	18518	1.18	8017	15573
85	2.01E-06	4514	14046	1.66	7324	11502
100	3.38E-06	3101	8973	1.28	3807	7331
4% Creep Curve						
Stress (Mpa)	MinRate (s^-1)	Time at min creep rate (h)	Time at failure (h)	Tertiary creep onset strain (%)	Time at onset of tertiary creep (h)	Time at 5% strain
75	1.51E-06	7338	19046	1.18	7789	16836
85	2.19E-06	5069	14046	1.66	7067	12068
100	3.78E-06	3274	9407	1.28	3323	7564
Experimental Results						
Stress (Mpa)	MinRate (s^-1)	Time at min creep rate (h)	Time at failure (h)	Tertiary creep onset strain (%)	Time at onset of tertiary creep (h)	Time at 5% strain
75	8.43E-07	7038	15963	1.18	10426	15666
85	2.12E-06	4869	12165	1.66	8376	11327
100	3.02E-06	3574	8929	1.28	5031	8346

Table 10-17: Model and experimental creep time error values for CB8 after parameter optimisation at 85 MPa 650°C

% Error in Time at onset of Tertiary Creep				
75	23.10	0.72	15.09	16.52
85	19.69	0.06	8.65	10.76
100	22.45	8.35	13.71	19.13
% Error in Time at Minimum creep rate				
75	13.81	6.48	5.80	1.88
85	8.18	4.30	2.92	1.64
100	11.31	11.30	5.29	3.36
% Error in Time at 5% strain				
75	15.57	1.98	0.59	7.47
85	15.83	1.22	1.54	6.54
100	28.64	20.02	12.16	9.37

Parameters Optimised at 75 MPa 650°C

Table 10-18: Model and experimental creep time results after for CB8 after parameter optimisation at 75 MPa 650°C

Full Curve Model Results						
Stress (Mpa)	MinRate (s^-1)	Time at min creep rate (h)	Time at failure (h)	Tertiary creep onset strain (%)	Time at onset of tertiary creep (h)	Time at 5% strain
75	1.06E-06	5428	16210	1.18	9237	14416
85	1.58E-06	4211	12509	1.66	7575	10220
100	2.91E-06	2510	7113	1.28	3833	6158
8% Creep Curve						
Stress (Mpa)	MinRate (s^-1)	Time at min creep rate (h)	Time at failure (h)	Tertiary creep onset strain (%)	Time at onset of tertiary creep (h)	Time at 5% strain
75	9.60E-07	5656	16771	1.18	9663	14808
85	1.53E-06	4078	12722	1.66	7416	10004
100	3.19E-06	2565	6539	1.28	3484	5526
6% Creep Curve						
Stress (Mpa)	MinRate (s^-1)	Time at min creep rate (h)	Time at failure (h)	Tertiary creep onset strain (%)	Time at onset of tertiary creep (h)	Time at 5% strain
75	8.21E-07	6563	18487	1.18	10490	15915
85	1.21E-06	4612	14046	1.66	8540	11357
100	2.19E-06	3117	8407	1.28	4609	6981
4% Creep Curve						
Stress (Mpa)	MinRate (s^-1)	Time at min creep rate (h)	Time at failure (h)	Tertiary creep onset strain (%)	Time at onset of tertiary creep (h)	Time at 5% strain
75	7.69E-07	6701	18258	1.18	11337	16252
85	1.14E-06	4839	14046	1.66	8946	11524
100	2.08E-06	3146	8095	1.28	4886	6963
Experimental Results						
Stress (Mpa)	MinRate (s^-1)	Time at min creep rate (h)	Time at failure (h)	Tertiary creep onset strain (%)	Time at onset of tertiary creep (h)	Time at 5% strain
75	8.43E-07	7138	15963	1.18	10426	15666
85	2.12E-06	5069	12165	1.66	8376	11327
100	3.02E-06	3574	8929	1.28	5031	8346

Table 10-19: Model and experimental creep time error values for CB8 after parameter optimisation at 75 MPa 650°C

% Error in Time at onset of Tertiary Creep				
75	7.45	4.78	0.40	5.70
85	6.58	7.89	1.35	4.68
100	13.42	17.32	4.72	1.62
% Error in Time at Minimum creep rate				
75	10.71	11.16	7.99	2.73
85	7.05	11.44	4.58	1.89
100	11.91	15.78	7.36	4.79
% Error in Time at 5% strain				
75	7.98	5.48	1.59	3.74
85	9.77	11.68	0.26	1.74
100	26.21	33.78	16.36	16.57

Appendix A3 P92 Model Result Values Optimised across Stress range 93-104 MPa and 650 °C

Table 10-20: Model and experimental creep time results after for P92 after parameter optimisation across stress range 92-104 MPa at 650°C

Full Curve Model Results						
Stress (Mpa)	MinRate (s^-1)	Time at min creep rate (h)	Time at failure (h)	Tertiary creep onset strain (%)	Time at onset of tertiary creep (h)	Time at 5% strain
104	6.77E-06	1328	6802	2.25	3013	4535
92	3.60E-06	3011	13076	2.44	5688	8238
11% Creep Curve						
Stress (Mpa)	MinRate (s^-1)	Time at min creep rate (h)	Time at failure (h)	Tertiary creep onset strain (%)	Time at onset of tertiary creep (h)	Time at 5% strain
104	6.15E-06	2494	6802	2.25	3359	5357
92	2.92E-06	4998	13076	2.44	7416	10607
8% Creep Curve						
Stress (Mpa)	MinRate (s^-1)	Time at min creep rate (h)	Time at failure (h)	Tertiary creep onset strain (%)	Time at onset of tertiary creep (h)	Time at 5% strain
104	4.66E-06	2494	6802	2.25	3732	5469
92	1.99E-06	4998	13076	2.44	9359	11631
6% Creep Curve						
Stress (Mpa)	MinRate (s^-1)	Time at min creep rate (h)	Time at failure (h)	Tertiary creep onset strain (%)	Time at onset of tertiary creep (h)	Time at 5% strain
104	6.89E-06	3359	6802	2.25	3159	6167
92	4.08E-06	5688	13076	2.44	5688	10228
Experimental Results						
Stress (Mpa)	MinRate (s^-1)	Time at min creep rate (h)	Time at failure (h)	Tertiary creep onset strain (%)	Time at onset of tertiary creep (h)	Time at 5% strain
104	6.80E-06	2913	6802	2.25	3359	5001
92	3.02E-06	6016	13076	2.44	8322	11259

Table 10-21: Model and experimental creep time error values for P92 after parameter optimisation across stress range 92-104 MPa at 650°C

% Error in Time at onset of Tertiary Creep				
104	5.09	0.00	5.49	5.95
92	20.14	6.93	7.93	20.14
% Error in Time at Minimum creep rate				
104	23.30	6.15	6.15	6.56
92	22.98	7.79	7.79	2.50
% Error in Time at 5% strain				
104	9.32	7.12	9.36	23.32
92	26.84	5.79	3.30	9.16

Appendix B1 Derivations

Fourth order *Runge-Kutta* with an adaptive stepsize

Consider the initial value problem:

$$\frac{dx}{dt} = f\big(t, x(t)\big), \tag{A.1}$$

Where,

$$x(t) = \big(x_1(t), x_2(t), \dots x_n(t)\big), f\epsilon[a,b] \times R^n \to R^n \tag{A.2}$$

With the initial condition

$$x(0) = x_0$$

To obtain the numerical approximation of the Initial Value Problem over the time interval $[a, b]$, the interval needs to be divided into M equal subintervals and mesh points t_j selected:

$$t_j = a + jh, \;\; j = 0,1 \dots . M \; and \; h = \frac{b-a}{M}$$

Here, h is referred to as the step size.

The family of Runge-Kutta (RK) methods is given by:

$$x(t_{n+1}) \coloneqq x_{n+1} = x_n + h\sum_{i=1}^{m} c_i k_i, \tag{A.3}$$

Where m denotes the Order of Differential equation. For $m = 4$:

$$k_1 = f(t_n, x_n), \tag{A.4-1}$$

$$k_2 = f\big(t_n + \alpha_2 h, x_n + h\beta_{21} k_1(t_n, x_n)\big) \tag{A.4-2}$$

$$k_3 = f\Big(t_n + \alpha_3 h, x_n + h\big(\beta_{31} k_1(t_n, x_n) + \beta_{32} k_1(t_n, x_n)\big)\Big) \tag{A.4-3}$$

$$k_4 = f\Big(t_n + \alpha_4 h, x_n + h\big(\beta_{41} k_1(t_n, x_n) + \beta_{42} k_1(t_n, x_n)\big) + \beta_{43} k_1(t_n, x_n)\Big) \tag{A.4-4}$$

By matching the coefficients in the equation set A.4 with those of the *Taylor series* the following is obtained:

$$k_1 = f(t_n, x_n) \tag{A.5-1}$$

$$k_2 = f\left(t_n + \frac{h}{2}, x_n + \frac{h}{2}k_1\right) \tag{A.4-2}$$

$$k_4 = f(t_n + h, x_n + hk_3) \tag{A.4-3}$$

$$k_3 = f\left(t_n + \frac{h}{2}, x_n + \frac{h}{2}k_2\right) \tag{A.5-4}$$

$$x_{n+1} = x_n + \frac{h}{6}(k_1 + k_2 + k_3 + k_4) \tag{A.5-5}$$

The equation set A.5 is the commonly used fourth order *Runge-Kutta* method (RK4) for approximating the solutions to ODE's. In order to improve the accuracy of the approximation an adaptive stepsize control can be implemented when finding the solution to A.5. This technique can be illustrated by considering the stepsizes h and $h/2$ used to compute the approximate solutions x_1 and x_2 respectively for The RK method of order p. If the exact solution is denoted by $\tilde{x}_{n+1}$ then,

$$\tilde{x}_{n+1} = x_1 + Ch^{p+1} + \vartheta(h^{p+2}), \tag{A.6}$$

$$\tilde{x}_{n+1} = x_2 + 2C\left(\frac{h}{2}\right)^{p+1} + \vartheta(h^{p+2}), \tag{A.7}$$

Therefore,

$$|x_1 - x_2| = Ch^{(p+1)}\left(1 - \frac{1}{2p}\right) \tag{A.8}$$

Or,

$$C = \frac{|x_1 - x_2|}{(1 - 2^{-p})h^{p+1}} \tag{A.9}$$

By substituting the formulation of C into A.7, the following is obtained:

$$\tilde{x}_{n+1} = x_2 + \varepsilon + \vartheta(h^{p+2}), \tag{A.10}$$

Where,

$$\varepsilon = \frac{|x_1 - x_2|}{(2^p - 1)}$$

The expression denoted by ε is an indicator of the truncation error. Therefore the estimate has been improved to the order $p + 1$. For a fourth order formulation i.e. $p = 4$,

$$\tilde{x}_{n+1} = x_2 + \frac{|x_1 - x_2|}{15} + \vartheta(h^{p+2}), \tag{A.11}$$

Appendix C1- Graphical user interface screenshot

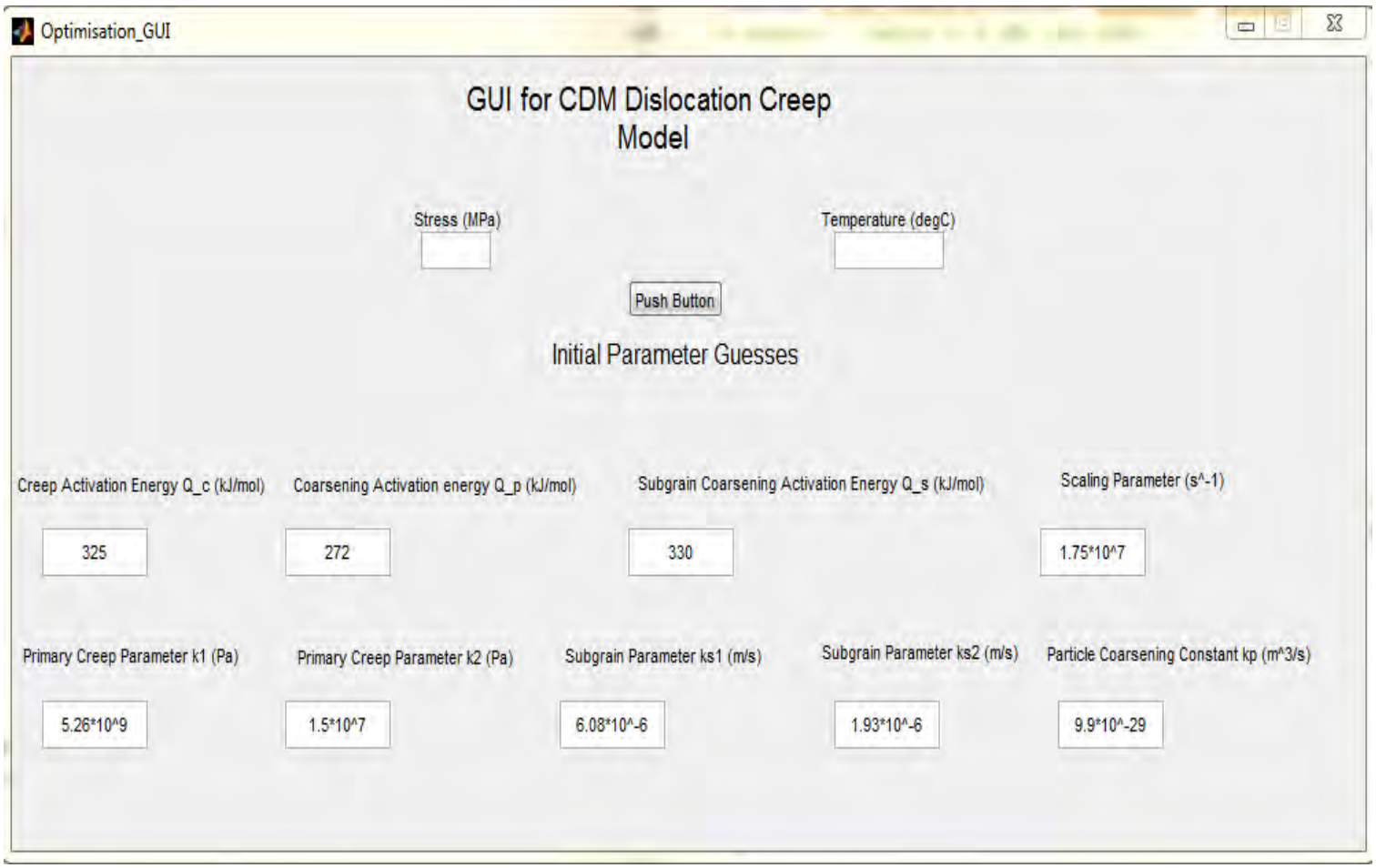

Appendix C2 – Source Code (Implemented in Matlab™)

Graphical User Interface (GUI) code

```
function varargout = CDM_GUI(varargin)
% CDM_GUI MATLAB code for CDM_GUI.fig
%      CDM_GUI, by itself, creates a new CDM_GUI or raises the existing
%      singleton*.
%
%      H = CDM_GUI returns the handle to a new CDM_GUI or the handle to
%      the existing singleton*.
%
%      CDM_GUI('CALLBACK',hObject,eventData,handles,...) calls the local
%      function named CALLBACK in CDM_GUI.M with the given input arguments.
%
%      CDM_GUI('Property','Value',...) creates a new CDM_GUI or raises the
%      existing singleton*.  Starting from the left, property value pairs
are
%      applied to the GUI before CDM_GUI_OpeningFcn gets called.  An
%      unrecognized property name or invalid value makes property
application
%      stop.  All inputs are passed to CDM_GUI_OpeningFcn via varargin.
%
%      *See GUI Options on GUIDE's Tools menu.  Choose "GUI allows only one
%      instance to run (singleton)".
%
% See also: GUIDE, GUIDATA, GUIHANDLES

% Edit the above text to modify the response to help CDM_GUI

% Last Modified by GUIDE v2.5 10-Jun-2016 14:26:41

% Begin initialization code - DO NOT EDIT
gui_Singleton = 1;
gui_State = struct('gui_Name',       mfilename, ...
                   'gui_Singleton',  gui_Singleton, ...
                   'gui_OpeningFcn', @CDM_GUI_OpeningFcn, ...
                   'gui_OutputFcn',  @CDM_GUI_OutputFcn, ...
                   'gui_LayoutFcn',  [] , ...
                   'gui_Callback',   []);
if nargin && ischar(varargin{1})
    gui_State.gui_Callback = str2func(varargin{1});
end

if nargout
    [varargout{1:nargout}] = gui_mainfcn(gui_State, varargin{:});
else
    gui_mainfcn(gui_State, varargin{:});
end
% End initialization code - DO NOT EDIT


% --- Executes just before CDM_GUI is made visible.
function CDM_GUI_OpeningFcn(hObject, eventdata, handles, varargin)
% This function has no output args, see OutputFcn.
% hObject    handle to figure
% eventdata  reserved - to be defined in a future version of MATLAB
```

```
% handles    structure with handles and user data (see GUIDATA)
% varargin   command line arguments to CDM_GUI (see VARARGIN)

% Choose default command line output for CDM_GUI
handles.output = hObject;

% Update handles structure
guidata(hObject, handles);

% UIWAIT makes CDM_GUI wait for user response (see UIRESUME)
% uiwait(handles.figure1);


% --- Outputs from this function are returned to the command line.
function varargout = CDM_GUI_OutputFcn(hObject, eventdata, handles)
% varargout  cell array for returning output args (see VARARGOUT);
% hObject    handle to figure
% eventdata  reserved - to be defined in a future version of MATLAB
% handles    structure with handles and user data (see GUIDATA)

% Get default command line output from handles structure
varargout{1} = handles.output;



function Stress_Callback(hObject, eventdata, handles)
% hObject    handle to Stress (see GCBO)
% eventdata  reserved - to be defined in a future version of MATLAB
% handles    structure with handles and user data (see GUIDATA)

% Hints: get(hObject,'String') returns contents of Stress as text
%        str2double(get(hObject,'String')) returns contents of Stress as a
double


% --- Executes during object creation, after setting all properties.
function Stress_CreateFcn(hObject, eventdata, handles)
% hObject    handle to Stress (see GCBO)
% eventdata  reserved - to be defined in a future version of MATLAB
% handles    empty - handles not created until after all CreateFcns called

% Hint: edit controls usually have a white background on Windows.
%       See ISPC and COMPUTER.
if ispc && isequal(get(hObject,'BackgroundColor'),
get(0,'defaultUicontrolBackgroundColor'))
    set(hObject,'BackgroundColor','white');
end



function Temperature_Callback(hObject, eventdata, handles)
% hObject    handle to Temperature (see GCBO)
% eventdata  reserved - to be defined in a future version of MATLAB
% handles    structure with handles and user data (see GUIDATA)

% Hints: get(hObject,'String') returns contents of Temperature as text
%        str2double(get(hObject,'String')) returns contents of Temperature
as a double
```

```
% --- Executes during object creation, after setting all properties.
function Temperature_CreateFcn(hObject, eventdata, handles)
% hObject    handle to Temperature (see GCBO)
% eventdata  reserved - to be defined in a future version of MATLAB
% handles    empty - handles not created until after all CreateFcns called

% Hint: edit controls usually have a white background on Windows.
%       See ISPC and COMPUTER.
if ispc && isequal(get(hObject,'BackgroundColor'),
get(0,'defaultUicontrolBackgroundColor'))
    set(hObject,'BackgroundColor','white');
end



function QC_Callback(hObject, eventdata, handles)
% hObject    handle to QC (see GCBO)
% eventdata  reserved - to be defined in a future version of MATLAB
% handles    structure with handles and user data (see GUIDATA)

% Hints: get(hObject,'String') returns contents of QC as text
%        str2double(get(hObject,'String')) returns contents of QC as a
double


% --- Executes during object creation, after setting all properties.
function QC_CreateFcn(hObject, eventdata, handles)
% hObject    handle to QC (see GCBO)
% eventdata  reserved - to be defined in a future version of MATLAB
% handles    empty - handles not created until after all CreateFcns called

% Hint: edit controls usually have a white background on Windows.
%       See ISPC and COMPUTER.
if ispc && isequal(get(hObject,'BackgroundColor'),
get(0,'defaultUicontrolBackgroundColor'))
    set(hObject,'BackgroundColor','white');
end



function QP_Callback(hObject, eventdata, handles)
% hObject    handle to QP (see GCBO)
% eventdata  reserved - to be defined in a future version of MATLAB
% handles    structure with handles and user data (see GUIDATA)

% Hints: get(hObject,'String') returns contents of QP as text
%        str2double(get(hObject,'String')) returns contents of QP as a
double


% --- Executes during object creation, after setting all properties.
function QP_CreateFcn(hObject, eventdata, handles)
% hObject    handle to QP (see GCBO)
% eventdata  reserved - to be defined in a future version of MATLAB
% handles    empty - handles not created until after all CreateFcns called
```

```
% Hint: edit controls usually have a white background on Windows.
%       See ISPC and COMPUTER.
if ispc && isequal(get(hObject,'BackgroundColor'),
get(0,'defaultUicontrolBackgroundColor'))
    set(hObject,'BackgroundColor','white');
end



function QS_Callback(hObject, eventdata, handles)
% hObject    handle to QS (see GCBO)
% eventdata  reserved - to be defined in a future version of MATLAB
% handles    structure with handles and user data (see GUIDATA)

% Hints: get(hObject,'String') returns contents of QS as text
%        str2double(get(hObject,'String')) returns contents of QS as a
double


% --- Executes during object creation, after setting all properties.
function QS_CreateFcn(hObject, eventdata, handles)
% hObject    handle to QS (see GCBO)
% eventdata  reserved - to be defined in a future version of MATLAB
% handles    empty - handles not created until after all CreateFcns called

% Hint: edit controls usually have a white background on Windows.
%       See ISPC and COMPUTER.
if ispc && isequal(get(hObject,'BackgroundColor'),
get(0,'defaultUicontrolBackgroundColor'))
    set(hObject,'BackgroundColor','white');
end



function STRAIN0_Callback(hObject, eventdata, handles)
% hObject    handle to STRAIN0 (see GCBO)
% eventdata  reserved - to be defined in a future version of MATLAB
% handles    structure with handles and user data (see GUIDATA)

% Hints: get(hObject,'String') returns contents of STRAIN0 as text
%        str2double(get(hObject,'String')) returns contents of STRAIN0 as a
double


% --- Executes during object creation, after setting all properties.
function STRAIN0_CreateFcn(hObject, eventdata, handles)
% hObject    handle to STRAIN0 (see GCBO)
% eventdata  reserved - to be defined in a future version of MATLAB
% handles    empty - handles not created until after all CreateFcns called

% Hint: edit controls usually have a white background on Windows.
%       See ISPC and COMPUTER.
if ispc && isequal(get(hObject,'BackgroundColor'),
get(0,'defaultUicontrolBackgroundColor'))
    set(hObject,'BackgroundColor','white');
end
```

```
function K_ONE_Callback(hObject, eventdata, handles)
% hObject    handle to K_ONE (see GCBO)
% eventdata  reserved - to be defined in a future version of MATLAB
% handles    structure with handles and user data (see GUIDATA)

% Hints: get(hObject,'String') returns contents of K_ONE as text
%        str2double(get(hObject,'String')) returns contents of K_ONE as a
double


% --- Executes during object creation, after setting all properties.
function K_ONE_CreateFcn(hObject, eventdata, handles)
% hObject    handle to K_ONE (see GCBO)
% eventdata  reserved - to be defined in a future version of MATLAB
% handles    empty - handles not created until after all CreateFcns called

% Hint: edit controls usually have a white background on Windows.
%       See ISPC and COMPUTER.
if ispc && isequal(get(hObject,'BackgroundColor'),
get(0,'defaultUicontrolBackgroundColor'))
    set(hObject,'BackgroundColor','white');
end



function K_TWO_Callback(hObject, eventdata, handles)
% hObject    handle to K_TWO (see GCBO)
% eventdata  reserved - to be defined in a future version of MATLAB
% handles    structure with handles and user data (see GUIDATA)

% Hints: get(hObject,'String') returns contents of K_TWO as text
%        str2double(get(hObject,'String')) returns contents of K_TWO as a
double


% --- Executes during object creation, after setting all properties.
function K_TWO_CreateFcn(hObject, eventdata, handles)
% hObject    handle to K_TWO (see GCBO)
% eventdata  reserved - to be defined in a future version of MATLAB
% handles    empty - handles not created until after all CreateFcns called

% Hint: edit controls usually have a white background on Windows.
%       See ISPC and COMPUTER.
if ispc && isequal(get(hObject,'BackgroundColor'),
get(0,'defaultUicontrolBackgroundColor'))
    set(hObject,'BackgroundColor','white');
end



function KS_ONE_Callback(hObject, eventdata, handles)
% hObject    handle to KS_ONE (see GCBO)
% eventdata  reserved - to be defined in a future version of MATLAB
% handles    structure with handles and user data (see GUIDATA)

% Hints: get(hObject,'String') returns contents of KS_ONE as text
```

```
%        str2double(get(hObject,'String')) returns contents of KS_ONE as a
double


% --- Executes during object creation, after setting all properties.
function KS_ONE_CreateFcn(hObject, eventdata, handles)
% hObject    handle to KS_ONE (see GCBO)
% eventdata  reserved - to be defined in a future version of MATLAB
% handles    empty - handles not created until after all CreateFcns called

% Hint: edit controls usually have a white background on Windows.
%       See ISPC and COMPUTER.
if ispc && isequal(get(hObject,'BackgroundColor'),
get(0,'defaultUicontrolBackgroundColor'))
    set(hObject,'BackgroundColor','white');
end



function KS_TWO_Callback(hObject, eventdata, handles)
% hObject    handle to KS_TWO (see GCBO)
% eventdata  reserved - to be defined in a future version of MATLAB
% handles    structure with handles and user data (see GUIDATA)

% Hints: get(hObject,'String') returns contents of KS_TWO as text
%        str2double(get(hObject,'String')) returns contents of KS_TWO as a
double


% --- Executes during object creation, after setting all properties.
function KS_TWO_CreateFcn(hObject, eventdata, handles)
% hObject    handle to KS_TWO (see GCBO)
% eventdata  reserved - to be defined in a future version of MATLAB
% handles    empty - handles not created until after all CreateFcns called

% Hint: edit controls usually have a white background on Windows.
%       See ISPC and COMPUTER.
if ispc && isequal(get(hObject,'BackgroundColor'),
get(0,'defaultUicontrolBackgroundColor'))
    set(hObject,'BackgroundColor','white');
end



function KP_Callback(hObject, eventdata, handles)
% hObject    handle to KP (see GCBO)
% eventdata  reserved - to be defined in a future version of MATLAB
% handles    structure with handles and user data (see GUIDATA)

% Hints: get(hObject,'String') returns contents of KP as text
%        str2double(get(hObject,'String')) returns contents of KP as a
double


% --- Executes during object creation, after setting all properties.
function KP_CreateFcn(hObject, eventdata, handles)
% hObject    handle to KP (see GCBO)
% eventdata  reserved - to be defined in a future version of MATLAB
```

```
% handles    empty - handles not created until after all CreateFcns called

% Hint: edit controls usually have a white background on Windows.
%       See ISPC and COMPUTER.
if ispc && isequal(get(hObject,'BackgroundColor'),
get(0,'defaultUicontrolBackgroundColor'))
    set(hObject,'BackgroundColor','white');
end



% --- Executes on selection change in popupmenu1.
function popupmenu1_Callback(hObject, eventdata, handles)
% hObject    handle to popupmenu1 (see GCBO)
% eventdata  reserved - to be defined in a future version of MATLAB
% handles    structure with handles and user data (see GUIDATA)

% Hints: contents = cellstr(get(hObject,'String')) returns popupmenu1
contents as cell array
%        contents{get(hObject,'Value')} returns selected item from
popupmenu1



% --- Executes during object creation, after setting all properties.
function popupmenu1_CreateFcn(hObject, eventdata, handles)
% hObject    handle to popupmenu1 (see GCBO)
% eventdata  reserved - to be defined in a future version of MATLAB
% handles    empty - handles not created until after all CreateFcns called

% Hint: popupmenu controls usually have a white background on Windows.
%       See ISPC and COMPUTER.
if ispc && isequal(get(hObject,'BackgroundColor'),
get(0,'defaultUicontrolBackgroundColor'))
    set(hObject,'BackgroundColor','white');
end



% --- If Enable == 'on', executes on mouse press in 5 pixel border.
% --- Otherwise, executes on mouse press in 5 pixel border or over
popupmenu1.
function popupmenu1_ButtonDownFcn(hObject, eventdata, handles)
% hObject    handle to popupmenu1 (see GCBO)
% eventdata  reserved - to be defined in a future version of MATLAB
% handles    structure with handles and user data (see GUIDATA)



% --- Executes on button press in pushbutton1.
function pushbutton1_Callback(hObject, eventdata, handles)
% hObject    handle to pushbutton1 (see GCBO)
% eventdata  reserved - to be defined in a future version of MATLAB
% handles    structure with handles and user data (see GUIDATA)
sigma1 = str2num(get( handles.Stress,'string'));

Temp = str2num(get( handles.Temperature,'string'))
T = Temp+273
sigma=sigma1*10^6
R = 8.314
steel = {get(handles.popupmenu1,'Value')};
steel = cell2mat(steel);
if steel == 1
```

```
P_i = (108*10^-9)^3;    % Initial M23C6 ppt size in m
S_i = 0.7*10^-6;        % Initial subgrain size in m

Q_c = (str2num(get( handles.QC,'string')))*10^3;
Q_p = (str2num(get( handles.QP,'string')))*10^3;
Q_s = (str2num(get( handles.QS,'string')))*10^3;
k_one = (str2num(get( handles.K_ONE,'string')));
k_two = (str2num(get( handles.K_TWO,'string')));
kp = (str2num(get( handles.KP,'string')))/P_i;
ks_one = (str2num(get( handles.KS_ONE,'string')));
ks_two = (str2num(get( handles.KS_TWO,'string')));
strainO = (str2num(get( handles.STRAIN0,'string')));

 [t,y] = CDM_Dislocation_creep_Model_function ( sigma,T, k_one, k_two, kp,
R, ks_one, ks_two, Q_c, Q_p, Q_s, P_i, S_i, strainO);

else if steel == 2


P_i = (95*10^-9)^3;    % Initial M23C6 ppt size in m
S_i = 0.79*10^-6;        % Initial subgrain size in m

Q_c = (str2num(get( handles.QC,'string')))*10^3;
Q_p = (str2num(get( handles.QP,'string')))*10^3;
Q_s = (str2num(get( handles.QS,'string')))*10^3;
k_one = (str2num(get( handles.K_ONE,'string')));
k_two = (str2num(get( handles.K_TWO,'string')));
kp = (str2num(get( handles.KP,'string')))/P_i;
ks_one = (str2num(get( handles.KS_ONE,'string')));
ks_two = (str2num(get( handles.KS_TWO,'string')));
strainO = (str2num(get( handles.STRAIN0,'string')));

[t,y] = CDM_Dislocation_creep_Model_function_P92 ( sigma,T, k_one, k_two,
kp, R, ks_one, ks_two, Q_c, Q_p, Q_s, P_i, S_i, strainO);
    end
end
```

CDM Execution Function – CB8

File name:CDM_Dislocation_creep_Model_function.m

```
function [t,y] = CDM_Dislocation_creep_Model_function (  sigma,T, k_one,
k_two, kp, R, ks_one, ks_two, Q_c, Q_p, Q_s, P_i, S_i, strainO);

%global k T sigma k_one k_two kp R ks_one ks_two Q_c Q_p Q_s P_i S_i
strainO ; % Global Constants
%% Model Time vector (may need to be adjusted depending on model
parameters)
if  sigma == 100*10^6;
        tspan=[0 30666800];     % Time vector for 100 MPa stress condition
else if sigma == 85*10^6;
        tspan=[0 39566800];     % Time vector for 85 MPa stress condition
else if sigma == 75*10^6;
```

```
        tspan=[0 50566800];     % Time vector for 75 MPa stress condition
    end
    end
end;

% initialize solution vector,

y(1,1) = 0;             % Initial Creep Strain in 1/s
y(2,1) = 2*10^6;        % Initial Primary creep stress in MPa
y(3,1) = 0;             % Initial Subgrain coarsening D_s damage
y(4,1) = 0;             % Initial M23C6 evolution coarsening D_p
y(5,1)= 0.35;           % Initial stress redistribution value
y(6,1) = sigma;         % Initial applied stress in MPa
y(7,1) = (108*10^-9);   % Initial M23C6 ppt size in m
y(8,1)= S_i;            % Initial Subgrain size in m
y(9,1) = 0;

%% Call Experimental data
if  sigma == 100*10^6;
        sample_number = 8.74;
else if sigma == 85*10^6;
        sample_number = 8.93;
else if sigma == 75*10^6;
        sample_number = 8.96;
    end
    end
end

[td,RawStrain]= expdata(sample_number); % Call experimental creep-time data

%%
[t,y]=ode45('Orut_no_voids',tspan,y,sigma,T, k_one, k_two, kp, R, ks_one,
ks_two, Q_c, Q_p, Q_s, P_i, S_i, strain0);   % Call Fourth Order Runge-
Kuttta solver ODE45

RawStrain = smooth(RawStrain);


% Model strain rate evaluation
dy= diff(y(:,1));
dt= diff(t./3600);
dydt= dy./dt;
%% Error Calculations

 yb(1,1) = 0;                       % Strain
 yb(2,1) = 2*10^6;                  % Primary creep
 yb(3,1) = 0;                       % Subgrain evolution D_s
 yb(4,1) = 0;                       % MX evolution D_p
 yb(5,1)= 0.4;                      % Initial stress redistribution value
 yb(6,1) = sigma;                   % Initial applied stress in MPa
 yb(7,1) = (108*10^-9);             % Initial M23C6 ppt size in m
 yb(8,1)= S_i;                      % Initial Subgrain size in m
 yb(9,1) = 0;

[t2,yb]=ode45('Orut_no_voids',td,yb,sigma,T, k_one, k_two, kp, R, ks_one,
ks_two, Q_c, Q_p, Q_s, P_i, S_i, strain0);        % Run Model with Exp data
time vector

%Time at 5% Strain
```

```
I = find(yb(:,1)<=0.05);
QI = max(I);                                % Identify model strain vector
position at 5% strain
Mod_time_at_5perC_strain = t2(QI)/3600       % Model time vector value at 5
percent strain

%%

RawStrain2 = smooth(RawStrain);             % Smooth experimental strain
data

tm = t2./3600;                              % Model time vector in hours
rate = yb(:,1)./tm;                         % Model strain rate

td1 = td./3600;                             % Experimental time vector in
hours
rateExp = smooth(RawStrain2./td1);           % Experimental strain rate
minMod = min(rate);                         % Model minimum strain rate

%%
ffm = find(rate==minMod);                   % Model minimum strain rate
vector position
fftm = t2(ffm);                             % Model Time vector at which
minimum strain rate occurs
pos_tm = find(t2==fftm);
strain_minratem = yb(pos_tm,1)*100;         % Model minimum strain rate in
percent
wm= yb(:,1)*100;
Ter_onsetm = strain_minratem +0.2;          % Model Onset of tertiary
creep strain
[v ,index] = min(abs(wm-Ter_onsetm));
closestValuesm = wm(index);
pos_clvalm=find(wm==closestValuesm);
Mod_Time_at_teronset=t2(pos_clvalm)/3600    % Model Time at which onset of
tertiary creep occurs
Mod_time_at_minrate = fftm/3600             % Model Time at which minimum
creep rate occurs


%% Experimental M23C6 precipitate size/time  data
pptexp = [108
109
141
145
156]*10^-9;

ppttime =[0
100
500
1000
1500];

% M23C6 size error
errorppt=[6.4,5.7,6.8,6.8,7.4];

%% Experimental subgrain size/time data
expsubd = [0.7
0.89
0.93
```

```
0.98
1.6];
D =[0
2000
4000
7000
16500];

% Subgrain size error
E=[0.2,0.2,0.2,0.2,0.2];

%% Graphs

% Plot of creep strain vs time for model
figure(1)
plot(t/3600, y(:,1)*100, 'g-' , 'LineWidth' , 2) , grid on
hold on
plot(td/3600,RawStrain*100, 'r--' , 'LineWidth' , 2),grid on
ylabel('Strain (%)' , 'FontSize' , 15)
xlabel('Time (h)' , 'FontSize' , 15)
title('Graph of Dislocation Creep ' , 'FontSize' , 15)
legend('Model','Sample 8.89');
hold off

% Plot of primary creep stress evolution
figure(2)
plot(t/3600, y(:,2), 'r-' , 'LineWidth' , 2) , grid
hold on
ylabel('Strain (%)' , 'FontSize' , 15)
xlabel('Time (h)' , 'FontSize' , 15)
title('Primary Creep ' , 'FontSize' , 15)
hold off

% Plot of subgrain size and subgrain damage evolution
figure(3)
subplot(2,1,1)
plot(t/3600, y(:,3), 'bl-' , 'LineWidth' , 2) , grid
ylabel('Subgrain Evolution Damage ' , 'FontSize' , 15)
xlabel('Time (h)' , 'FontSize' , 15)
title('Subgrain Evolution Model ' , 'FontSize' , 15)
subplot(2,1,2)
plot(t/3600,y(:,8)*10^6, 'g-' , 'LineWidth' , 2) , grid
 hold on
errorbar(D,expsubd,E, 'r--' , 'LineWidth' , 2)
ylabel('Subgrain size (microns)' , 'FontSize' , 15)
xlabel('Time (h)' , 'FontSize' , 15)
title('Graph of subgrain growth' , 'FontSize' , 15)

% Plot of M23C6 size and M23C6 damage evolution
figure(4)
subplot(2,1,1)
plot(t/3600, y(:,4), 'bl-' , 'LineWidth' , 2) , grid
ylabel('M23C6 Coarsening Damage' , 'FontSize' , 15)
xlabel('Time (h)' , 'FontSize' , 15)
title('Graph of M23C6 Coarsening' , 'FontSize' , 15)
subplot(2,1,2)
title('Graph of M23C6 Coarsening' , 'FontSize' , 15)
hold on
plot(t/3600,y(:,7)*10^9, 'g-' , 'LineWidth' , 2) , grid
errorbar(ppttime,pptexp*10^9,errorppt, 'r--', 'LineWidth' , 2)
```

```
axis([0,1600,100,180]);
ylabel('Precipitate diameter (nm)' , 'FontSize' , 15)
xlabel('Time (h)' , 'FontSize' , 15)
title('Graph of M23C6 Coarsening' , 'FontSize' , 15)
hold off

% Plot of Strain rate data
figure(5)
loglog(t(2:end)./3600,dydt, 'g-' , 'LineWidth' , 2) , grid
hold on
loglog(td1,rateExp, 'b-' , 'LineWidth' , 2)
ylabel('Log Strain Rate (h^-1)' , 'FontSize' , 15)
xlabel('Log Time (h)' , 'FontSize' , 15)
title('Graph of creep Strain Rate' , 'FontSize' , 15)
hold off
end
```

CDM Execution Function – P92

File name: CDM_Dislocation_creep_Model_function_P92.m

```
% Muhammad Stracey
% Center for Materials Engineering UCT 2016
% CB8 CDM Dislocation Creep Model
%%%%%%%%%%%%%%%%%%%%%%%%%%%%%%%%%%%%%%%%%%%%%%%%%%%%%%%%%%%%%%%%%%%%%%%%%%%%%%%
function [t,y] = CDM_Dislocation_creep_Model_function_P92 (  sigma,T,
k_one, k_two, kp, R, ks_one, ks_two, Q_c, Q_p, Q_s, P_i, S_i, strain0);

%global k T sigma k_one k_two kp R ks_one ks_two Q_c Q_p Q_s P_i S_i
strain0 ; % Global Constants
%% Model Time vector (may need to be adjusted depending on model
parameters)
if  sigma == 104*10^6;
        tspan=[0 25566800];     % Time vector for 100 MPa stress condition
else if sigma == 92*10^6;
        tspan=[0 48566800];     % Time vector for 85 MPa stress condition
    end
end;

% initialize solution vector,

y(1,1) = 0;             % Initial Creep Strain in 1/s
y(2,1) = 2*10^6;        % Initial Primary creep stress in MPa
y(3,1) = 0;             % Initial Subgrain coarsening D_s damage
y(4,1) = 0;             % Initial M23C6 evolution coarsening D_p
y(5,1)= 0.35;           % Initial stress redistribution value
y(6,1) = sigma;         % Initial applied stress in MPa
y(7,1) = (95*10^-9);    % Initial M23C6 ppt size in m
y(8,1)= S_i;            % Initial Subgrain size in m


%% Call Experimental data

 if sigma == 104*10^6;
        sample_number = 104;
else if sigma == 92*10^6;
        sample_number = 92;
```

```
    end
end

[td,RawStrain]= expdataP92(sample_number); % Call experimental creep-time
data

%%
[t,y]=ode45('CDM_equation_loop',tspan,y,sigma,T, k_one, k_two, kp, R,
ks_one, ks_two, Q_c, Q_p, Q_s, P_i, S_i, strain0);   % Call Fourth Order
Runge-Kuttta solver ODE45

RawStrain = smooth(RawStrain);


% Model strain rate evaluation
dy= diff(y(:,1));
dt= diff(t./3600);
dydt= dy./dt;
%% Error Calculations

 yb(1,1) = 0;                          % Strain
 yb(2,1) = 2*10^6;                     % Primary creep
 yb(3,1) = 0;                          % Subgrain evolution D_s
 yb(4,1) = 0;                          % MX evolution D_p
 yb(5,1)= 0.35;                         % Initial stress redistribution value
 yb(6,1) = sigma;                      % Initial applied stress in MPa
 yb(7,1) = (95*10^-9);                % Initial M23C6 ppt size in m
 yb(8,1)= S_i;                          % Initial Subgrain size in m


[t2,yb]=ode45('CDM_equation_loop',td,yb,sigma,T, k_one, k_two, kp, R,
ks_one, ks_two, Q_c, Q_p, Q_s, P_i, S_i, strain0);        % Run Model with
Exp data time vector

%Time at 5% Strain
I = find(yb(:,1)<=0.05);
QI = max(I);                                  % Identify model strain vector
position at 5% strain
Mod_time_at_5perC_strain = t2(QI)/3600        % Model time vector value at 5
percent strain

%%

RawStrain2 = smooth(RawStrain);               % Smooth experimental strain
data

tm = t2./3600;                                % Model time vector in hours
rate = yb(:,1)./tm;                           % Model strain rate

td1 = td./3600;                               % Experimental time vector in
hours
rateExp = smooth(RawStrain2./td1);             % Experimental strain rate
minMod = min(rate);                           % Model minimum strain rate

%%
ffm = find(rate==minMod);                     % Model minimum strain rate
vector position
```

```
fftm = t2(ffm);                                % Model Time vector at which
minimum strain rate occurs
pos_tm = find(t2==fftm);
strain_minratem = yb(pos_tm,1)*100;            % Model minimum strain rate in
percent
wm= yb(:,1)*100;
Ter_onsetm = strain_minratem +0.2;             % Model Onset of tertiary
creep strain
[v ,index] = min(abs(wm-Ter_onsetm));
closestValuesm = wm(index);
pos_clvalm=find(wm==closestValuesm);
Mod_Time_at_teronset=t2(pos_clvalm)/3600      % Model Time at which onset of
tertiary creep occurs
Mod_time_at_minrate = fftm/3600               % Model Time at which minimum
creep rate occurs



%% Graphs

% Plot of creep strain vs time for model
figure(1)
plot(t/3600, y(:,1)*100, 'g-' , 'LineWidth' , 2) , grid on
hold on
plot(td/3600,RawStrain*100, 'r--' , 'LineWidth' , 2),grid on
ylabel('Strain (%)' , 'FontSize' , 15)
xlabel('Time (h)' , 'FontSize' , 15)
title('Graph of Dislocation Creep ' , 'FontSize' , 15)
legend('Model','Sample 8.89');
hold off

% Plot of primary creep stress evolution
figure(2)
plot(t/3600, y(:,2), 'r-' , 'LineWidth' , 2) , grid
hold on
ylabel('Strain (%)' , 'FontSize' , 15)
xlabel('Time (h)' , 'FontSize' , 15)
title('Primary Creep ' , 'FontSize' , 15)
hold off

% Plot of subgrain size and subgrain damage evolution
figure(3)
subplot(2,1,1)
plot(t/3600, y(:,3), 'bl-' , 'LineWidth' , 2) , grid
ylabel('Subgrain Evolution Damage ' , 'FontSize' , 15)
xlabel('Time (h)' , 'FontSize' , 15)
title('Subgrain Evolution Model ' , 'FontSize' , 15)
subplot(2,1,2)
plot(t/3600,y(:,8)*10^6, 'g-' , 'LineWidth' , 2) , grid
ylabel('Subgrain size (microns)' , 'FontSize' , 15)
xlabel('Time (h)' , 'FontSize' , 15)
title('Graph of subgrain growth' , 'FontSize' , 15)

% Plot of M23C6 size and M23C6 damage evolution
figure(4)
subplot(2,1,1)
plot(t/3600, y(:,4), 'bl-' , 'LineWidth' , 2) , grid
ylabel('M23C6 Coarsening Damage' , 'FontSize' , 15)
xlabel('Time (h)' , 'FontSize' , 15)
title('Graph of M23C6 Coarsening' , 'FontSize' , 15)
```

```
subplot(2,1,2)
title('Graph of M23C6 Coarsening' , 'FontSize' , 15)
hold on
plot(t/3600,y(:,7)*10^9, 'g-' , 'LineWidth' , 2) , grid
axis([0,1600,100,180]);
ylabel('Precipitate diameter (nm)' , 'FontSize' , 15)
xlabel('Time (h)' , 'FontSize' , 15)
title('Graph of M23C6 Coarsening' , 'FontSize' , 15)
hold off

% Plot of Strain rate data
figure(5)
loglog(t(2:end)./3600,dydt, 'g-' , 'LineWidth' , 2) , grid
hold on
loglog(td1,rateExp, 'b-' , 'LineWidth' , 2)
ylabel('Log Strain Rate (h^-1)' , 'FontSize' , 15)
xlabel('Log Time (h)' , 'FontSize' , 15)
title('Graph of creep Strain Rate' , 'FontSize' , 15)
hold off
end
```

CDM Equation Loop Function (Nested in ODE45)

File name: Orut.m

```
function F = Orut(t,y,sigma,T, k_one, k_two, kp, R, ks_one, ks_two, Q_c,
Q_p, Q_s, P_i, S_i, strain0);


F = zeros(8,1);
F(1) = strain0*exp(-Q_c/(R*T)).*sinh( (y(6).*(1-y(5).*(1-
y(3)))).*(y(2).*(1-y(4))));   % Creep Rate differential equation
F(2) = k_one.*(1-y(2)./k_two)*F(1); % Primary creep differential equation
F(3) =  F(1)./S_i.*(ks_one+ks_two).*(1-y(3)).^2; %Subgrain Damage Evolution
F(4) = (kp/3).*((1-y(4)).^4); % M23C6 Precipitate Damage Evolution
F(5) = -(y(5).*(1-y(5))./2.*(1+y(3)).^-1.*F(3);% Backstress Damage
F(6) = 0; % Applied Stress Rate
F(7) = kp./3.*y(7); % M23C6 Precipitate Growth Equation
F(8)= F(1).*(ks_one+ks_two); % Subgrain Growth Equation
```

Optimisation Routine Across Stress Range – CB8

Execution File

File name: Optimisation_multiple_stresses_CB8.m

```
clear all; close all; clc
global k sigma T sigma2 sigma3


%tic
```

```
sigma =  75*10^6;        % Stress condition one (MPa)
sigma2 = 85*10^6;        % Stress condition two (MPa)
sigma3 = 100*10^6;       % Stress condition three (MPa)

T = 650+273;              % Temperature
%% Initial Guess values

Q_cg = 3.30E+05;          % Creep activation energy guess (kJ/mol)
strainOg = 4.84E+07;      % Normalising strain guess value (1/s)
k_oneg = 7.14E+09 ;       % Primary creep rate constant guess value(MPa)
k_twog= 1.17E+07;         % Primary creep limiting stress guess value (MPa)
ks_oneg = 7.14E-06;       % Temperature independent subgrain coarseing
constant guess value
ks_twog = 6E-06;          % Temperature dependent subgrain coarseing
constant guess value
kpg = 6E-29;              % M23C6 ppt coarsening constant

%% Initialise optimisation routine
v = [Q_cg   strainOg    k_oneg  k_twog  ks_oneg  ks_twog kpg];    % Initial
guess vector

LB = [290*10^3  5*10^6 5*10^9 8*10^6   6*10^-6 5*10^-7 1*10^-29]; %
Optimisation lower bound values
UB = [340*10^3  5*10^7 10*10^9 15*10^6 6*10^-5 5*10^-6 6*10^-28]; %
Optimisation upper bound values

[k,fval,exitflag,output] =
fminsearchbnd(@myobj_multiple_stresses_CB8,v,LB,UB); % Call objective
function myobj_P92 nested in Nelder-Mead simplex fminsearchbnd
display('optimisation complete')
```

Objective Function

File name: `myobj_multiple_stresses_CB8.m`

```
%least squares Objective function for P92 across stress range
% Muhammad Stracey
function obj = myobj_multiple_stresses_CB8(k)
global R T P_i S_i sigma  sigma2 sigma3;

[td,RawStrain]= expdata(8.96);
[td2,RawStrain2]= expdata(8.93);
[td3,RawStrain3]= expdata(8.74);

%% Constants

R = 8.314;          % Boltzman Constant in J/(K mol)
P_i = (108*10^-9)^3; % Initial M23C6 ppt size ^3 in m
S_i = 0.7*10^-6;   % Initial subgrain size in m

%% Update parameter trial values

Q_c = k(1);     % Creep activation energy in kJ/mol
strainO = k(2); % Normalising strain in 1/s
k_one = k(3) ;  % Primary creep rate constant in MPa
k_two= k(4);    % Primary creep limiting stress in MPa
```

```
ks_one = k(5);  % Temperature independent subgrain coarseing constant
ks_two = k(6);  % Temperature dependent subgrain coarseing constant
kp = k(7)/P_i;  % M23C6 ppt coarsening constant

% initialize solution vector,

 x0(1,1) = 0;             % Initial Creep Strain in 1/s
 x0(2,1) = 2*10^6;        % Initial Primary creep stress in MPa
 x0(3,1) = 0;             % Initial Subgrain coarsening D_s damage
 x0(4,1) = 0;             % Initial M23C6 evolution coarsening D_p
 x0(5,1) = 0.35;          % Initial stress redistribution value

   %f = @(t,x) myodefcn(tspan,p,y);  %function to call ode45
  [t,x] = ode45(@(t,x) myodefcn_stress1(t,x,Q_c,strain0, k_one, k_two,
ks_one, ks_two,kp), td, x0);  %xs is the state variable predicted by the
model
  [t2,x2] = ode45(@(t2,x2) myodefcn_stress2(t,x2,Q_c,strain0, k_one, k_two,
ks_one, ks_two,kp), td2, x0);
  [t3,x3] = ode45(@(t3,x3) myodefcn_stress3(t,x3,Q_c,strain0, k_one, k_two,
ks_one, ks_two,kp), td3, x0);

y = smooth(RawStrain);
y2 = smooth(RawStrain2);
y3 = smooth(RawStrain3);



%% Plot model and experimental results
figure(1)
subplot(3,1,1)
plot(t/3600, x(:,1)*100, 'g-' , 'LineWidth' , 2) , grid
ylabel('Strain (%)' , 'FontSize' , 15)
xlabel('Time (h)' , 'FontSize' , 15)
title('Graph of Dislocation Creep ' , 'FontSize' , 15)
hold on
plot(td/3600, y(:,1)*100, 'b-' , 'LineWidth' , 2)
 hold off
subplot(3,1,2)
plot(t2/3600, x2(:,1)*100, 'g-' , 'LineWidth' , 2) , grid
ylabel('Strain (%)' , 'FontSize' , 15)
xlabel('Time (h)' , 'FontSize' , 15)
title('Graph of Dislocation Creep ' , 'FontSize' , 15)
hold on
plot(td2/3600, y2(:,1)*100, 'r-' , 'LineWidth' , 2)
hold off
subplot(3,1,3)
plot(t3/3600, x3(:,1)*100, 'g-' , 'LineWidth' , 2) , grid
ylabel('Strain (%)' , 'FontSize' , 15)
xlabel('Time (h)' , 'FontSize' , 15)
title('Graph of Dislocation Creep ' , 'FontSize' , 15)
hold on
plot(td3/3600, y3(:,1)*100, 'b-' , 'LineWidth' , 2)
hold off

%% Calculate Sum of squares error
n1 = numel(y);  % Get number of data points from model result 1
n2 = numel(y2); % Get number of data points from model result 2
n3 = numel(y3); % Get number of data points from model result 3
SSE= max((x(:,1)-y).^2);      % Calculate SSE for stress 1
SSE_2 = max((x2(:,1)-y2).^2); % Calculate SSE for stress 2
```

```
SSE_3 = max((x3(:,1)-y3).^2); % Calculate SSE for stress 3
SSE_1_N = (SSE/n1);           % Normalise error using number of data points
SSE_2_N = (SSE_2/n2);         % Normalise error using number of data points
SSE_3_N = (SSE_3/n3);         % Normalise error using number of data points
SSEM = [SSE_1_N,SSE_2_N,SSE_3_N]; % Vectorise errors

%% Impose condition to ensure error is distributed aprox. equally between
stresses
if sqrt(SSE) < 10^-4 && sqrt(SSE_2)< 10^-4 && sqrt(SSE_3)< 10^-4
        obj = (SSE_1_N + SSE_2_N +SSE_3_N)/3; % USSE value when conditions
are not met
else
        obj = max(SSEM)                       % USSE value when conditions
are met
end

end
```

Optimisation Routine across Stress Range – P92

Execution File

File name: Optimisation_multiple_stresses_P92.m

```
%% Optimisation initialisation for P92
% Muhammad Stracey

clear all; close all; clc
global k sigma T sigma2

sigma = 92*10^6;          % Stress condition one (MPa)
sigma2 = 104*10^6;        % Stress condition two (MPa)
T = 650+273;              % Temperature

%% Initial Guess values

Q_cg = 3.38E+05;          % Creep activation energy guess (kJ/mol)
strainOg = 4.17E+07;      % Normalising strain guess value (1/s)
k_oneg = 5.00E+09 ;       % Primary creep rate constant guess value(MPa)
k_twog= 1.37E+07;         % Primary creep limiting stress guess value (MPa)
ks_oneg = 6.13E-06;       % Temperature independent subgrain coarseing
constant guess value
ks_twog = 8.09E-07;       % Temperature dependent subgrain coarseing
constant guess value
kpg = 9.51E-29;           % M23C6 ppt coarsening constant

%% Initialise optimisation routine
v = [Q_cg   strainOg    k_oneg  k_twog  ks_oneg  ks_twog    kpg]; % Initial
guess vector

LB = [290*10^3  5*10^6   5*10^9 8*10^6   6*10^-6 5*10^-7 1*10^-29];    %
Optimisation lower bound values
UB = [340*10^3  5*10^7   10*10^9 15*10^6 6*10^-5 5*10^-6 6*10^-28];    %
Optimisation upper bound values

[k,fval,exitflag,output] = fminsearchbnd(@myobj_P92,v,LB,UB); % Call
objective function myobj_P92 nested in Nelder-Mead simplex fminsearchbnd
display('optimisation complete')
```

Objective Function

File name: myobj_P92.m

```
%least squares function Objective function for P92 across stress range
% Muhammad Stracey
function obj = myobj_P92(k)
global R T P_i S_i sigma  sigma2 ;

[td,RawStrain]= expdataP92(92);     % Call experimental creep-time data for
stress condition 1
[td2,RawStrain2]= expdataP92(104);  % Call experimental creep-time data for
stress condition 2
y = smooth(RawStrain);              % Smooth creep-time data for stress
condition 1
y2 = smooth(RawStrain2);            % Smooth creep-time data for stress
condition 2
%% Constants

R = 8.314;          % Boltzman Constant in J/(K mol)
P_i = (95*10^-9)^3; % Initial M23C6 ppt size ^3 in m
S_i = 0.79*10^-6;   % Initial subgrain size in m

%% Update parameter trial values

Q_c = k(1);     % Creep activation energy in kJ/mol
strain0 = k(2); % Normalising strain in 1/s
k_one = k(3) ;  % Primary creep rate constant in MPa
k_two= k(4);    % Primary creep limiting stress in MPa
ks_one = k(5);  % Temperature independent subgrain coarseing constant
ks_two = k(6);  % Temperature dependent subgrain coarseing constant
kp = k(7)/P_i;  % M23C6 ppt coarsening constant

% initialize solution vector,

 x0(1,1) = 0;             % Initial Creep Strain in 1/s
 x0(2,1) = 2*10^6;        % Initial Primary creep stress in MPa
 x0(3,1) = 0;             % Initial Subgrain coarsening D_s damage
 x0(4,1) = 0;             % Initial M23C6 evolution coarsening D_p
 x0(5,1) = 0.35;          % Initial stress redistribution value

%% Run model with updated parameter set
 [t,x] = ode45(@(t,x) myodefcn_stress1(t,x,Q_c,strain0, k_one, k_two,
ks_one, ks_two,kp), td, x0);  % Model predictions for stress 1
 [t2,x2] = ode45(@(t2,x2) myodefcn_stress2(t,x2,Q_c,strain0, k_one, k_two,
ks_one, ks_two,kp), td2, x0); % Model predictions for stress 2



%% Plot model and experimental results
figure(1)
subplot(2,1,1)
plot(t/3600, x(:,1)*100, 'g-' , 'LineWidth' , 2) , grid
ylabel('Strain (%)' , 'FontSize' , 15)
xlabel('Time (h)' , 'FontSize' , 15)
title('Graph of Dislocation Creep ' , 'FontSize' , 15)
hold on
```

```
plot(td/3600, y(:,1)*100, 'b-' , 'LineWidth' , 2)
hold off
subplot(2,1,2)
plot(t2/3600, x2(:,1)*100, 'g-' , 'LineWidth' , 2) , grid
ylabel('Strain (%)' , 'FontSize' , 15)
xlabel('Time (h)' , 'FontSize' , 15)
title('Graph of Dislocation Creep ' , 'FontSize' , 15)
hold on
plot(td2/3600, y2(:,1)*100, 'r-' , 'LineWidth' , 2)
hold off

%% Calculate Sum of squares error
n1 = numel(y);                  % Get number of data points from model
result 1
n2 = numel(y2);                 % Get number of data points from model
result 2
SSE_1= max((x(:,1)-y).^2);       % Calculate SSE for stress 1
SSE_2 = max((x2(:,1)-y2).^2);    % Calculate SSE for stress 2
SSE_1_N = (SSE_1/n1);            % Normalise error using number of data
points
SSE_2_N = (SSE_2/n2);            % Normalise error using number of data
points
SSEM = [SSE_1_N,SSE_2_N];       % Vectorise errors

%% Impose condition to ensure error is distributed aprox. equally between
stresses
if sqrt(SSE_1) < 10^-6 && sqrt(SSE_2)< 10^-6
      obj = (SSE_1_N + SSE_2_N)/2;          % USSE value when conditions
are not met
else
    obj = max(SSEM)                         % USSE value when conditions
are met
end

end
```

CDM Loop

Stress condition 1

File name: myodefcn_stress1

```
function F = myodefcn_stress1(t,x,Q_c,strainO, k_one, k_two, ks_one,
ks_two,kp)

global  R T P_i S_i sigma A B ;

F = zeros(5,1);
F(1) = strainO*exp(-Q_c/(R*T)).*sinh( (sigma.*(1-x(5).*(1-
x(3)))).*(x(2).*(1-x(4)))); % Creep Rate differential equation
F(2) = k_one.*(1-x(2)./k_two).*F(1);
% Primary creep differential equation
F(3) = F(1)./S_i.*(ks_one+ks_two).*(1-x(3)).^2;
% Subgrain Damage  Evolution
```

```
F(4) = kp/3.*(1-x(4)).^4;
% M23C6 Precipitate Damage Evolution
F(5) = -(x(5).*(1-x(5))./2*(1+x(3)).^-1.*F(3);
```

Stress condition 2

File name: myodefcn_stress2

```
function F = myodefcn_stress2(t,x2,Q_c, strain0, k_one, k_two, ks_one,
ks_two,kp)

global  R T P_i S_i sigma2  ;


F = zeros(5,1);
F(1) = strain0*exp(-Q_c/(R*T)).*sinh( (sigma2.*(1-x2(5).*(1-
x2(3)))./(x2(2).*(1-x2(4)))); % Creep Rate differential equation
F(2) = k_one.*(1-x2(2)./k_two).*F(1);
% Primary creep differential equation
F(3) = F(1)./S_i.*(ks_one+ks_two).*(1-x2(3)).^2;
% Subgrain Damage  Evolution
F(4) = kp/3.*(1-x2(4)).^4;
% M23C6 Precipitate Damage Evolution
F(5) = -(x2(5).*(1-x2(5))./2*(1+x2(3)).^-1.*F(3);
% Backstress Damage Evolution
```

Stress condition 3

File name: myodefcn_stress3

```
function F = myodefcn_stress3(t,x3,Q_c, strain0, k_one, k_two, ks_one,
ks_two,kp)

global   R T P_i S_i sigma3  ;


F = zeros(5,1);
F(1) = strain0*exp(-Q_c/(R*T)).*sinh( (sigma3.*(1-x3(5).*(1-
x3(3)))./(x3(2).*(1-x3(4)))); % Creep Rate differential equation
F(2) = k_one.*(1-x3(2)./k_two).*F(1);
% Primary creep differential equation
F(3) = F(1)./S_i.*(ks_one+ks_two).*(1-x3(3)).^2;
% Subgrain Damage  Evolution
F(4) = kp/3.*(1-x3(4)).^4;
% M23C6 Precipitate Damage Evolution
F(5) = -(x3(5).*(1-x3(5))./2*(1+x3(3)).^-1.*F(3);
% Backstress Damage Evolution
```

Nelder-Mead Routine

Routine adapted from [68]

File name: fminsearchbnd

```
function [x,fval,exitflag,output] =
fminsearchbnd(fun,x0,LB,UB,options,varargin)


% size checks
xsize = size(x0);
x0 = x0(:);
n=length(x0);

if (nargin<3) || isempty(LB)
  LB = repmat(-inf,n,1);
else
  LB = LB(:);
end
if (nargin<4) || isempty(UB)
  UB = repmat(inf,n,1);
else
  UB = UB(:);
end

if (n~=length(LB)) || (n~=length(UB))
  error 'x0 is incompatible in size with either LB or UB.'
end

% set default options if necessary
if (nargin<5) || isempty(options)
   options = optimset('MaxFunEvals',1000000);
end

% stuff into a struct to pass around
params.args = varargin;
params.LB = LB;
params.UB = UB;
params.fun = fun;
params.n = n;
% note that the number of parameters may actually vary if
% a user has chosen to fix one or more parameters
params.xsize = xsize;
params.OutputFcn = [];

% 0 --> unconstrained variable
% 1 --> lower bound only
% 2 --> upper bound only
% 3 --> dual finite bounds
% 4 --> fixed variable
params.BoundClass = zeros(n,1);
for i=1:n
  k = isfinite(LB(i)) + 2*isfinite(UB(i));
  params.BoundClass(i) = k;
  if (k==3) && (LB(i)==UB(i))
    params.BoundClass(i) = 4;
  end
end
```

```
% transform starting values into their unconstrained
% surrogates. Check for infeasible starting guesses.
x0u = x0;
k=1;
for i = 1:n
  switch params.BoundClass(i)
    case 1
      % lower bound only
      if x0(i)<=LB(i)
        % infeasible starting value. Use bound.
        x0u(k) = 0;
      else
        x0u(k) = sqrt(x0(i) - LB(i));
      end

      % increment k
      k=k+1;
    case 2
      % upper bound only
      if x0(i)>=UB(i)
        % infeasible starting value. use bound.
        x0u(k) = 0;
      else
        x0u(k) = sqrt(UB(i) - x0(i));
      end

      % increment k
      k=k+1;
    case 3
      % lower and upper bounds
      if x0(i)<=LB(i)
        % infeasible starting value
        x0u(k) = -pi/2;
      elseif x0(i)>=UB(i)
        % infeasible starting value
        x0u(k) = pi/2;
      else
        x0u(k) = 2*(x0(i) - LB(i))/(UB(i)-LB(i)) - 1;
        % shift by 2*pi to avoid problems at zero in fminsearch
        % otherwise, the initial simplex is vanishingly small
        x0u(k) = 2*pi+asin(max(-1,min(1,x0u(k))));
      end

      % increment k
      k=k+1;
    case 0
      % unconstrained variable. x0u(i) is set.
      x0u(k) = x0(i);

      % increment k
      k=k+1;
    case 4
      % fixed variable. drop it before fminsearch sees it.
      % k is not incremented for this variable.
  end

end
% if any of the unknowns were fixed, then we need to shorten
% x0u now.
```

```
if k<=n
  x0u(k:n) = [];
end

% were all the variables fixed?
if isempty(x0u)
  % All variables were fixed. quit immediately, setting the
  % appropriate parameters, then return.

  % undo the variable transformations into the original space
  x = xtransform(x0u,params);

  % final reshape
  x = reshape(x,xsize);

  % stuff fval with the final value
  fval = feval(params.fun,x,params.args{:});

  % fminsearchbnd was not called
  exitflag = 0;

  output.iterations = 0;
  output.funcCount = 1;
  output.algorithm = 'fminsearch';
  output.message = 'All variables were held fixed by the applied bounds';

  % return with no call at all to fminsearch
  return
end

% Check for an outputfcn. If there is any, then substitute my
% own wrapper function.
if ~isempty(options.OutputFcn)
  params.OutputFcn = options.OutputFcn;
  options.OutputFcn = @outfun_wrapper;
end

% now we can call fminsearch, but with our own
% intra-objective function.
[xu,fval,exitflag,output] = fminsearch(@intrafun,x0u,options,params);

% undo the variable transformations into the original space
x = xtransform(xu,params);

% final reshape to make sure the result has the proper shape
x = reshape(x,xsize);

% Use a nested function as the OutputFcn wrapper
  function stop = outfun_wrapper(x,varargin);
    % we need to transform x first
    xtrans = xtransform(x,params);

    % then call the user supplied OutputFcn
    stop = params.OutputFcn(xtrans,varargin{1:(end-1)});

  end

end % mainline end
```

```
% ====================================
% ========= begin subfunctions =========
% ====================================
function fval = intrafun(x,params)
% transform variables, then call original function

% transform
xtrans = xtransform(x,params);

% and call fun
fval = feval(params.fun,reshape(xtrans,params.xsize),params.args{:});

end % sub function intrafun end

% ====================================
function xtrans = xtransform(x,params)
% converts unconstrained variables into their original domains

xtrans = zeros(params.xsize);
% k allows some variables to be fixed, thus dropped from the
% optimization.
k=1;
for i = 1:params.n
  switch params.BoundClass(i)
    case 1
      % lower bound only
      xtrans(i) = params.LB(i) + x(k).^2;

      k=k+1;
    case 2
      % upper bound only
      xtrans(i) = params.UB(i) - x(k).^2;

      k=k+1;
    case 3
      % lower and upper bounds
      xtrans(i) = (sin(x(k))+1)/2;
      xtrans(i) = xtrans(i)*(params.UB(i) - params.LB(i)) + params.LB(i);
      % just in case of any floating point problems
      xtrans(i) = max(params.LB(i),min(params.UB(i),xtrans(i)));

      k=k+1;
    case 4
      % fixed variable, bounds are equal, set it at either bound
      xtrans(i) = params.LB(i);
    case 0
      % unconstrained variable.
      xtrans(i) = x(k);

      k=k+1;
  end
end

end % sub function xtransform end
```

Appendix D- Engineering Ethics Form

EBE Faculty: Assessment of Ethics in Research Projects

Any person planning to undertake research in the Faculty of Engineering and the Built Environment at the University of Cape Town is required to complete this form before collecting or analysing data. When completed it should be submitted to the supervisor (where applicable) and from there to the Head of Department. If any of the questions below have been answered YES, and the applicant is NOT a fourth year student, the Head should forward this form for approval by the Faculty EIR committee: submit to Ms Zulpha Geyer (Zulpha.Geyer@uct.ac.za; Chem Eng Building, Ph 021 650 4791). Students must include a copy of the completed form with the thesis when it is submitted for examination.

Name of Principal Researcher/Student: MUHAMMAD G. STRACEY Department: MECHANICAL ENGINEERING

If a Student: Degree: MSC. ENG Supervisor: Prof. R. Knutsen

If a Research Contract indicate source of funding/sponsorship: THRIP

Research Project Title: Continuum Damage Mechanics (CDM) modelling of Dislocation Creep in 9-12% Cr Streels

Overview of ethics issues in your research project:

Question 1: Is there a possibility that your research could cause harm to a third party (i.e. a person not involved in your project)?	YES	(NO)
Question 2: Is your research making use of human subjects as sources of data? If your answer is YES, please complete Addendum 2.	YES	(NO)
Question 3: Does your research involve the participation of or provision of services to communities? If your answer is YES, please complete Addendum 3.	YES	(NO)
Question 4: If your research is sponsored, is there any potential for conflicts of interest? If your answer is YES, please complete Addendum 4.	YES	(NO)

If you have answered YES to any of the above questions, please append a copy of your research proposal, as well as any interview schedules or questionnaires (Addendum 1) and please complete further addenda as appropriate.

I hereby undertake to carry out my research in such a way that

- there is no apparent legal objection to the nature or the method of research; and
- the research will not compromise staff or students or the other responsibilities of the University;
- the stated objective will be achieved, and the findings will have a high degree of validity;
- limitations and alternative interpretations will be considered;
- the findings could be subject to peer review and publicly available; and
- I will comply with the conventions of copyright and avoid any practice that would constitute plagiarism.

Signed by:

	Full name and signature	Date
Principal Researcher/Student: Signed	MUHAMMAD GHALIB STRACEY	29/01/15

This application is approved by:

Supervisor (if applicable):	Signed	23/02/15
HOD (or delegated nominee): Final authority for all assessments with NO to all questions and for all undergraduate research.	R.D. KNUTSEN	23/02/15
Chair : Faculty EIR Committee For applicants other than undergraduate students who have answered YES to any of the above questions.		

ADDENDUM 1:
Please append a copy of the research proposal here, as well as any interview schedules or questionnaires.

ADDENDUM 2: To be completed if you answered YES to Question 2:

It is assumed that you have read the UCT Code for Research involving Human Subjects (available at http://web.uct.ac.za/depts/educate/download/uctcodeforresearchinvolvinghumansubjects.pdf) in order to be able to answer the questions in this addendum.

2.1 Does the research discriminate against participation by individuals, or differentiate between participants, on the grounds of gender, race or ethnic group, age range, religion, income, handicap, illness or any similar classification?	YES	NO
2.2 Does the research require the participation of socially or physically vulnerable people (children, aged, disabled, etc) or legally restricted groups?	YES	NO
2.3 Will you not be able to secure the informed consent of all participants in the research? (In the case of children, will you not be able to obtain the consent of their guardians or parents?)	YES	NO
2.4 Will any confidential data be collected or will identifiable records of individuals be kept?	YES	NO
2.5 In reporting on this research is there any possibility that you will not be able to keep the identities of the individuals involved anonymous?	YES	NO
2.6 Are there any foreseeable risks of physical, psychological or social harm to participants that might occur in the course of the research?	YES	NO
2.7 Does the research include making payments or giving gifts to any participants?	YES	NO

If you have answered YES to any of these questions, please describe how you plan to address these issues (append to form)

ADDENDUM 3: To be completed if you answered YES to Question 3:

3.1 Is the community expected to make decisions for, during or based on the research?	YES	NO
3.2 At the end of the research will any economic or social process be terminated or left unsupported, or equipment or facilities used in the research be recovered from the participants or community?	YES	NO
3.3 Will any service be provided at a level below the generally accepted standards?	YES	NO

If you have answered YES to any of these questions, please describe how you plan to address these issues (append to form)

ADDENDUM 4: To be completed if you answered YES to Question 4

4.1 Is there any existing or potential conflict of interest between a research sponsor, academic supervisor, other researchers or participants?	YES	NO
4.2 Will information that reveals the identity of participants be supplied to a research sponsor, other than with the permission of the individuals?	YES	NO
4.3 Does the proposed research potentially conflict with the research of any other individual or group within the University?	YES	NO

If you have answered YES to any of these questions, please describe how you plan to address these issues(append to form)